NASA-CR-199665

NAG9-697

Lamar University

BEAUMONT, TEXAS

TECHNICAL REPORT

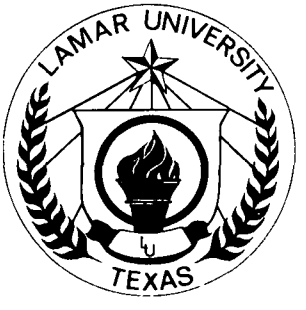

COLLEGE OF ENGINEERING

(NASA-CR-199665) SUPPORTING TECHNOLOGY FOR THE DEVELOPMENT OF CONTROLLED ECOLOGICAL LIFE SUPPORT SYSTEMS (CELSS) Final Report (Lamar Univ.) 118 p

N96-13450

Unclas

G3/54 0073760

Supporting Technology for the Development of Controlled Ecological Life Support Systems (CELSS)

FINAL REPORT
NASA Grant NAG9-697

by

Ku-Yen Li and Carl L.Yaws
Chemical Engineering Department
Lamar University
Beaumont, Texas 77710

and

William E. Simon and Harry T. Mei
Mechanical Engineering Department
Lamar University
Beaumont, Texas 77710

August 30, 1995

CONTENTS

LIST OF TABLES

LIST OF FIGURES

ABSTRACT

To support the development of Controlled Ecological Life Support Systems (CELSS) in the space program, a metabolic simulator has been selected for use in a closed chamber to test functions of the CELSS. This metabolic simulator is a catalytic reactor which oxidizes the methyl acetate to produce carbon dioxide and water vapor. In this project, kinetic studies of catalytic oxidation of methyl acetate were conducted using monolithic and pellet catalysts with 0.5% (by weight) platinum (Pt) on aluminum oxide (Al_2O_3). The reaction was studied at a pressure of one atmosphere and at temperatures varying from 160°C to 420°C. By-products were identified at the exit of the preheater and reactor.

For the kinetic study with the monolithic catalyst, a linear regression method was used to correlate the kinetic data with zero-order, first-order and Langmuir-Hinshelwood models. Results indicate that the first-order model represents the data adequately at low concentrations of methyl acetate. For higher concentrations of methyl acetate, the Langmuir-Hinshelwood model best represents the kinetic data. Both rate constant and adsorption equilibrium constants were estimated from the regression.

A Taguchi orthogonal array (L_9) was used to investigate the effects of temperature, flow rate, and concentration on the catalytic oxidation of methyl acetate. For the monolithic catalyst, temperature exerts the most significant effect, followed by concentration of methyl acetate. For the pellet catalyst, reaction temperature is the most significant factor, followed by gas flow rate and methyl acetate concentration. Concentrations of either carbon dioxide or oxygen were seen to have insignificant effect on the methyl acetate conversion process.

Experimental results indicate that the preheater with glass beads can accomplish thermal cracking and catalytic reaction of methyl acetate to produce acetic acid, methanol, methyl formate, and 1-propanol. The concentration of all byproducts was measured in ppmv (parts per million by volume). At higher temperatures, greater amounts of these products are produced, as expected. In all cases, methanol was the predominant concentration detected, followed by methyl formate.

At temperatures lower than 320°C for the P-type monolithic catalyst, methanol, acetic acid, and acetone were detected, whereas, for the E-type monolithic catalyst, only methanol was detected at 160°C. Both P and E types of the monolithic catalyst were specified with the same substrates (ceramic), washcoat (Al_2O_3), and promoter (Pt). However, the manufacturing and treatment procedures were quite different. It was therefore concluded that the performance

of the E-type monolithic catalyst is superior to that of the P-type for oxidation of methyl acetate. At higher reaction temperatures, e.g., above 420°C, all reactants and byproducts were completely oxidized using these two types of monolithic catalyst to produce carbon dioxide and water vapor.

A complex heterogenous catalytic reaction mechanism was proposed to explain the formation of the byproducts (methanol, acetic acid, and methyl formate) as the methyl acetate traveled through the preheater packed with glass beads. The byproduct, 1-propanol, may be formed only through a homogeneous reaction, since it is difficult to develop a reasonable sequence of heterogeneous reaction steps to explain its formation. The homogeneous thermal decomposition of methyl acetate to form free radicals was proposed to explain the formation of 1-propanol, and also methanol, in the preheater.

A dual-site catalytic reaction mechanism was proposed for the oxidation of methyl acetate over Pt/Al2O3 monolithic catalyst. The dual-site mechanism describes the chemisorption of oxygen molecules as well as a physical adsorption of methyl acetate on the active sites. On the active sites, methyl acetate is oxidized rapidly to form carbon dioxide and water vapor. A rate equation derived from this mechanism gives the Langmuir-Hinshelwood rate formula which has been observed from the experimental data obtained in this project for high methyl acetate concentration (>1000 ppmv) over a monolithic catalyst. If the oxygen concentration is very high and methyl acetate concentration is very low, the reaction rate equation is then reduced to a first-order with respect to methyl acetate concentration. The first-order model has also been observed from the experimental data obtained in this project for low methyl acetate concentration (<1000 ppmv).

I. INTRODUCTION

One of the most challenging problems associated with long-duration manned space flight is found in the development of Controlled Ecological Life Support Systems (CELSS). This includes the technologies of air revitalization, water recovery, waste processing and food production, and the integration of these systems into an optimal closed life support system for future space missions [Elikan, 1966; Schwartzkopf, 1992]. While early studies addressed some of these technology areas on an individual basis, little effort was put forth to develop an integrated, closed-cycle ecological space life support system. Johnson Space Center (JSC) engineers from the Crew and Thermal Systems Division (CTSD) have converted the 20' man-rated vacuum chamber in Building 7A to a full-up Systems Integration Research Facility (SIRF). JSC plans include a fully integrated, reduced-pressure (10.2 psia), test with four humans and all required closed-cycle life support equipment to sustain the crew for one year in an isolated condition.

To achieve this goal, subsystem development work has begun with the construction of experimental waste-processing and plant growth facilities at JSC, as well as contractor development of various subsystems. To facilitate efficient development and testing of these systems, expensive man-in-the-loop testing of early development subsystems must be avoided. To accomplish this, a human metabolic simulator is desired to simulate the presence of humans in the closed environment. Such a metabolic simulator has been conceptually designed by JSC and its support contractors. This conceptual design, in summary, is based on the catalytic oxidation of fuels. This catalytic simulator is designed to provide proper carbon dioxide, humidity, and metabolic heat load to a test-bed environment [Lin, 1982; Henninger, 1993].

The fuels are typically organic. Combustion of such a mixture of organic compounds is described by the following overall exothermic reaction, although the reaction mechanisms are very different [Van Der Vaart, 1991]:

$$C_xH_yO_z + \left(x+\frac{y}{4}-\frac{z}{2}\right) O_2 \rightarrow xCO_2 + \frac{y}{2}H_2O$$

Several different kinds of fuel such as methyl acetate, ethanol, and methanol were investigated. Their advantages and disadvantages were discussed in two graduate theses [Li, 1993; Chalasani, 1995]. Following a considerable amount of study, methyl acetate was selected because its respiratory quotient approximates closely that of a human being. However, experimental kinetic data associated with the methyl acetate oxidation were very limited [Maurel, 1982; Lang, 1991 & 1992], and specific data for this reaction at the design temperature were unavailable. Therefore, in an earlier project, a subscale reactor with pellet Pt/Al_2O_3 catalyst was built and used for the study of the catalytic oxidation of methyl acetate [Simon, et al. 1994].

This project continued the previous work of obtaining kinetic data for the oxidation of methyl acetate using a monolithic catalytic reactor. A monolithic reactor offers a low pressure drop with a high conversion factor. Two types, P-type and E-type, of the monolithic catalysts were investigated in this project. Both P- and E- types of the monolithic catalysts were specified with the same substrates (ceramic), washcoat (Al_2O_3), and promoter (Pt). It should be noted, however, that manufacturing and treatment procedures could be quite different for these catalysts.

Heretofore, byproduct identification has not been performed during the catalytic oxidation of methyl acetate (MA). Even a trace quantity of hazardous byproducts could be fatal in a closed life support system. Therefore, it is important not only to identify the byproduct but also to determine optimum reaction conditions to avoid or minimize the production of any unwanted byproducts during the catalytic oxidation of methyl acetate. If concentration of the hazardous by-products produced from the oxidation of methyl acetate is excessive, ethanol may be considered as the alternative fuel for future work.

To investigate the effects of controlled variables such as reaction temperature, gas flow rate, and MA concentration on catalytic oxidation of MA, Taguchi orthogonal arrays (OAs), L_9, were developed and ANOVA (analysis of variance) tables were used for data analysis. Two types of monolithic catalysts, v.i.z., P-type and E-type, dispersed with platinum, were used for this study. The byproducts of this study were also collected following the OA experimental design and identified by gas chromatograph/mass spectrometer (GC/MS) analysis to determine the optimum parameters for byproduct control.

The 0.5% Pt/Al_2O_3 pelletized catalysts were also used to determine the effect of the interaction factors, such as reaction temperature, gas flow rate, and MA concentration, and the no-interaction factors, such as CO_2 concentration and O_2 concentration, on conversion of methyl acetate. A Taguchi orthogonal array, or L_{27} table, and ANOVA tables were used for the data analysis.

The Taguchi techniques in the statistical design of experiments simplify the assignment of factors and interactions to the columns of an orthogonal array to obtain a desired pattern of interactions [Czitrom, 1990]. This experimental design method is helpful in analyzing a system with several uncertainties because it offers maximum information with minimum sets of experiments [Ross, 1988].

The information obtained from this study should be beneficial for the design and operation of both the metabolic simulator and industrial catalytic oxidation units [Kesselring, 1986; Becker, 1989].

II. EXPERIMENT

II.1 Equipment and Materials

An overall flow diagram of the experimental system is shown in Figure 1. Figure 2 illustrates a modified flow diagram with on-line sorbent tubing for the study of byproduct identification. Details of the preheater and the reactor as well as the gas sampling system are shown in Figure 3. Each of the components shown in Figures 1 and 2 is described in the following paragraphs.

Methyl Acetate Tank

Liquid Methyl Acetate was stored in a tank constructed of schedule 80 stainless steel, 8-inch pipe with 5 1/4" NPT threads on the top. The methyl acetate tank has four tubes connected at the top, one for a pressure gauge, one for inlet air, one for outlet air and methyl acetate, and one for reducing tank pressure and adding methyl acetate. The air inlet tube was connected to a 1/4" pipe running to the bottom of the tank to pick up methyl acetate by bubbling air through the liquid methyl acetate.

Float-Type Flow Meter

Four float-type flow meters (Omega Engineering, Inc.) with different capacities, ranging from 0.036 to 8.695 l/min (STD), were used to control the concentration of methyl acetate (MA) and to monitor the flow rate from sampling ports on the reactor flowing to the gas chromatograph.

Electronic Mass Flow Meter and Controller

An electronic mass flow meter with two independent controllers (model no. 902C, Sierra Instruments, Inc.) ranging from 0 to 10 l/min (STD), was used to control and monitor the flow rate. The flow setpoint for flow controller is at the front panel adjustment potentiometers. Linear operation with LCD readout is standard. The back pack panel connectors, providing outputs of 0-5 VDC and 4-20 mA with 0-100% analogs of the flow range, have two 20-pin headers labeled Channel 1 and Channel 2. Each channel was set up for a specific transducer. Great care was taken to avoid plugging a transducer into the wrong channel, as flow values may be extremely inaccurate and/or damage may result to system electronics and transducer. Both voltage and current outputs were simultaneously available. Two controllers can be operated simultaneously.

Three more flow monitors with display were bought from Sierra Instruments, Inc., model 821Top Trak™, ranging from 0 to 1 l/min. One was installed for monitoring the flow rate of the vaporized MA immediately leaving the MA tank. This mass flow monitor controls the flowrate of MA stream at different constant air flowrates. Two others were installed on two gas sampling lines (as shown in Figure 2), one before and another after the reactor. To accommodate corrosive gas, all wetted surfaces of flow monitors were constructed of 316 stainless steel.

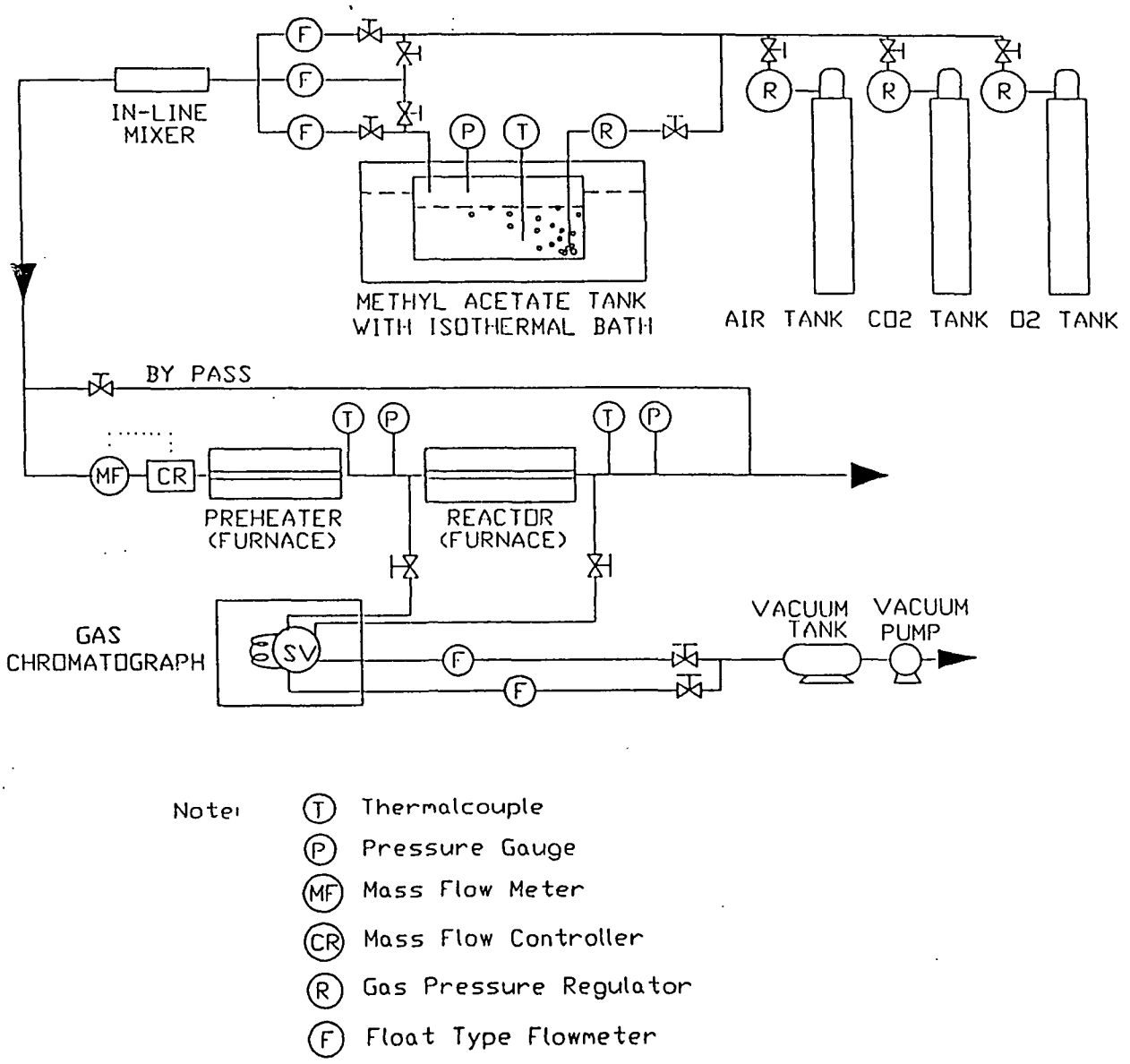

Figure 1. Flow Diagram of Experimental Setup for Conversion Study

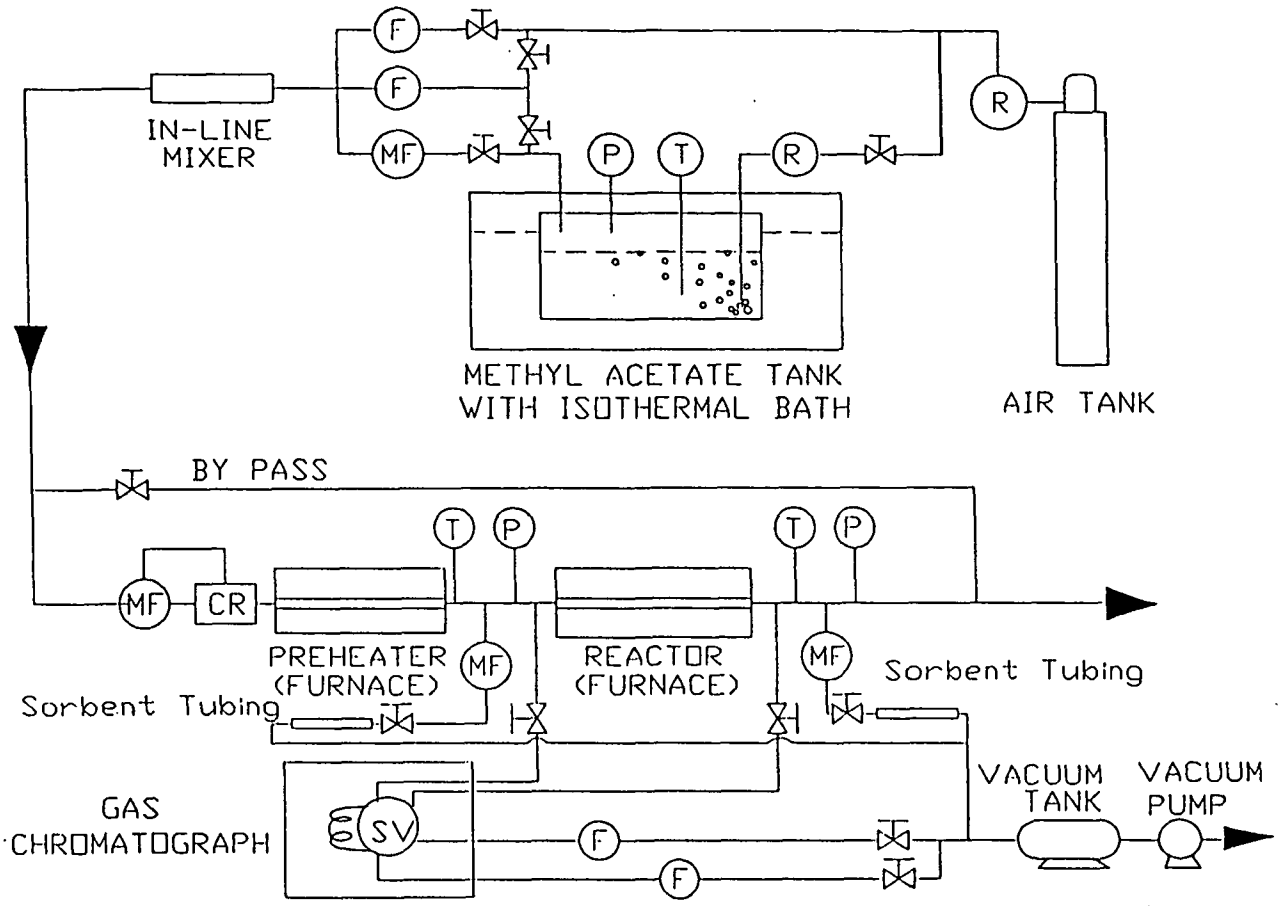

Note:

- (T) Thermalcouple
- (P) Pressure Gauge
- (MF) Mass Flow Meter
- (CR) Mass Flow Controller
- (R) Gas Pressure Regulator
- (F) Float Type Flowmeter

Figure 2. Flow Diagram of Experimental Setup with On-Line Sorbent Tubing for Byproduct Identification

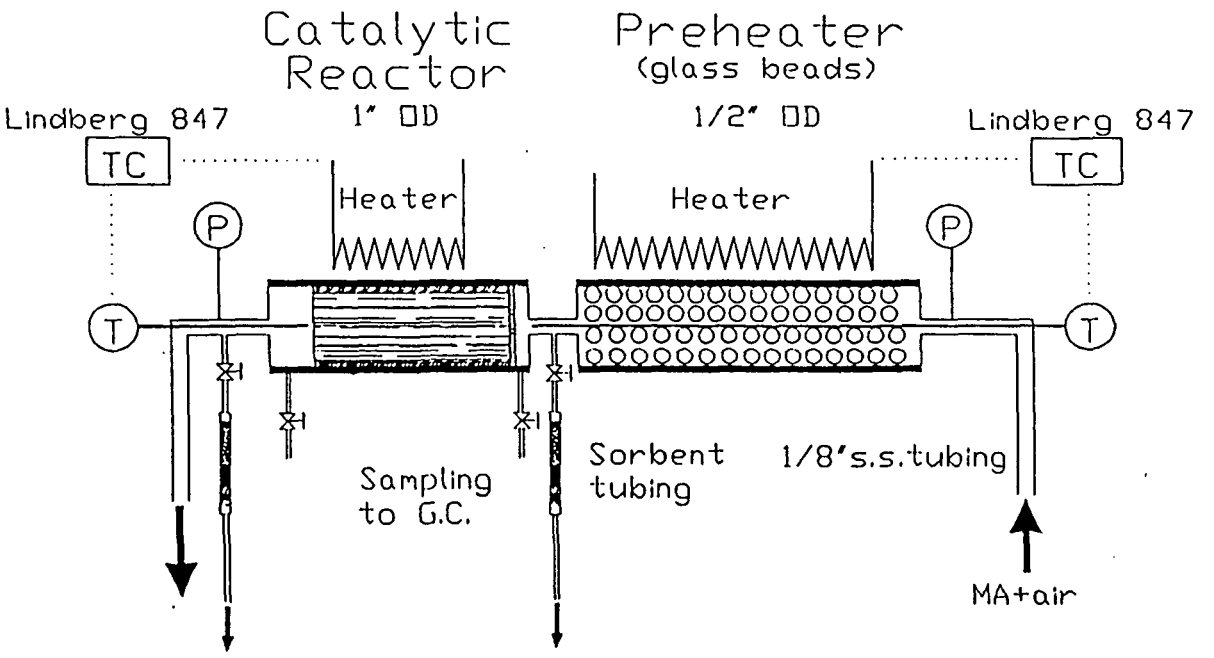

Figure 3. Structure of the Preheater and Reactor

Water Bath

Immersed in a 10-liter isothermal water bath, the water temperature was set at 25 °C and controlled within ±0.5 °C to reduce the fluctuation of both methyl acetate vapor pressure and downstream concentration.

Feed Gas Regulator System

Gas cylinders of hydrogen, helium and breathing air were obtained from the Big Three Gas Company. For the gas chromatograph, helium (He) was used as the carrier gas, and a mixture of H_2 and breathing air was used as fuel for the FID (flame ionization detector). Breathing air was also used as process air.

The effluent pressure of each gas cylinder was controlled by two-stage gas regulators manufactured by the Victor Equipment Company. Between the gas cylinder and the regulator, an inline filter of stainless steel wire was installed to prevent particulate migration to the downstream equipment.

In-Line Static Pipe Mixer

An In-Line Mixer from Cole Parmer, (model No.G-04669-18) consisted of a series of fixed right- and left-hand elements of stainless steel to provide efficient mixing with less pressure drop. To ensure complete mixing, the mixer was installed immediately after dilution of the vaporized MA stream with breathing air.

Thermocouples

Chromel Alumel K-type thermocouples, (catalogue number TJ36-CAIN-116U), with heavy duty transition joints, 1/16" inconel sheath, ungrounded junction and various lengths were ordered from Omega. To avoid electrical noise, the ungrounded junction at the end is the only choice with small sacrifice in response time. Additionally, the K-type thermocouple with a high temperature limit (approximately 1400°F) is suitable for the reaction temperature range of this investigation.

Preheater

A detailed diagram of the preheater and reactor is shown in Figure 3. A ½" OD and 6" long stainless steel tube purchased from Rawson, filled with 3 mm diameter glass beads from Kimble, served as the preheater. This preheater was placed in the center of a tube furnace to get efficient and uniform heating in a short travel distance.

Reactor

The fixed-bed reactor was made of 1" OD stainless steel tube and cut into 3" lengths. For the reactor with the pellet catalyst, at both ends of the catalyst region, two pieces of stainless steel wire mesh were used to support the 1/8" pellet catalyst bed. In front of the pellet catalyst bed, glass beads were packed with an axial length about 1/3" to serve as a distributor for the elimination of both eddies and non-uniform flow distribution. For the monolithic catalyst reactor, at the reactant entrance one piece of stainless steel

wire mesh was used to support a mass of glass wool used to eliminate flow eddies and non-uniform flow distribution. Welded to the stainless steel 1" unions were two sampling ports, which consisted of 1/8"-1/16" tube end reducers as shown in Figure 3.

Tube Furnace

Two tube furnaces, (model 55035 with 847 digital controls) were ordered from the Lindberg Company. The furnace, with a maximum operating temperature of 1000 °C at 2400 watts, consisted of a 1"×12" chamber and a convenient LED (light-emitting diode) digital indicator for furnace set point and chamber temperature. The exposed thermocouple inside the furnace chamber was disconnected, and another identical thermocouple, inserted adjacent to the catalyst bed, was wired to the temperature controller to assure accurate control of the reaction temperature within the reactor. Great care was taken to avoid electric shorting while reconfiguring this equipment. The critical setting of the operating parameters on the front panel of the controllers is discussed in the next chapter.

Valves

Three types of valves, ball valve, needle valve, and check valve, were installed for different purposes. The needle valves, 4Z-V4LN-SS CPI valves with 1/4" tubing connectors, were ordered from Parker and used when complete closure was important or accurate control was needed, such as for flow rate control. The ball valves, 4Z-B6LJ2-SSP CPI valves with 1/4" tubing connectors, ordered from Parker, were used where quick opening and closing were necessary. The other type of ball valves, SS-41S1CPI valves with 1/16" tubing connectors, obtained from Whitey, were connected for effluent analysis. The check valves, 4Z-C4L-1-SS valves with 1/4" tubing connectors, obtained from Parker, were used in the flow lines of hydrogen and MA entering the preheater to avoid accidental backfire.

Pressure Gauge

For pressure measurement, four ½" dial diameter pressure gauges and two ½" vacuum- pressure gauges were installed with a vacuum air tank and a line after the reactor and before the preheater. These types of gauge, (G-68800-40 and G6880048) with 1/4" npt bottom connections, were purchased from Cole-Parmer.

Heating Tape

The heavy insulated Samox tapes with maximum heating temperature 760 °C, (catalog number G-03115-21 and G-03115-40) suitable for direct contact on conductive surfaces, were ordered from Cole-Parmer. For safety reasons these tapes were not overlapped. In this experiment, the heating tape was connected with power regulators to limit temperature and to keep the transport lines at constant temperature.

Power Regulator

Power regulators rated at 1.1 KW (catalog number MC228) were purchased from

Electrothermal. They were designed to regulate power input to laboratory heating equipment and to ensure that the intended load would not exceed the maximum current rating of the power regulator as shown on its base label.

On-Line Sampling System

A detailed description of this equipment is shown in Figures 4 and 5. Taking gas samples before and after the catalyst bed was accomplished by connecting two pretreated 1/16" stainless steel tubes (washed, heated and purged) to the unions at the ends of the reactor. The other ends of these two tubes were connected to the first automatic valve housed on the top of the Gas Chromatograph, Varian Star 3400. By switching the 1st valve, a gas sample from either before or after reaction was sent to the sample loop (250 µl) installed on the 2nd automatic valve. The gas inside the sample loop was then flushed by the carrier gas (He) and sent to the separation column later when the injection command was generated to switch to the 2nd valve. Each valve was driven by a pneumatic actuator installed vertically above the valve. Additionally, a flow meter between the first automatic valve and the sampling port on the reactor was used to monitor the gas sample flowing to the 250 µl sample loop.

Vacuum System

The vacuum system consisted of a vacuum pump, (model 400-1901) from Barnant and an air tank (model 4F694) from Speedaire. This digraphragm-operated pump was designed for pressure, suction and gas circulation applications. To decrease the noise level a muffler was installed at the outlet. Usually, three-foot lengths of plastic tubing at both ends were more than adequate for quiet operation.

Gas Chromatograph

The analytical instrument for this function was the Varian Star 3400 equipped with a Flame Ionization Detector (FID), a Thermal Conductivity Detector (TCD), two 1041 universal injectors, and a plotter.

The FID was commonly used to detect hydrocarbons where high sensitivity was required. In the FID, the eluate coming from the column (CTR column) was combined with hydrogeny and air to form a combustible mixture. This ignited mixture formed a flame which provided sufficient energy to ionize most organic and some inorganic sample components of the eluate. Upon striking the collector electrode, the current flowing through the circuit was proportional to the number of ions striking the collector, which in turn was proportional to the concentration of ionizable sample components entering the flame. Thus detector response increased with increasing carbon atoms in the component molecule.

The TCD was used to monitor the rate of heat transfer away from an electrically heated wire by the column eluate. Passing the eluate through one filament and the carrier gas through the other filament, the relative resistance of the two heated filaments was then

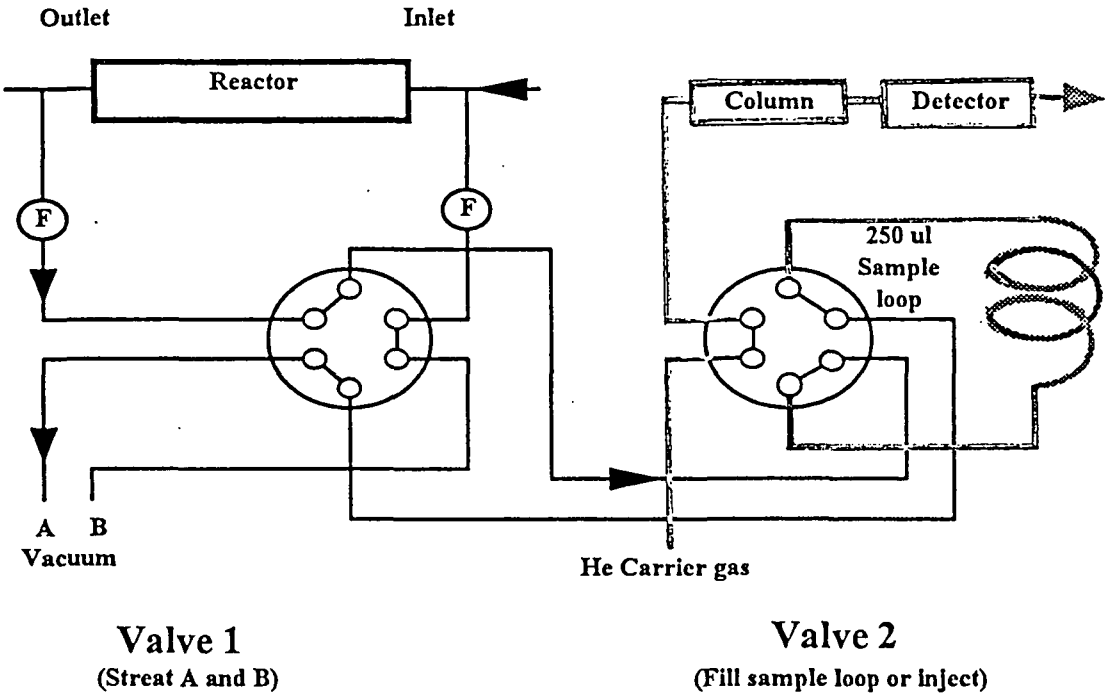

Figure 4
Flow Diagram of On-Line Sampling System

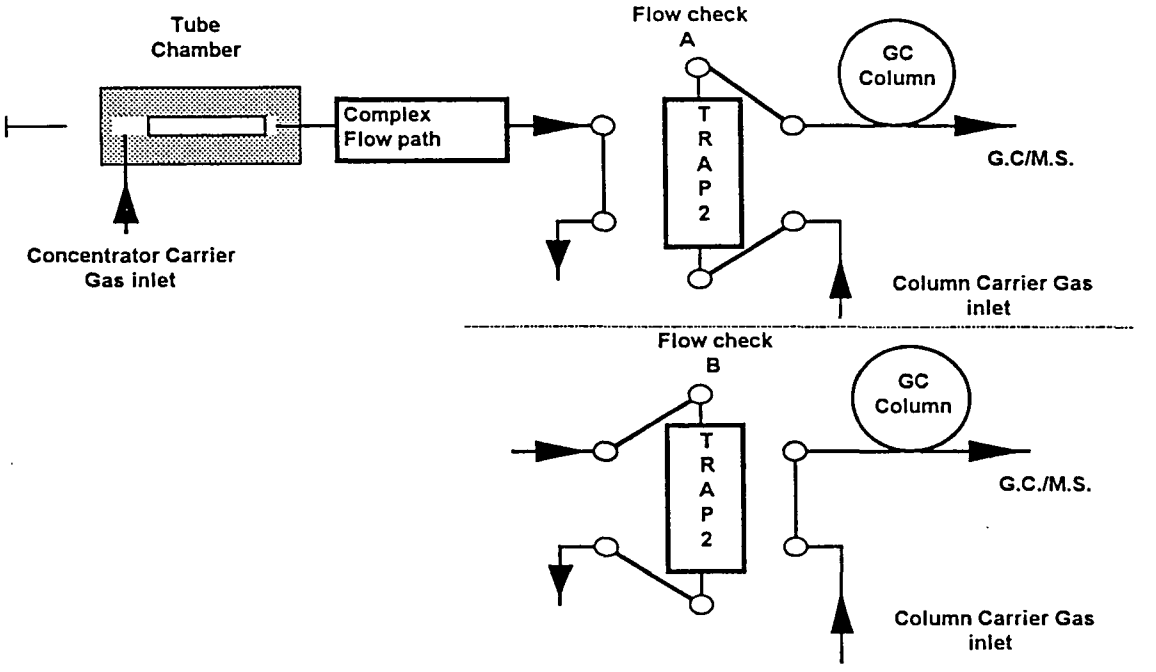

Figure 5
Experimental Setup for Byproduct Identification
(Concentrator/GC/MS)

continuously monitored with a Wheatstone bridge. When a signal was produced due to a difference in resistance, the detector responded to changes in the type and amount of gas flowing through the filament.

Column

The CTR column, (catalog number 8700, sample size 250 µl) installed in the GC was Alltech's designation of concentric columns which offers many advantages for certain types of difficult analyses. A CTR column is essentially a column within a column. This permitted two different packings to be used simultaneously for one analysis. This invention was helpful to permit the separation of oxygen, nitrogen, carbon monoxide, carbon dioxide and methane in one analysis at a carrier gas flowrate of 59 ml/min and room temperature. Usually this analysis was accomplished by either making two separate runs on the sample of interest, or employing a switching valve and polarity change during the analysis. The reason for this difficulty is that carbon dioxide was irreversibly adsorbed on molecular sieves which are necessary for obtaining an oxygen/nitrogen split.

Microliter Syringe

For the calibration of methyl acetate, Hamilton 7000 series microliter syringes with 1 μl capacity were purchased from Fisher. The included guide assembly was most commonly used on syringes with a small-diameter plunger wire to minimize damage due to excessive force. Additionally, the Chaney adapter ensured reproducibility within 1% when injections of identical volumes were required.

Data Acquisition System

A 386 DX 40MHz computer, purchased from UL-Tech was the major device used for signal analysis from the TCD and FID. The software, Star Workstation from Varian, provided a convenient way to handle a large amount of experimental results and to accomplish remote control of the GC. Two data acquisition boards were installed inside the computer, one for the Star Workstation, the other for digital/analog signal conversion.

Integrator

An integrator manufactured from Varian, model no.4270, was used to process output data and generate analytical reports for the GC. It was placed near detector B (FID) of the GC. The plus (+) lead of the analog signal cable (1 volt max.) was attached to the red connector, with the minus (-) lead attached to the black connector on the back of the integrator. The critical setting of the operating parameters on the integrator is discussed in the next chapter.

Gas Chromatograph/Mass Spectrometer

The HP 5970B Mass Selective Detector (MSD), ordered from Hewlett Packard, with the right side of HP 5890 GC, ordered from Hewlett Packard, is a standalone capillary GC detector designed for use with a variety of gas chromatographs. It is capable of analyzing minute amounts of material usually in the program range by fragmenting the

sample into charged ions, separating them on the basis of molecular weight-to-charge ratio, then counting the ions as they enter the detector. The counted ions identified by mass can be plotted, with mass on the abscissa and the counted ions or abundances on the ordinate.

The Mass Selective Detector can be thought of as having four major components: analyzer, detector, vacuum system, and workstation. They are described below.

1. Analyzer: The analyzer of the mass spectrometer separates the ions generated in an ion source or collision cell according to their mass-to-charge ratios. The mass analyzer can consist of a magnetic, electric, or quadrupole sector, or of a combination of sectors.
2. Detector: The detector of a mass spectrometer converts the ion's beam from the mass analyzer into a signal that can be digitized. This signal is then processed by the data system to provide information about the sample. The more ions hitting the detector, the more current is generated. The electrons in the Mass Selective Detector convert current into an analog voltage which is then converted into a digital signal. The ion abundance information is sent to the Workstation, which in turn stores it in the disc memory.
3. Vacuum: The key to operating a Mass Selective Detector is a good vacuum. Normal operating conditions require a vacuum in the range of 10^{-6} to10^{-5} Torr. Insufficient vacuum may lead to decreased sensitivity, excessive contamination of parts, and a shorter life expectancy of the electron multiplier. Two pumps are responsible for maintaining the vacuum: the mechanical roughing pump and the turbomolecular pump. In series, they create and maintain the vacuum needed to operate the Mass Selective Detector.
4. Workstation: The Mass Selective Detector requires a Workstation to (1) turn the detector off and on, (2) optimize the potentials in the analyzer, (3) select the mass (amu) that the quadrupole is to filter, (4) receive data from the detector, (5) present data in a suitable form to the user, and (6) receive instructions from the user. MS Chemstation software is used for the above purposes.

The mass spectrometer has a very fast response time and can detect the concentrations of several gases simultaneously. By the nature of its design, it is unaffected by pressure fluctuations, and the presence of water vapor for its diluting effect is easily achieved. Mass spectrometers are linear over a wide range of gas concentrations and are accurate.

Capillary Column

The capillary column, Ultra 2, HP part no.19091B-102 and 25 m×0.2 mm×0.33μm film thickness, ordered from Hewlett Packard, was used to separate byproducts in the GC/MS. This column is manufactured to the highest specifications, exceeding industry standards. Available in methyl siloxane and 5% phenyl methyl siloxane phases, this column is ideal for applications requiring extreme column-to-column reproducibility, and

is recommended for the use with the Sadtler Retention Index Library.

Data Acquisition System

A 486 DX 40MHz computer was used to perform the signal analysis. The software, ChemStation, provides a convenient way of controlling MSD and GC operation, and of handling a large amount of mass spectral data. Once acquired, the data can be displayed and manipulated in various ways including integration, quantification, and library search. The library search compares the spectrum of the unknown compound with a library or database of known spectra, and it identifies those spectra from the reference library which are most like the spectrum of the unknown compound. This software allows custom report generation and has a rich command set. Command parameters set in the software for this experiment are discussed in the next section.

Spectrum Gas Syringe

The various spectrum gas syringes, ordered from Fisher, were used for calibrations of methyl formate, 1-proponal, acetone, methanol, and acetic acid, by injecting head-space vapor into the concentrator and GC/MS. In this device the plunger face contacts are positioned snugly against the bottom of the glass barrel, assuring virtually total gas displacement from the measuring chamber. Also, the plunger has stationary PTFE seals at its tip. Contact by the seal against the flat glass tip face of the syringe assures a leak-proof connection.

Concentrating/Capillary Inletting System for GC/MS

The concentrator (810 Envirochem) was used to sparge, inject or thermally desorbe samples for GC/MS analysis. The heart of the concentrator is its patented two-stage gradient trapping system. This system is constructed of the highest quality inert materials, and all transfer lines which come in to contact with the sample are of nickel and are heated to eliminate potential sample degradation or condensation. The gradient trapping system allows direct on-column capillary inletting without splitting. The 810 Envirochem Concentrator has a pair of traps - one with a large bore and a second with a small bore. The flow path is complex. Once a sample is deposited onto trap 2, there will be two positions: check A and check B. A detailed description is shown in Figure 5. In check A position, concentrator carrier gas enters valve 2, port 3, through the trap 2 desorbing sample; exits valve 2, port 2, and enters the transfer line to the GC. In check B position, valve 2 has turned and the gas flow is no longer through trap 2.

Sorbent Tube

The sorbent tubes, model number ST-032, packed with glass beads/75mg 20: 35 mesh Tenax-TA/Ambersorb/Charcoal in order of increasing affinity for low boiling compounds, were ordered from Envirochem. During sample collection, flow enters at the glass bead end. The higher molecular weigh compounds in the sample are absorbed on the surface area of the glass beads, while those compounds which penetrate the beads proceed to the Tenax layer. The lower boiling components passing through the glass beads and

Tenax layers are adsorbed on the Ambersorb, or charcoal, layers. Thus each layer of sorbent protects succeeding, more active layers.

During thermal desorption, the tube was positioned in the concentrator so that carrier gas passes through the tube in the reverse direction of sample collection flow. Each molecular weight range of compounds is then " backed off' of the adsorbent material.

Sorbent Tube Conditioner

The sorbent tube conditioner, consisting of a gas inlet on/off toggle valve and adjustable needle valve for the carrier gas, a sleeve heater and variable transformer for temperature control, and a pyrometer connection (from Envirochem), were useful for conditioning the sampling tubes prior to taking samples. Extra-pure grade N_2 carrier gas was connected, the flowrate was set at 55 cc/min, and the sleeve heater temperature was set to 300 ^{0}C for two hours of conditioning. The conditioned tubes were checked by GC/MS to assure they were clean before sampling.

Catalyst

Aldrich provided the 0.5% platinum content catalyst, catalogue number 20601-6, for laboratory use (1/8"×1/8" nonporous alumina pellet with platinum coating on the surface).

The two different monolithic catalysts, with alumina and supported platinum, were provided by two different companies. The monolithic catalyst consists of a large number of narrow, parallel channels separated by thin walls. The characteristics of monolithic catalysts are listed in Table 1.

Table 1
Characteristics of Monolithic Catalyst

	P-type of monolithic	E-type of monolithic
Dia. x Length	1" dia. by 3" length	1" dia. by 3" length
Substrate	Corning Celcor Brand	Corning Celcor Brand
Washcoat	25-50 μm Al_2O_3	25-50 μm Al_2O_3
Number of Cells	135	86
Weight (gram)	15.10	13.68
Diameter (inch)	0.827	0.875
Cell dimension (inch)	0.048	0.055

II.2 Experimental Procedure

II.2.1 Pre-test and Pre-condition Operations

Catalyst Preparation

The 1/8"×1/8" pellet catalyst was first weighed by an analytical balance (0.1 mg accuracy) before being placed into the reactor. Normally the amount of catalysts used in this study was between 0.5 - 5.0 gram. To support the catalyst in the reactor, a piece of stainless steel wire mesh was fixed at each end of the catalyst bed.

For the monolithic catalyst reactor, the diameter of the monolithic catalyst was first reduced to fit the 1" O.D. stainless steel reactor. It was then weighed, the number of cells counted, and its total area calculated. The catalyst was then wrapped with a layer of ceramic paper to fit to the 1" stainless steel tubing. The ceramic paper prevents reactants passing through the gap between the monolithic catalyst and the stainless steel tube. Each reactor was checked at 30 psig for gas leaks before beginning the experimental runs.

Prior to the reaction exposure, the catalyst was pretreated by calcining in flowing air. The calcination was performed first by drying the catalyst at 125 °C in air flowing at 1.0 liter/min for 2 hours. The catalyst temperature was then gradually raised to 425 °C and maintained for 16 hours. After calcination, its temperature was decreased to 250 °C and hydrogen was then passed through the catalyst to reduce any oxidized surface. Extra care was taken when hydrogen was introduced into the process, e.g., to prevent a possible spark.

Column Preconditioning

To precondition the GC column, one end of the column was first connected to the injection port, with the other end left open. A normal flow of carrier gas was initiated through the column (i.e., 25 cc/min for 1/8" CTR column). The carrier gas (He) was required to be free of oxygen, moisture and oil, since this type of column deteriorates rapidly even with trace quantities of oxygen present in a highly purified carrier gas. This preconditioning process proceeded at room temperature for 30 minutes. The column was then programmed to a desired temperature at least 25 °C lower than the upper temperature limit (listed on the column tag). Alternatively, it was conditioned at 25 °C above the maximum operating temperature used in the analysis as long as it did not exceed the upper temperature limit minus 25 °C. In this study, the column was conditioned at 130 °C since the operating temperature was 105 °C.

The preconditioning process was continued for 24 hours at 130 °C. Overnight was usually sufficient. Nevertheless, for some cases, a longer period, up to 48 hours, was necessary. In addition, the carrier gas (He) valve was never closed before the column had cooled to room temperature. If a column had been out of use for awhile, it was reconditioned briefly by purging with pure carrier gas for 30 minutes, programming to the

desired temperature, and holding it at the desired temperature for 30 minutes to 2 hours before starting the analysis.

Pressure Test

A pressure test was performed before each run to check for leaks. The entire system was pressurized to 30 psig, after which the leak check was performed by observing the pressure gauge. If the pressure remained constant for more than 30 min., the test was acceptable. Otherwise, a soap solution was applied to determine the location of the faulty connection.

Calibration of Samples

The methyl acetate calibration curve for the GC-analysis was obtained by injecting several standard samples into the injection port of the GC with a Hamilton microsyringe. For methyl acetate, it was first diluted with methanol to form different weight-percent solutions. By injecting different amounts of the solutions, the area count related to a certain quantity of MA injected was then obtained. It was shown that the linearity for MA from FID is very good over a very wide range of concentration in a 250 μl sample loop. These results are shown in Appendix A.

The calibration curves of acetic acid, methanol, methyl formate, 1-propanol, and acetone were obtained by injecting head-space vapor samples into the injection port of the concentrator, after which the samples were deposited onto the capillary column of the GC/MS. The head-space vapor samples, prepared from 99+ % liquid samples, were placed in bottles and equilibrated for a predetermined time in an agitated, temperature-controlled environment (see Figure 6).

Henry's law (Equation 1) [Balzhiser, 1972] and the Antoine equation (Equation 2) [Yaws, 1992] were used for the calculation of vapor pressure. The area count was then obtained, related to absolute weight of sample injected. The parameters of A, B, C of the Antoine equation for identified byproducts and calculations are described in Appendix B.

$$x_i H_i = P_i = y_i P \tag{1}$$

Where x_i = Mole fraction of chemical specie i,
y_i = Mole fraction, particularly in gaseous phase,
P_i = Partial pressure, [atm.],
P = Pressure, [atm.],and
H_i = Henry law constant for component i, [atm.].

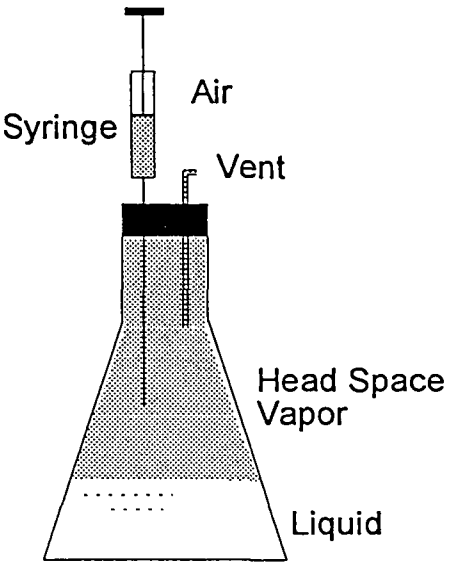

Figure 6

Sampling Head-Space Vapor with Syringe

In this calibration, the pressure is one atmosphere and the mole fraction x_i is 1. The Antoine equation is

$$\log P = A - [\frac{B}{T+C}] \quad (2)$$

Where P = Vapor pressure, mmHg
A = Antoine coefficients for the compound,
B = Antoine coefficients for the compound,
C = Antoine coefficients for the compound, and
T = Temperature, °C.

II.2.2 Operating Procedure for Catalytic Reactor

1. The liquid level in the methyl acetate vaporization tank was checked and the temperature of the isothermal water bath set to 25 °C.

2. Air supply pressure was set at 10 psig. This pressure was sufficient to produce the required flow rate, especially for the small pressure drop associated with the monolithic catalyst.

3. The methyl acetate tank pressure was set at 5 psig by adjusting the regulator located at the entrance of the MA tank.

4. The needle valves upstream of the flowmeter were adjusted, for both air and saturated methyl acetate vapor to dilute the methyl acetate to the desired concentration. Typical values were between 100 to 10,000 ppm. A rough estimate could be obtained through the readings on the mass flow meters, with the accurate concentration value obtained from GC analysis.

5. The reactor temperature was increased to the set point (160 - 460 °C). The parameters of the Lindberg 847 controller were recommended by the instruction manual and set as shown in Table 2. The thermocouple within the tube furnace was disconnected and another thermocouple, the same K-type, was connected to the 19th (yellow lines from thermocouples) and 20th (red lines from thermocouples) port on the back of the Eurotherm 847 controller. This modification was to assure that the temperature measured was the reaction temperature in the catalyst bed and not furnace temperature. This control scheme provided a stable catalyst bed temperature, as shown in Figure 7. Before taking samples, this temperature was maintained constant for at least 10 minutes to assure a uniform temperature distribution within the catalyst bed.

Table 2
Parameter Settings of the Lindberg 847 Temperature Controller

Basic Setpoint	460 °C
Tune	Off
Loop Counter	1
1st Ramp Rate	50
1st Dwell Level	400
1st Dwell Time	40
2nd Ramp Rate	0.01
2nd Dwell Level	460 °C
2nd Dwell Time	0
Holdback Band	20

II.2.3 Operating Procedure for On-Line Effluent Analysis

1. The catalytic reaction was assured to be in steady state.

2. The vacuum pump was started.

3. The breathing valve connected to the vacuum tank was adjusted to keep the tank at the desired vacuum, -1mmHg, for sampling.

4. The sampling flow rate was checked by the flowmeter brought on-line between the vacuum tank and the sampling port attached to the reactor. Typical flow rates were 20 to 30 cc/min to guarantee that the sample loop (250 μl) was entirely flushed within 20 sec by the fluid with the same concentration as that in the reactor.

5. A sample from the outlet of the reactor was taken first.

6. Immediately after the first injection, the sample from the inlet of the reactor was flushed into the sample loop. One minute later, both sample valves were closed. They are connected to the sample loop to hold the gas sample inside the loop waiting for the second injection.

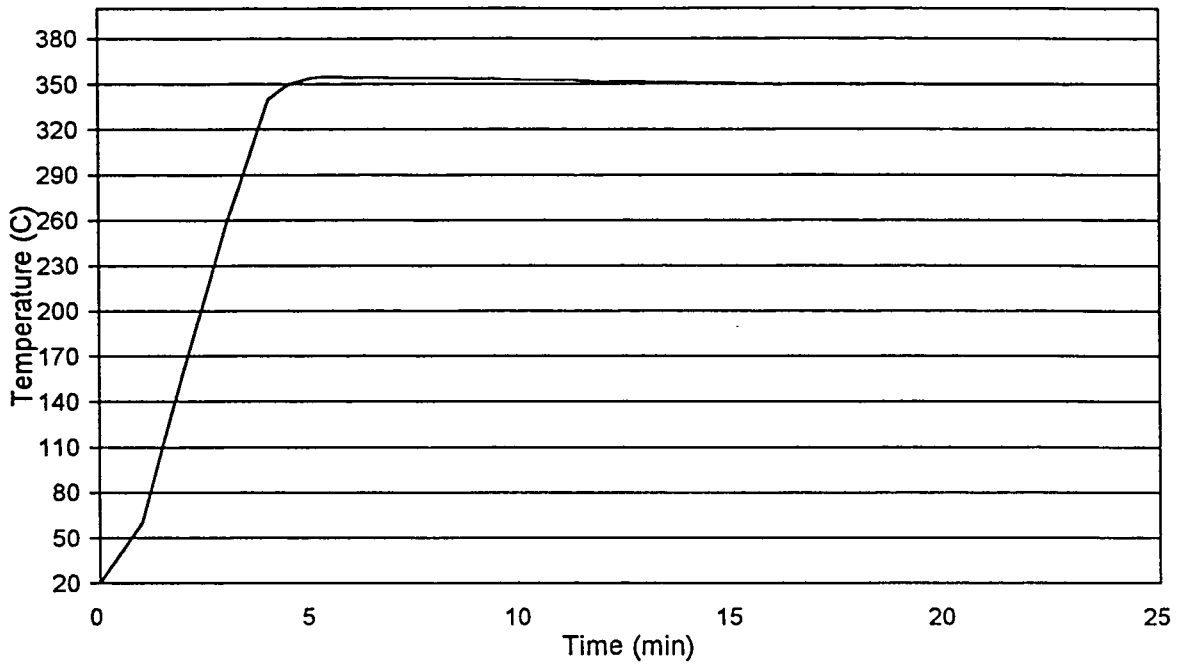

Figure 7

Temperature Stability of the Reactor and Preheater

II.2.4 Operating Procedure for Gas Chromatograph

1. The pressures of the He, H_2 and breathing air cylinders were checked. According to the menu, it was suggested that the He pressure be maintained at 80 psig, H_2 at 40 psig, and breathing air at 60 psig.

2. Leak checks were conducted on the 1/8" copper tubing connected between the gas chromatograph and the gas cylinders.

3. The carrier gas (He) flow rate was set at 60 cm^3/min.

4. The Star Work Station was initiated by typing win/s.

5. The parameters in the Method Editor were set as shown in Table 3.

6. The parameters for both relays were set as shown in Table 4.

7. The parameters of the integrator were set as shown in Table 5.

8. The stability of the baselines of the FID was checked. When the baseline was not stable, it was necessary to wait until there was no significant fluctuation, since an unstable baseline might be caused by an unstable column or detector temperature, which is an important factor for GC operation.

9. A run was then started by clicking on the "start" icon on the screen in the system control section.

II.2.5 Operating Procedure for Sample Collection

1. Before a sample was collected, the sorbent tube was checked using the GC/MS to assure no contamination. A typical figure such as that shown in Figure 8 should be achieved. The only peak is water which is condensed onto the column from the helium carrier gas.

2. According to the suggested Taguchi orthogonal arrays, air flow rate, oven temperature, and MA concentration were then adjusted to their desired values.

3. A constant room temperature was maintained for thermal adsorption of the gas stream through the sorbent tube. Normally, the collection temperature was 20 °C.

4. Sorbent tubes were used to collect samples from the bypass before and after the reactor. The sample flow rate was adjusted by a vacuum pump attached to the

sorbent tube and two needle valves on the line before and after the sorbent tube.

Table 3
Detailed Operation Parameters for Gas Chromatograph

TCD (Thermal Conductivity Detector)	
Temperature	150 °C
Attenuation	16
Range	0.5
Filament Temperature	250°C
FID (Flame Ionization Detector)	
Temperature	200 °C
Attenuation	32
Range	12
Column Temperature	105 °C
Injector Temperature	105 °C
Column Hold Time	15 min
Channel B	FID
Temperature Programming	Off

Table 4
The Settings of Relays for Sample Injection

Time	Relay# 1 position	Relay* 2 position
0.00	1	2
0.25	-1	-2
3.10	1	-2
3.35	-1	2
15	-1	2

Relay 1 refers to switch 1, which is used to choose either the injecting sample (position 1) or the fill sample loop (position -1)

* Relay 2 refers to switch 2, which is used to select a sample from either downstream of the reaction (position 2) or upstream of the reaction (position -2) for flow to switch 1.

Table 5
Detailed Operation Parameters for Integrator

Attenuation	32
Peak Width	6
Peak Threshold	500
Peak High	2
Function Time	15 min

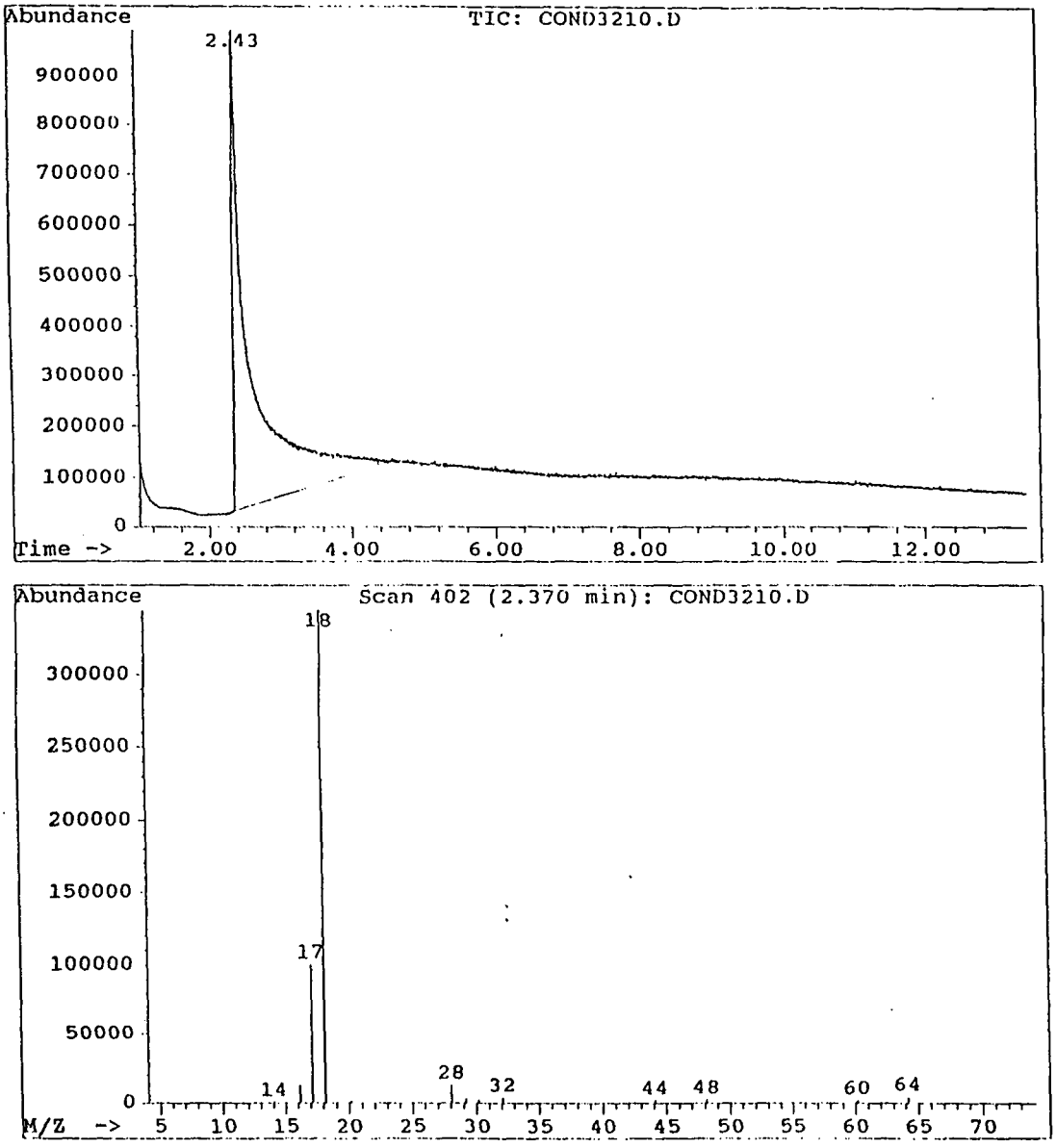

Figure 8
The GC/MS spectrum for the sorbent tubing before sampling

5. The sample flow rate and collection time were adjusted to moderate values to prevent excessive concentration of the adsorbates which may damage the GC/MS. Moderate values of flow rate and collection time were used (22 cc/min and 4 minutes, respectively).

6. After sample collection, the sorbent tubes were analyzed by desorption at the concentrator, where the samples were transferred to the capillary column of GC/MS for chemical analysis.

7. Before use, the sorbent tubes were desorbed using a sorbent tube conditioner at 300 °C and 55 mls/min of nitrogen gas for 2 hrs until they were completely clean.

II.2.6 Operating Procedure for Concentrator/GC/MS

1. Restart the MSD (HP 5970):

   A. Turn on the power switch.
   B. Press PUMPING UNIT. Wait 10 minutes.
   C. Press HEATING. Wait one hour.
   D. Check the He, H_2, and breathing air pressure. According to the suggested value of the menu, always keep He at 60 psig, H_2 at 40 psig and breathing air at 80 psig.
   E. Set the column carrier gas (He) flow rate to 1 ml/min.
   F. Turn on the computer and start the MS ChemStation software.
   G. Go to the EditParameters, set operating conditions. Table 6 lists these in detail.
   H. Go to Methods, load the edited method and start a run by clicking on the run method button on the screen in the "start run" section.

2. Restart the Envirochem Concentrator

   A. Return the auto/test/manual switch to the MANUAL position.
   B. Set the operation parameter from the front panel of the concentrator. Table 7 lists details of the operation parameter.
   C. Make sure the handle of the concentrator is on its side (pointing toward the sorbent tube).
   D. Make sure the desorber heater is in "auto" position.
   E. The mode should be "trap in"; sparger heater switch must be "off."
   F. Sequencer flow time and transfer time are as listed in Table 7.
   G. Place the sampling sorbent tube in the tube chamber with the glass frit end at the back of the tube chamber for desorption. Press "start."
   H. When the sequencer advances to the "trap 2" heat position, press "GC start" to

Table 6
Detailed Operation Parameters for GC/MS

Oven Program	
Oven Initial Temperature	30 °C
Oven Initial Time	5 min
Rate	8.0 C/min
Oven Final Temperature	230 °C
Detector B Temperature	200 °C
Solvent Delay	2.40 min
Electron Multiplier Voltage	1200 Volt
MS Scan Parameters	
Mass Range	12 to 150
Threshold	500
Scan/sec	3.0
On Time Window	30 min
Total Ion Max.	2000000
Injector B temperature	250 °C

Table 7
Detailed Operation Parameters for Concentrator

He Flow Rate	40 ml/min
Initial Carrier Flow Time	5 mins
Second Carrier Flow Time	3 mins
Trap 1 to Trap 2 Transfer Time	2 mins
Trap 1 Temperature	50 °C to 250 °C
Trap2 to GC Column Transfer Time	64 min
Trap 2 Temperature	50 °C to 250 °C

allow sample transfer to the GC column. The MS ChemStation program should be run before this.

I. Certify that the temperature of" trap 1" and "trap 2" are less than 50 °C before starting the second run.

J. When the analysis is complete (or the tube chamber cools to 50 °C or less) the sorbent tube may be removed. Install an empty tube in the tube chamber.

K. Turn the desorber switch on the concentrator to the "off" position.

III RESULTS AND DISCUSSION

III.1 Result of Pre-test

Prior to the experiment, the deactivation of the catalyst, the purity of methyl acetate reagent solution and the air purity were examined. The results of these operations are included in the following paragraphs.

Deactivation of Catalyst

Prior to the experiment, tests were performed to determine whether or not catalyst deactivation was significant. The two monolithic catalysts, P-type and E-type, were continuously exposed to a dry air stream containing 2000 ppmV methyl acetate at 390 °C for 85 hours and 74 hours, respectively. During this time, the conversion of methyl acetate was monitored. Results are presented in Figures 9 and 10. The conversion of MA was 100 % at all times. This suggests the two monolithic catalysts did not lose their activity for at least 74 hours. Thus, the catalyst used in obtaining the Taguchi experimental data was exposed to the oxidation of methyl acetate for less than 74 hours. If it took more than 74 hours, the catalyst was replaced or regenerated with hydrogen.

Methyl Acetate Purity Test

Prior to the experiment, the MA was tested to assure no byproducts or other contamination. After the methyl acetate tank was filled with liquid MA, the samples of MA liquid were then taken from the tank and bottled as shown in Figure 6. The head space vapor of the MA was injected into the concentrator/GC/MS system, which was used to identify byproducts. The results of Figure 11 suggest that only one peak (MA) is obtained, and no other compound exists. This indicates no contamination in the MA. It proves that the collected samples during the MA oxidation reaction process were free of contamination by this MA reagent solution.

Air Blank Run Test

The air blank run was tested to determine whether or not the breathing air contained any unwanted by-product. The sampling lines were wrapped with heating tape (50°C) to prevent any condensation of byproducts. The breathing air taken from the isothermal sampling line was collected into a sampling glass bottle between the preheater and the reactor. This air sample was then injected to the GC/MS for impurity analysis. The result is shown in Figure 12. The half-peak in Figure 12 is thought to be water from water vapor within the empty sorbent tubing. To prevent this water from interfering with the results and damaging the GC/MS, the solvent delay was set to 2.4 minutes. Because of the setting of the solvent delay, half the water peak was always shown and should be neglected. These results suggest that the breathing air and the sampling line were free of contamination. Before samples were collected, the breathing air was flushed through the sampling lines for 10 minutes to remove any contamination in the sampling lines.

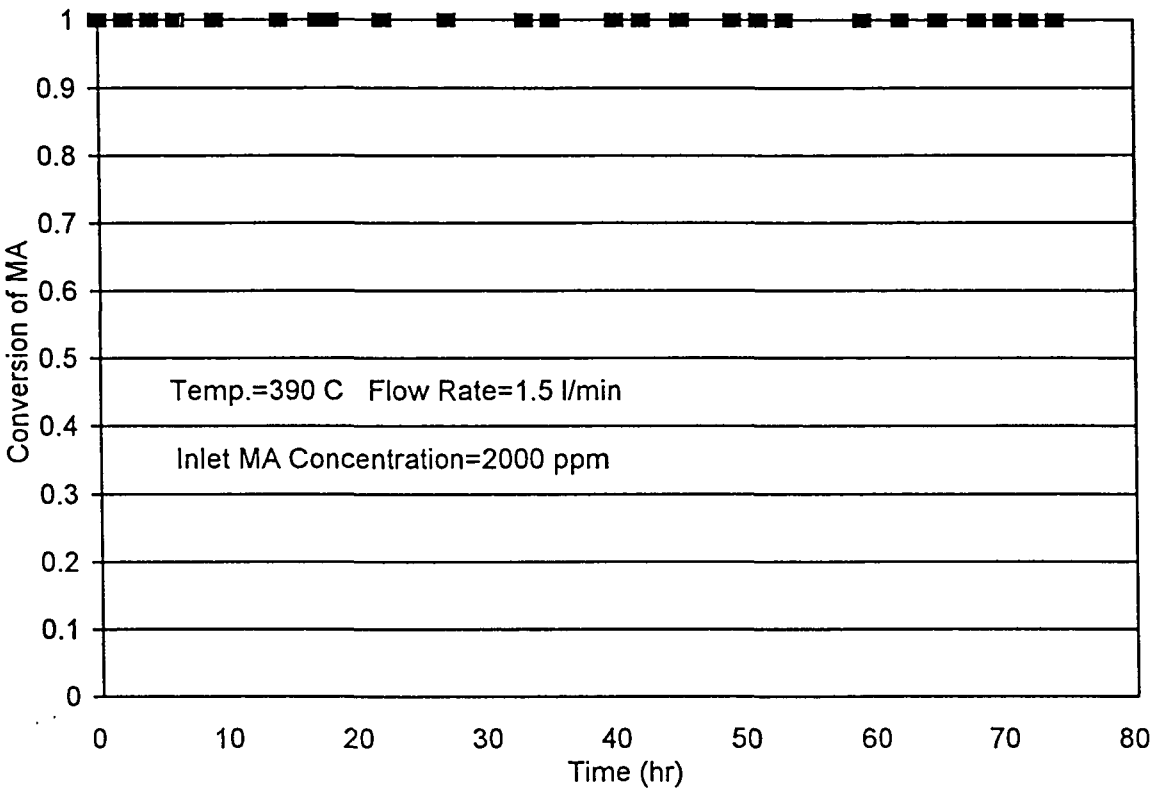

Figure 9

The Deactivation of P-type Monolithic Catalyst

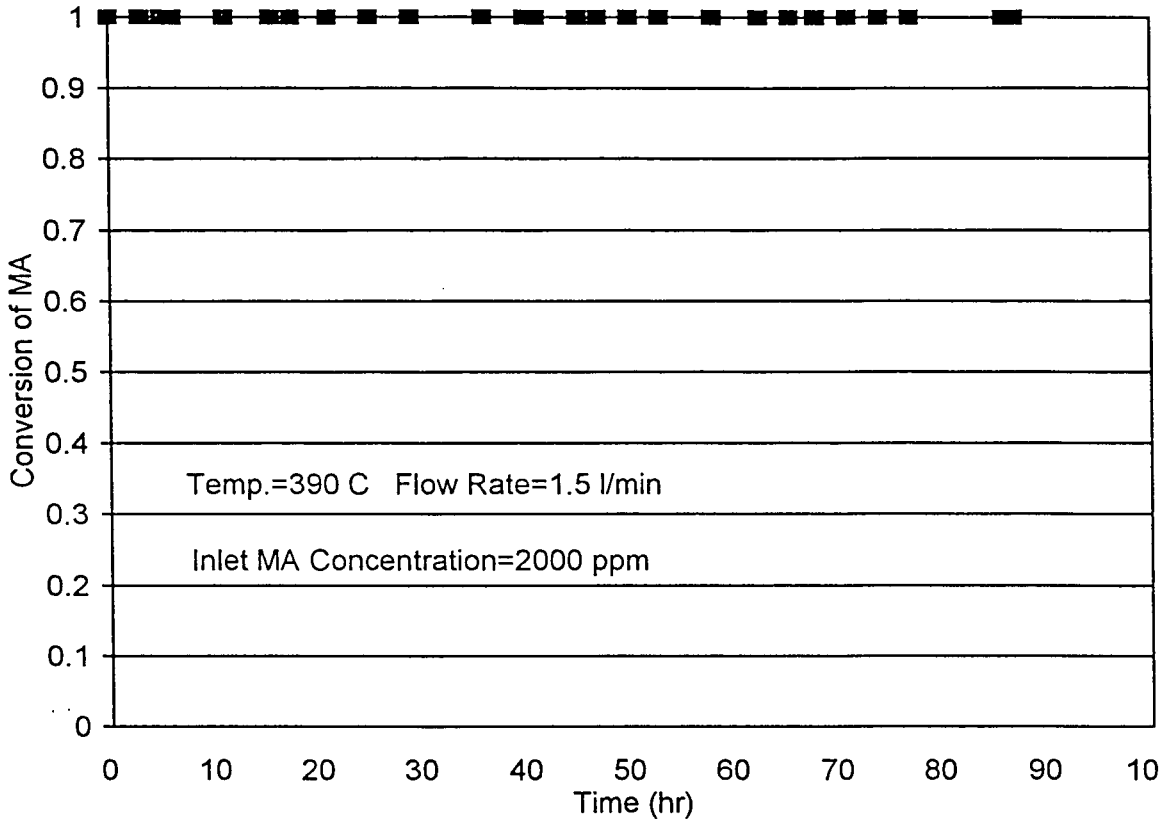

Figure 10

The Deactivation of E-type Monolithic Catalyst

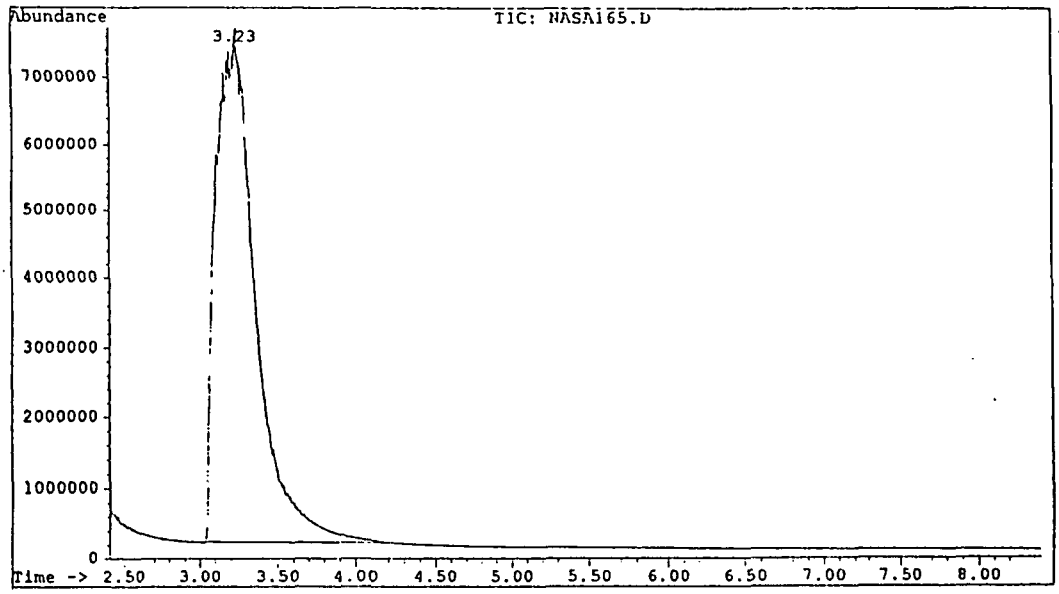

Figure 11 Results of MA Purity Test

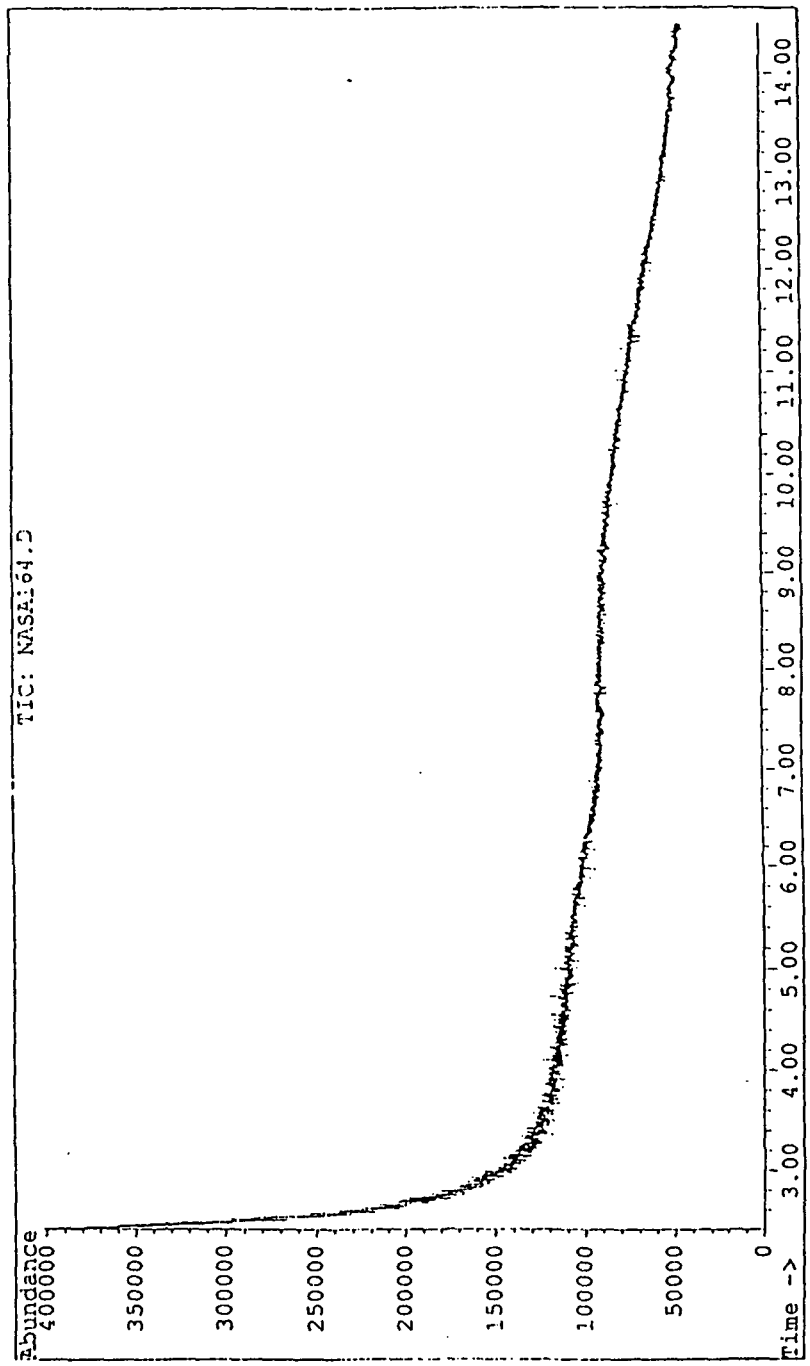

Figure 12 Results of Air Blank Test

III.2 Kinetic Study of Methyl Acetate Oxidation through Monolithic Catalytic Reactor

The mechanism of the oxidation reaction of methyl acetate is complex and can best be explained by breaking it up into several steps. The overall stoichiometric equation may be expressed as:

$$CH_3COOCH_3 + 3.5\ O_2 \rightarrow 3CO_2 + 3H_2O$$

If the adsorption step is not controlling or is not involved, the rate law may be represented as

$$rate = k\ [C_{MA}]^n \tag{3}$$

where n is the reaction order, i.e.
n = 1 for first order
n = 0 for zero order reaction
and C_{MA} = molal concentration, mole/L.

If the adsorption step is involved, the rate law may be written as

$$rate = k\ \frac{C_{MA}}{1 + K_a\ C_{MA}} \tag{4}$$

where K_a is the adsorption equilibrium constant in L/mole.

Conversion of Methyl Acetate

In order to analyze the data for an experimental integral reactor, the following conditions should be satisfied:

1. There should be no channeling or bypassing.
2. The conversion of MA should be reasonably high.
3. Catalyst should not decay during the time the conversion is in process.

The above conditions were satisfied for the reactor used in this experiment. Even though the reaction was exothermic, there may not be significant axial and radial temperature gradients. This is due to the low concentration of methyl acetate used in this experiment. Hence, the assumption of an isothermal nature of the reaction was used during data analysis.

For an integral reactor, the kinetic equation is

$$\frac{W}{F_{MA0}} = \int_0^X \frac{dx}{(-r)} \tag{5}$$

where W = mass of the catalyst, gram

F_{MA0} = Initial flow rate of methyl acetate in Moles/Sec
X = Conversion of methyl acetate, and
r = rate of disappearance of methyl acetate.

For the pellet catalyst, the mass of solid catalyst is of paramount importance to the rate of reaction. However, with the monolithic catalyst, the contact area between reactants and catalyst is the most important factor. Hence the following design equation was used for data analysis in this experiment.

$$\frac{A}{F_{MA0}} = \int_0^X \frac{dx}{(-r)} \tag{6}$$

where A = area of contact of monolithic cells, cm^2 and
r = rate in mole/(cm^2 sec)

Thus for a reactor of constant volume, conversion is a function of molar flow rate.

In summary, the following assumptions are made for analysis of the kinetic data:
1. Plug flow pattern (Reynolds number 9.8)
2. Uniform temperature profile in radial and axial directions
3. Constant activity of the catalyst, and
4. Negligible wall effect.

The feed concentrations of methyl acetate at different temperatures are tabulated in Table 8.

Data Analysis by Linear Regression

The kinetic data were regressed for the rate equations of zero-order, first-order and Langmuir-Hinshelwood models.

1. For the zero-order reaction model (n=0), by combining Equations (3) and (6), the following equation is obtained:

$$\frac{A}{F_{MA0}} = \frac{1}{k} X \tag{7}$$

2) For the first-order reaction model (n=1), again by combining Equations (3) and (6), a semi-logarithemic equation is obtained.

$$\frac{A}{F_{MA^\circ}} = -\frac{1}{k\, C_{MA^\circ}} \ln(1-X) \tag{8}$$

Table 8. Summary of Reaction Parameters

Catalyst	Temperature (°C)	Feed Concentration of MA(ppm)
P-type Monolithic Catalyst Diameter is 0.0827 inch; Length is three inches	271	1225
	280	1225
	285	310
	300	1400
	310	550
	320	825
	330	710

3) For the Langmuir-Hinshelwood model, obtained by combining Equations (4) and (6), the result is:

$$\frac{A}{F_{MA0}} = -\frac{1}{k\,C_{MA0}} \ln(1-X) + \frac{K_a}{k} X \qquad (9)$$

where C_{MA0} is the inlet molar concentration of methyl acetate to the reactor, moles/L.

In this experiment, the monolithic catalyst contained 135 cells and the total area(A) of these cells was 501.68 cm^2. The inlet concentration of MA was determined from GC analysis. The inlet flow rate was obtained with an electronic mass flow meter. Similarly, the exit concentration of MA was also measured by GC analysis. Conversion of methyl acetate was calculated by using inlet and outlet concentrations of methyl acetate. F_{MA0} (the inlet molar flow rate of methyl acetate, moles/sec) was calculated by multiplying inlet concentration (C_{MA0}) and the volumetric flow rate of the stream entering the reactor at room temperature. Retention time was calculated by dividing the total volume of monolithic cells by the volumetric flow rate. After

calculating the values of C_{MAO}, F_{MA0}, A, and X; these values were used in Equations (7), (8), and (9) for regressions of the zero-order, first-order, and the Langmuir-Hinshelwood models for model selection. The conversion of methyl acetate versus A/F_{MA0} at different temperatures is shown in Figures 13 through 29.

Model Selection

During the data analysis, the concentration of oxygen was assumed constant because the consumption of oxygen is less than 0.53%(based on 1400 ppm of MA). The amount of water produced was also negligible, since it is also less than 0.5%.

After rate laws were selected, kinetic data were used to estimate parameters at each temperature. Linear regression was applied by using Equations (7), (8), and (9) to estimate parameters k and K_a. The results are tabulated in Tables 9 through 14.

Zero-Order Model

For egression of the zero-order rate equation, experimental data of A/F_{MA0} (independent) and conversion X (dependent) were computed and fitted to Equation (7). The linear regression can be performed with an intercept, i.e. $y = mx + c$, or through the original point, i.e. $y = mx$. Table 9 shows the results of regression through an intercept while Table 10 indicates the results of regression through the original point. Comparing the two tables, it is concluded that the regression with an intercept is preferred (R^2 is closer to one) over that through the original point. Thus the linear regression with an intercept was used in the calculation of rate constants. Values of rate constant from Table 9 are used to compute the model-predicted conversion. A comparison of the predicted model conversion with the experimental conversion of methyl acetate as a function of A/F_{MA0} is shown in Figures 13 through 19.

First-Order Model

For regression of the First-order rate equation, experimental data of A/F_{MA0} and $-Ln(1-X)/C_{MA0}$ were computed and fitted to Equation (8). Again, the linear regression can be performed either with an intercept, i.e. $y = mx + c$, or through the original point, i.e., $y = mx$. The reason for using an intercept is the same as before. The results are tabulated in Tables 11 and 12. Values of rate constant from Table 11 are used to calculate the model predicted conversion. The graphs showing the comparison of the predicted model conversion with the experimental conversion of methyl acetate as a function of A/F_{MA0} are shown in Figures 20 through 26.

Langmuir-Hinshelwood Model

For regression with the Langmuir-Hinshelwood Model, experimental data of A/F_{MA0}, and two independent factors, i.e. $-Ln(1-X)/C_{MA0}$ and X, were computed and fitted to Equation 10. The linear regression was performed using an intercept, i.e., $y = mx + c$. Table 13 shows the results of regression through the intercept. The results of the adsorption equilibrium constant are shown in Table 14. By using the values of k and K_a from the above tables, model conversion is calculated. A comparison of the experimental conversion of methyl acetate with the predicted model conversion as a function of A/F_{MA0}, is shown in Figures 27 through 29.

Zero-Order Model
Temperature = 271°C
[MA] = 1225 ppm

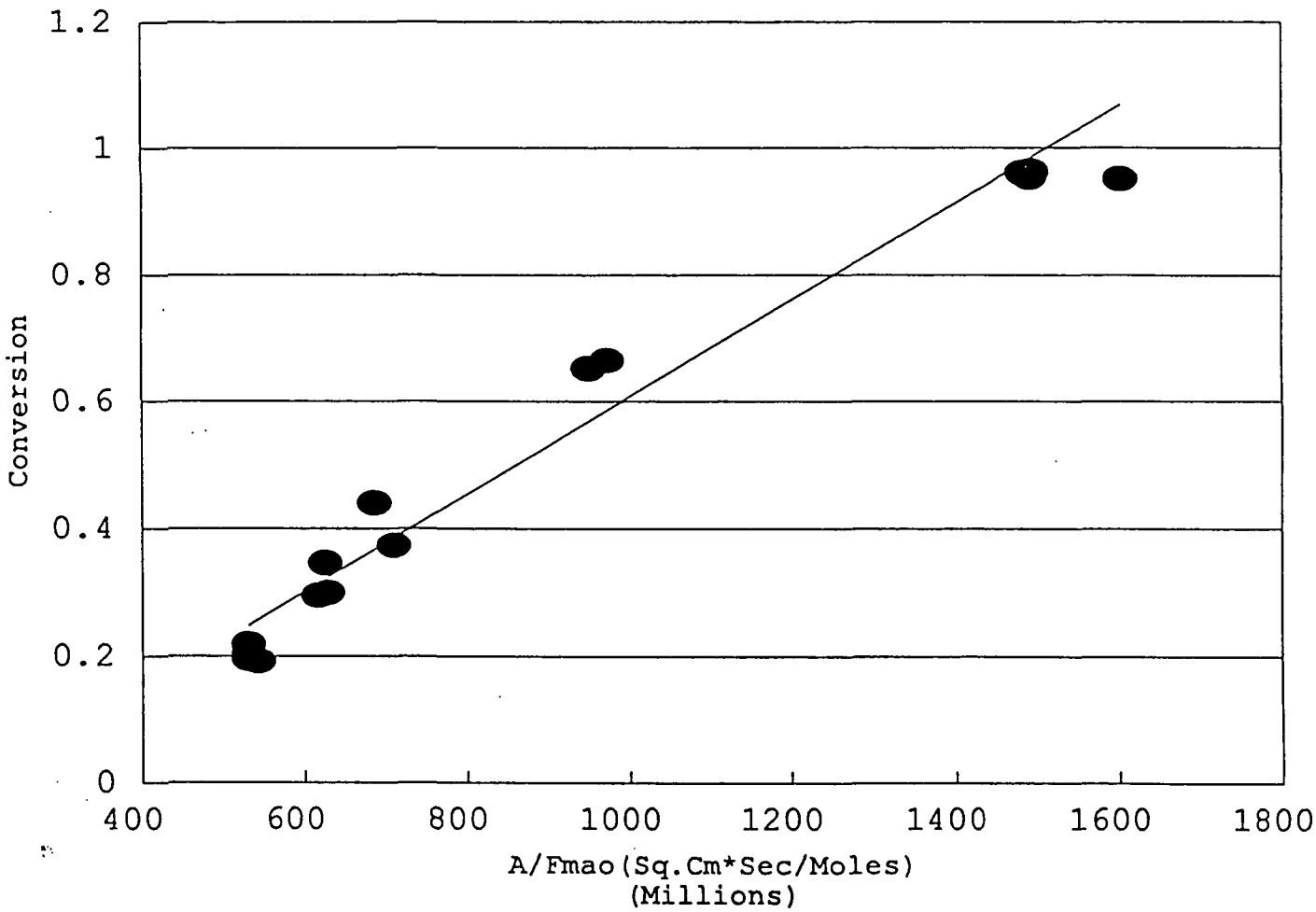

Figure 13. MA Conversion vs A/F_{MA0} at 271° C

Zero-Order Model
Temperature = 280°C
[MA] = 1225 ppm

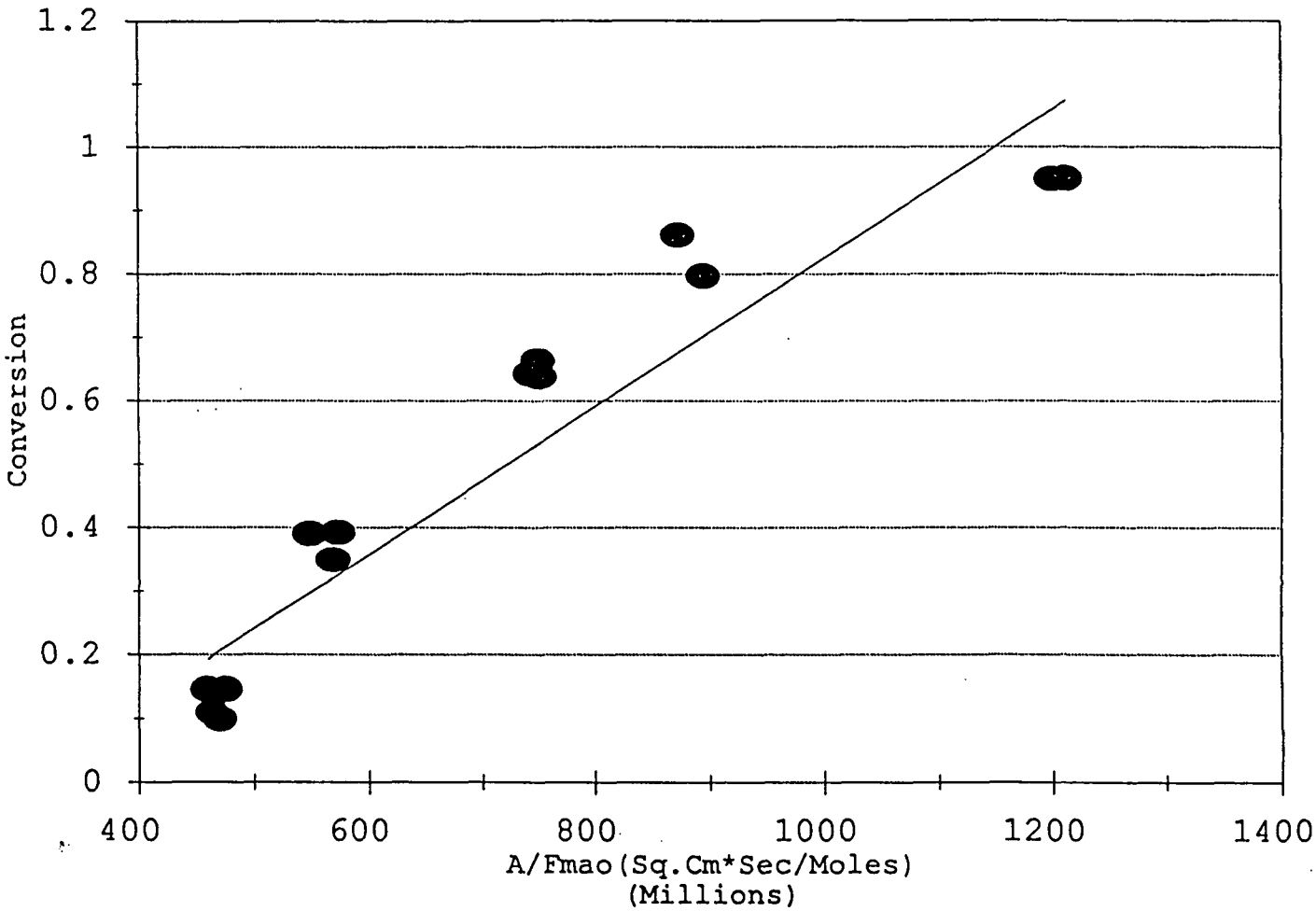

Figure 14. MA Conversion vs A/F_{MA0} at 280° C

Zero-Order Model
Temperature = 285°C
[MA] = 310 ppm

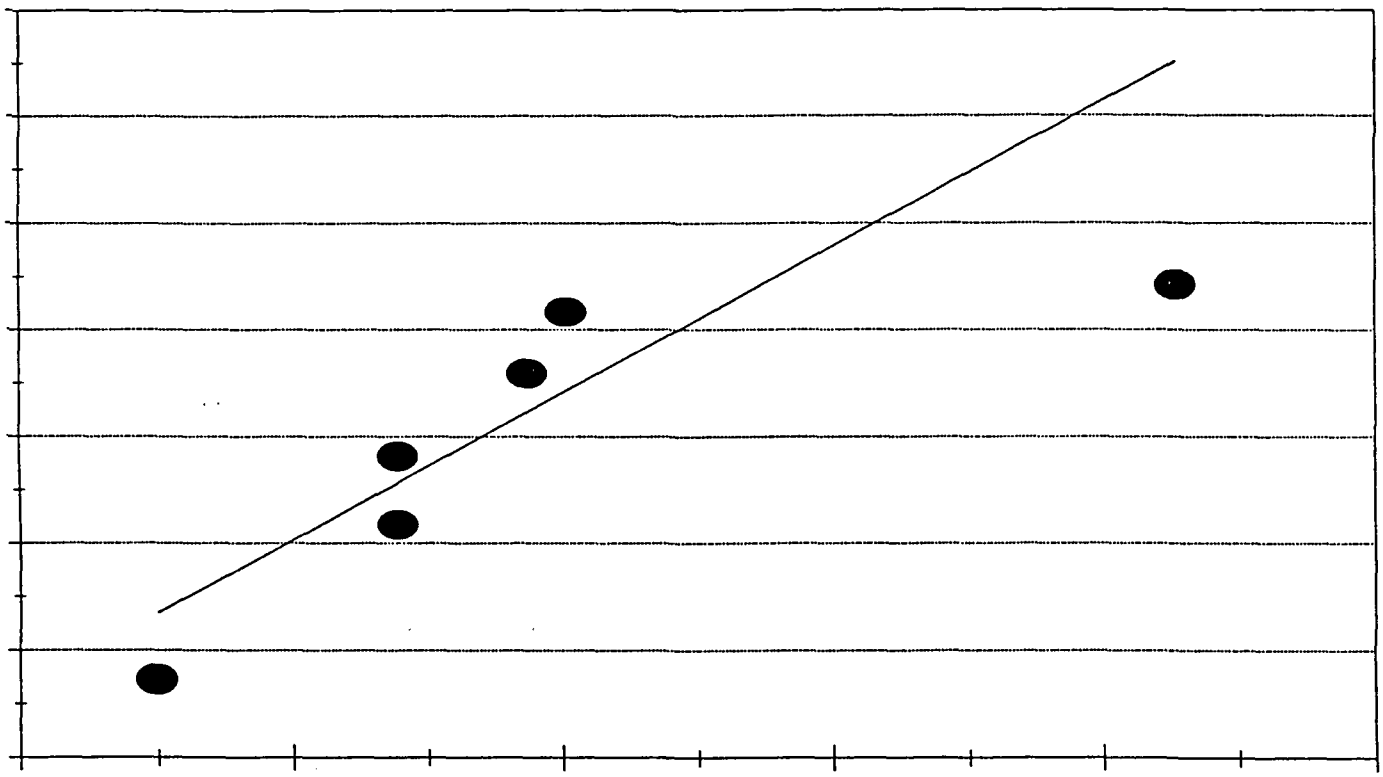

Figure 15. MA Conversion vs A/F_{MA0} at 285° C

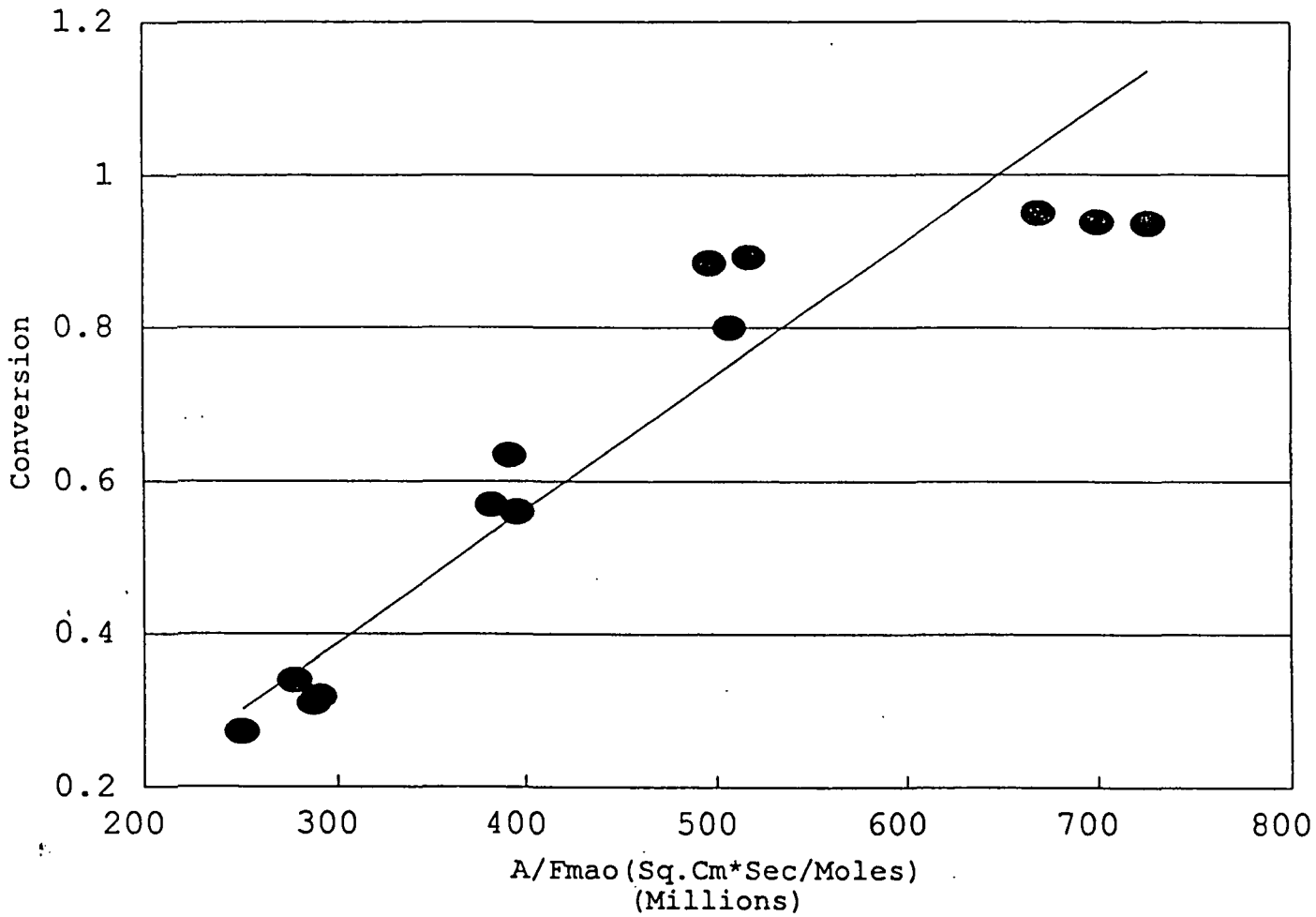

Figure 16. MA Conversion vs A/F_{MA0} at 300° C

Zero-Order Model
Temperature = 310°C
[MA] = 550 ppm

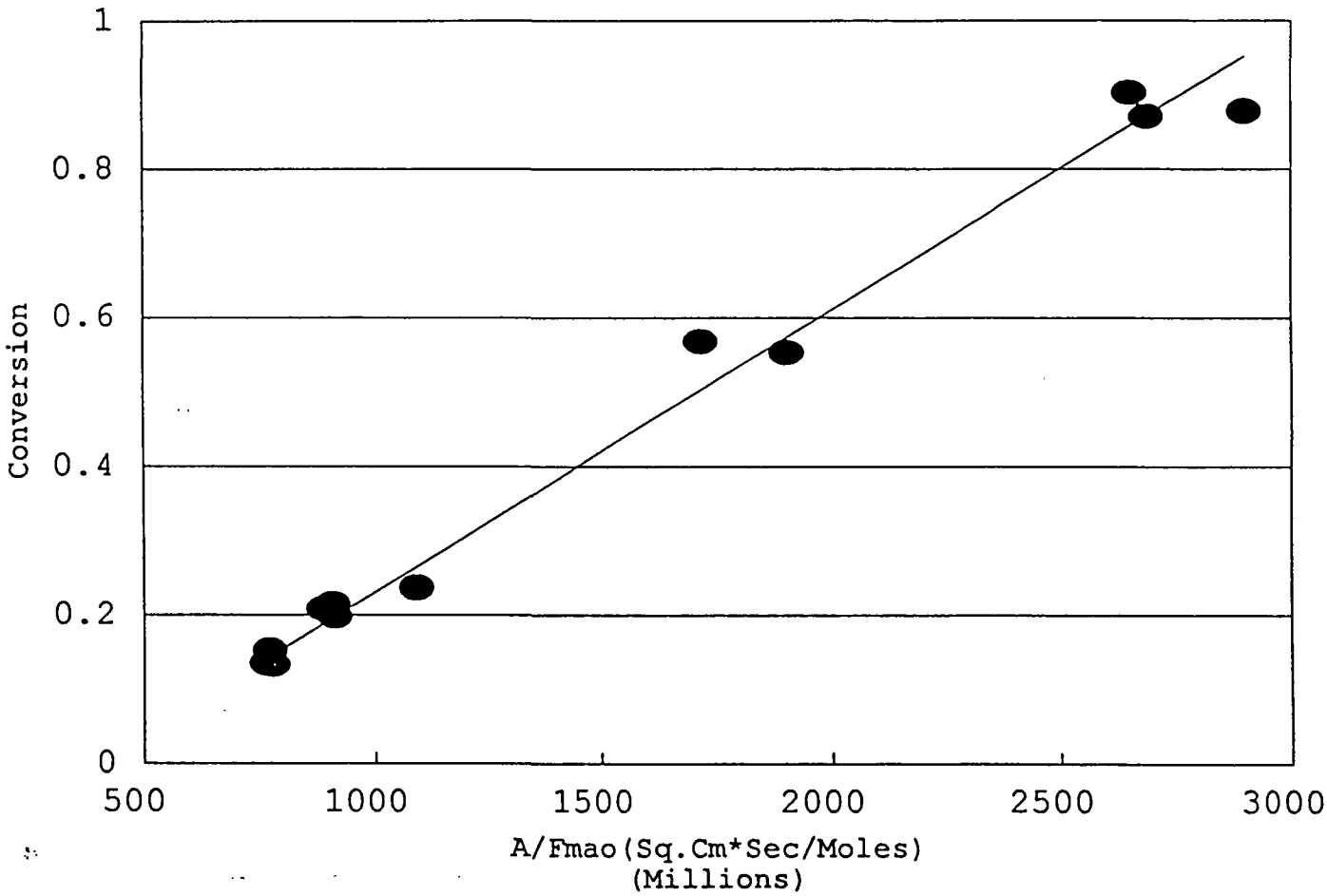

Figure 17. MA Conversion vs A/F_{MA0} at 310° C

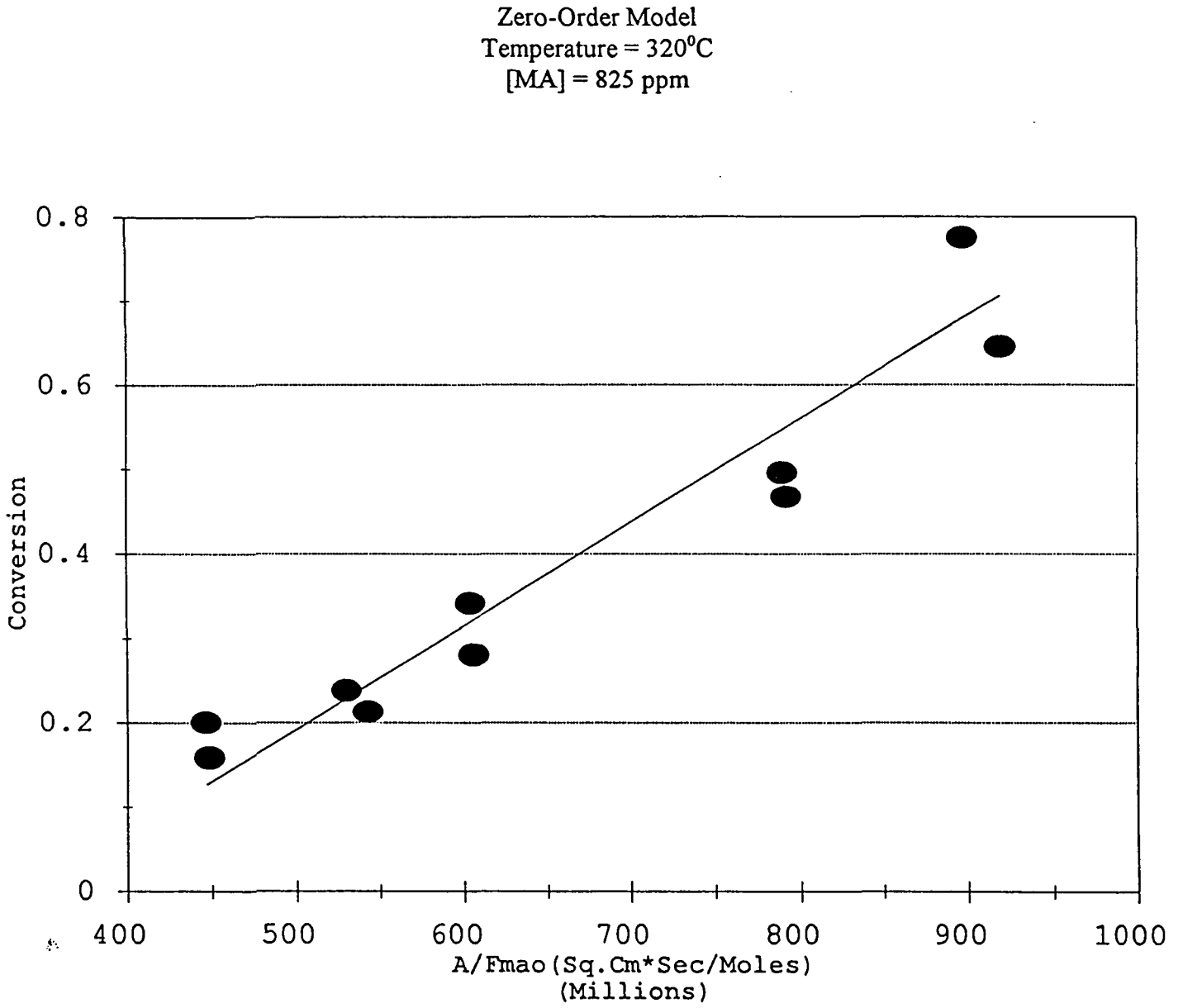

Figure 18. MA Conversion vs A/F_{MA0} at 320° C

Zero-Order Model
Temperature = 330°C
[MA] = 710 ppm

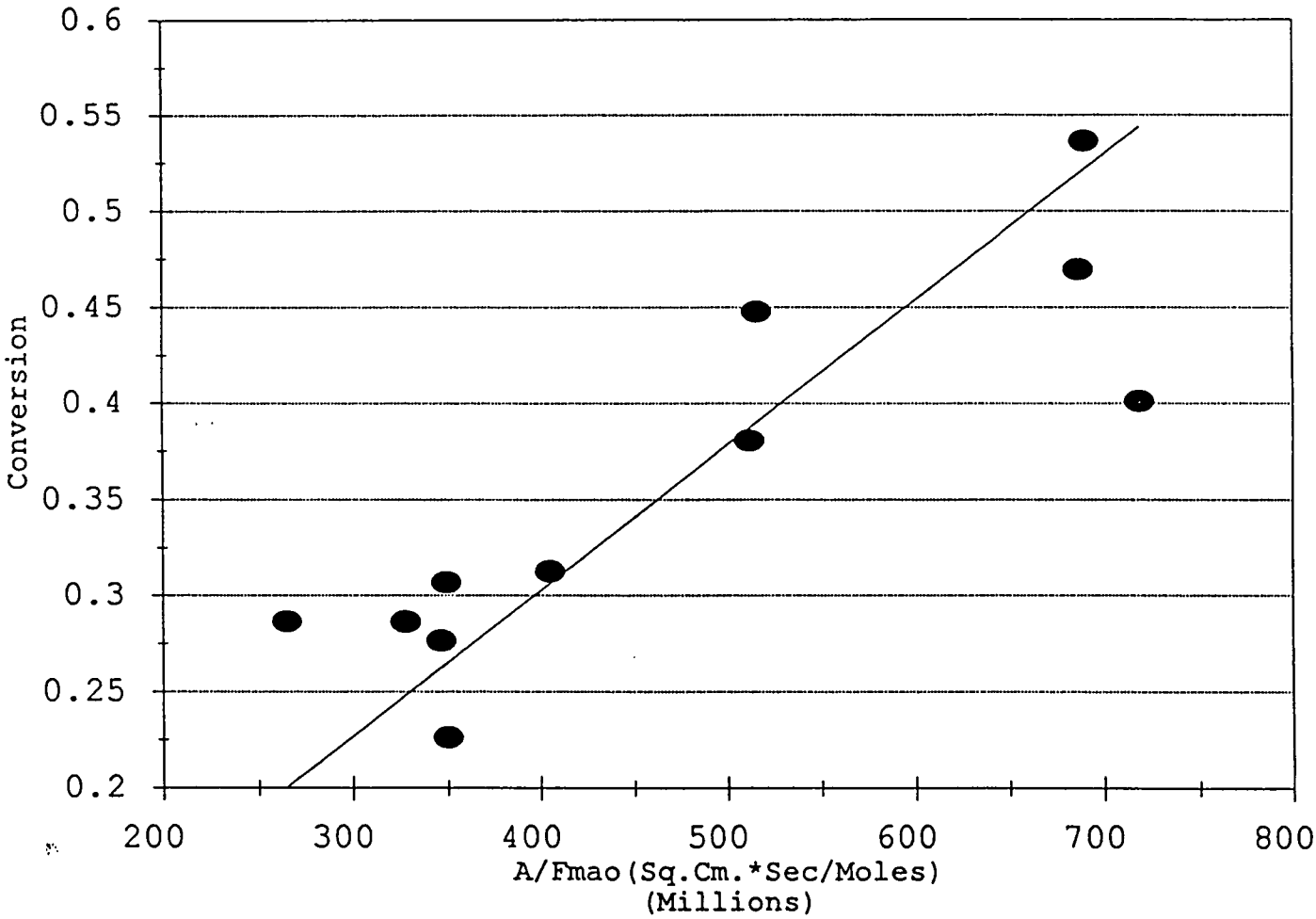

Figure 19. MA Conversion vs A/F_{MA0} at 330° C

First-Order Model
Temperature = 271°C
[MA] = 1225 ppm

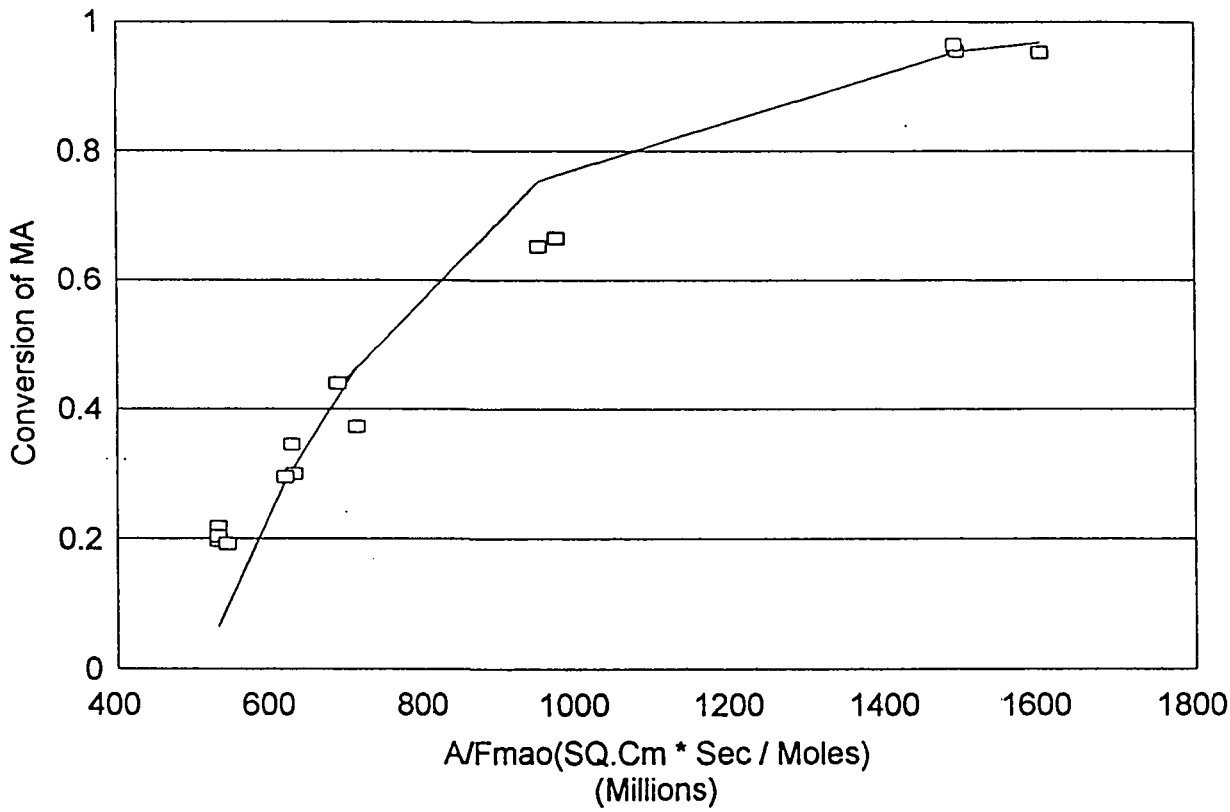

Figure 20. Conversion vs A/F_{MA0} at 271° C

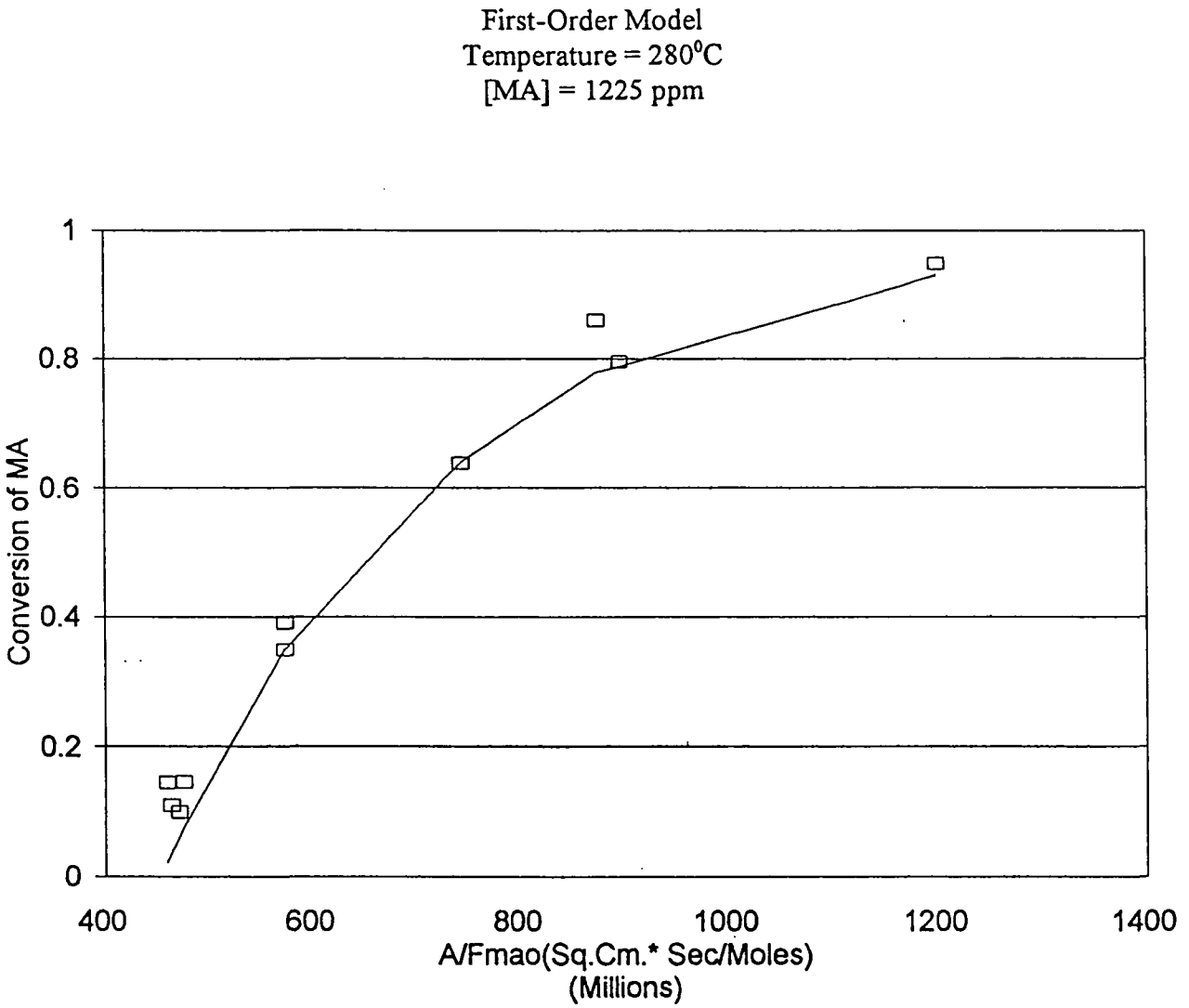

Figure 21. Conversion vs A/F_{MA0} at 280° C

First-Order Model
Temperature = 285°C
[MA] = 310 ppm

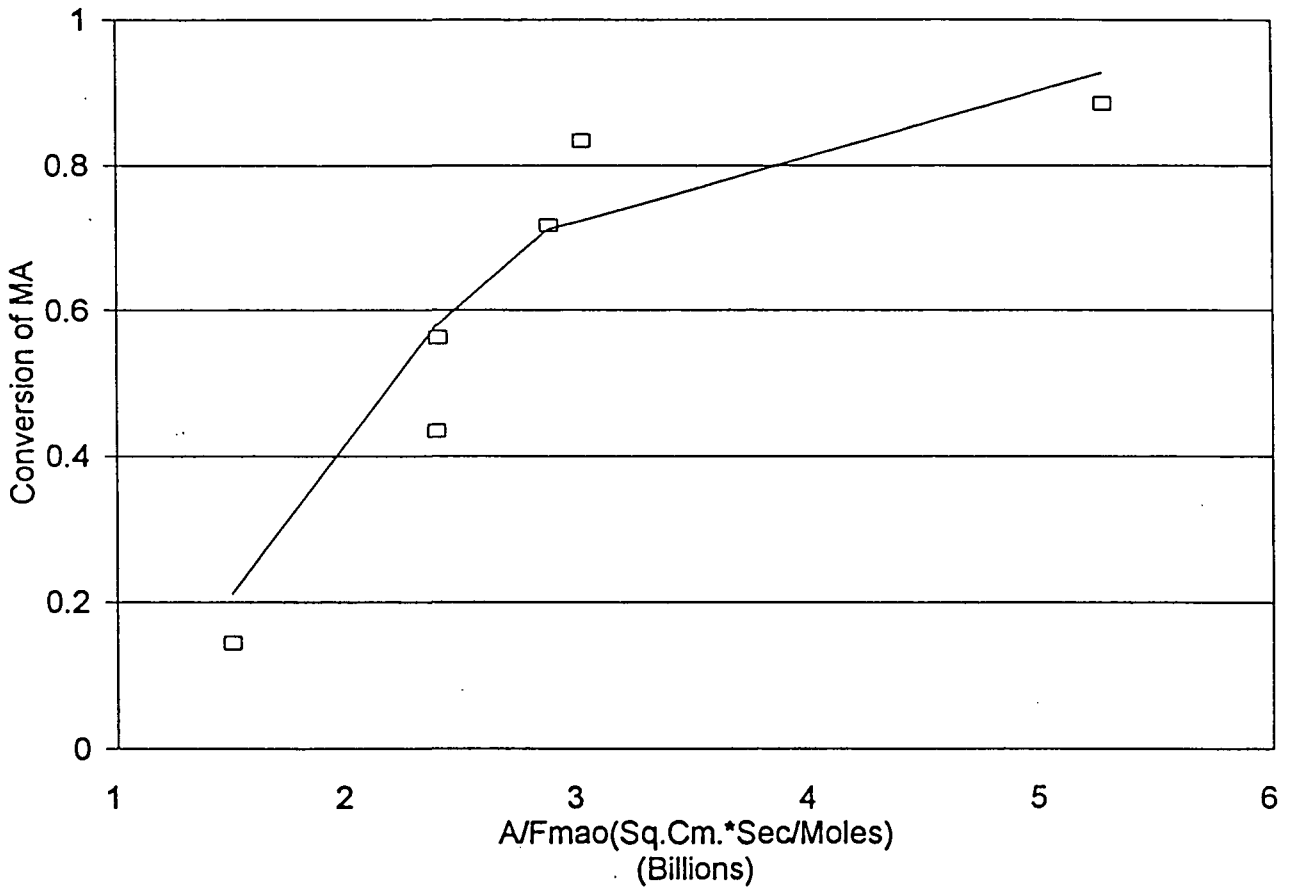

Figure 22. Conversion vs A/F_{MA0} at 285° C

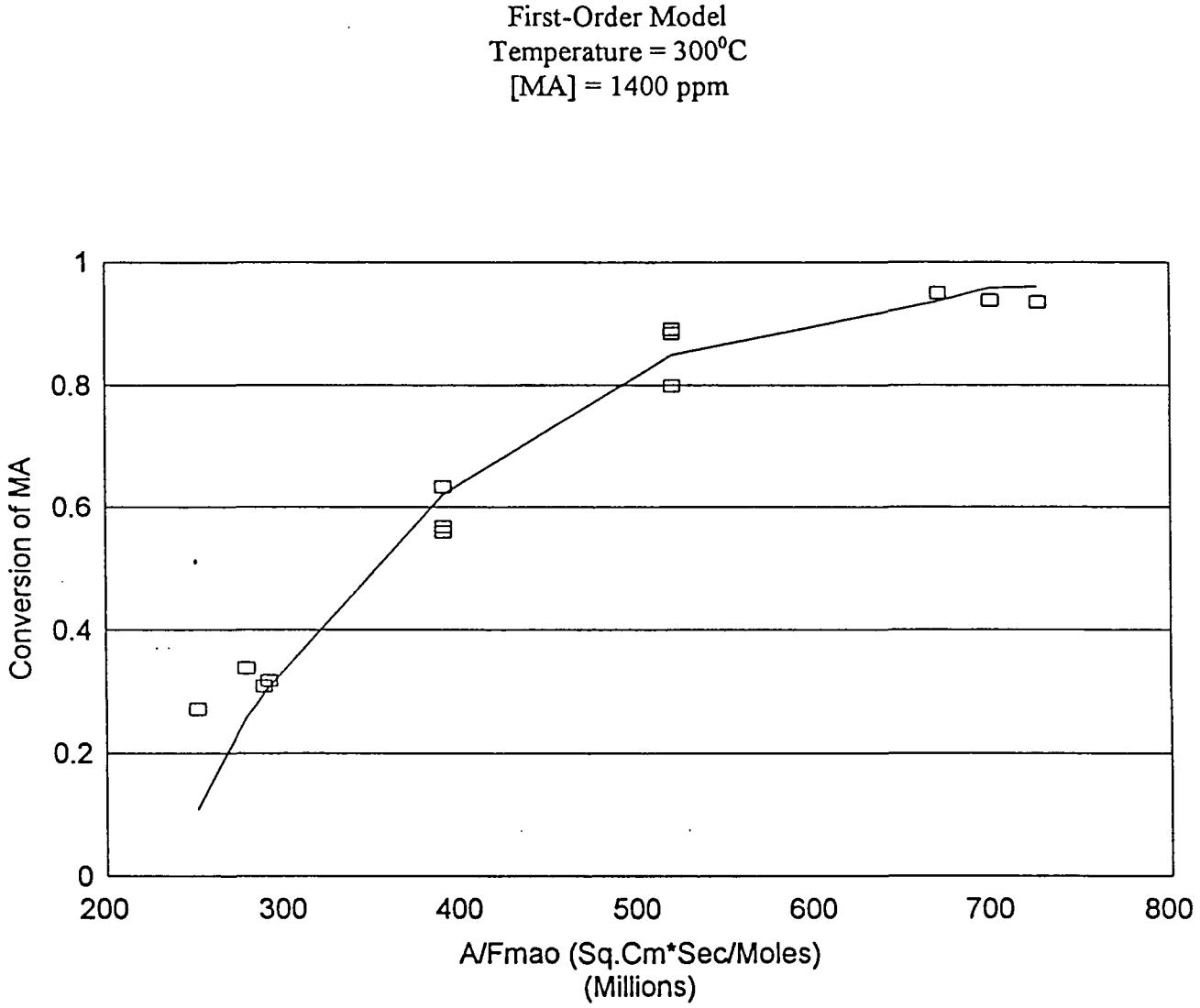

Figure 23. Conversion vs A/F_{MA0} at 300° C

First-Order Model
Temperature = 310°C
[MA] = 550 ppm

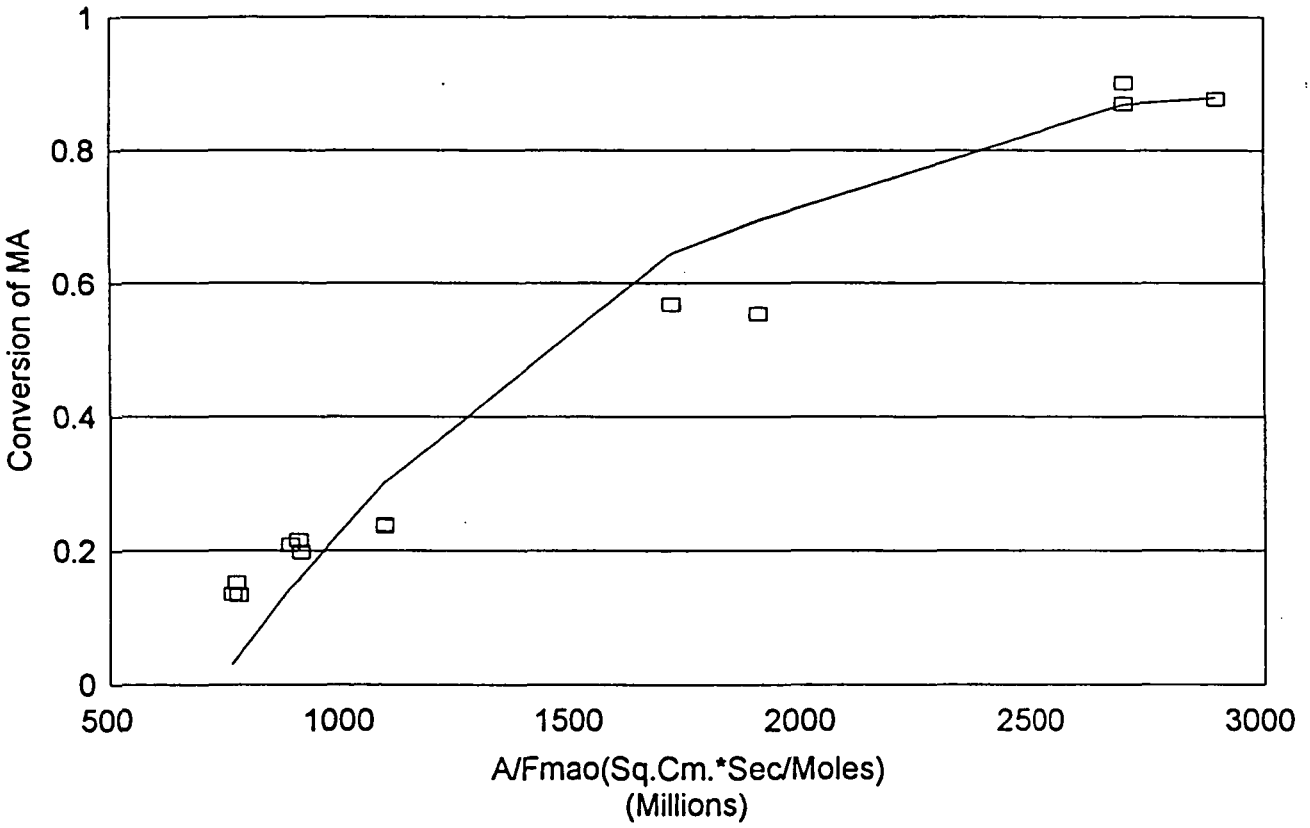

Figure 24. Conversion vs A/F_{MA0} at 310° C

First-Order Model
Temperature = 320°C
[MA] = 825 ppm

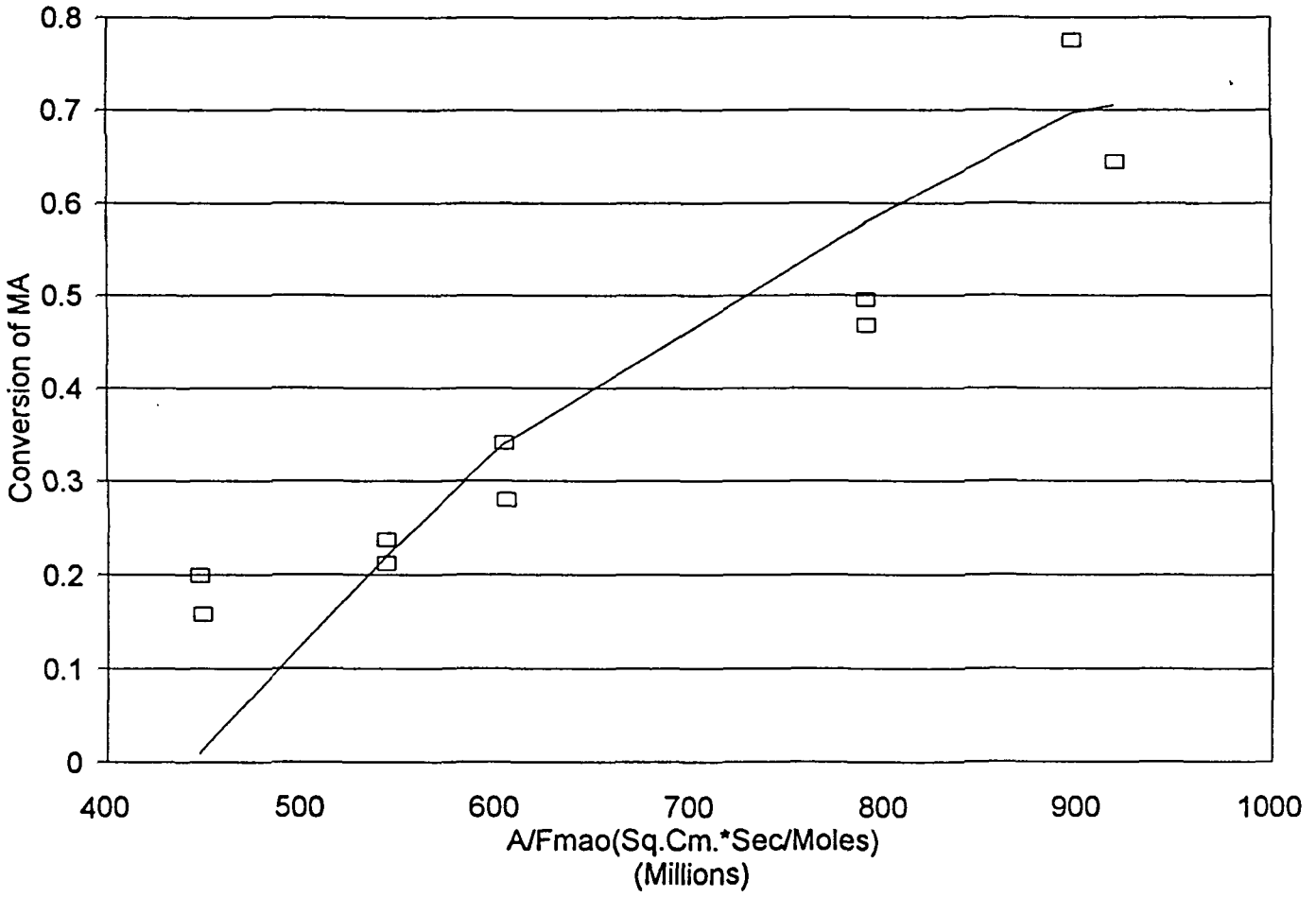

Figure 25. Conversion vs A/F_{MA0} at 320° C

First-Order Model
Temperature = 330°C
[MA] = 710 ppm

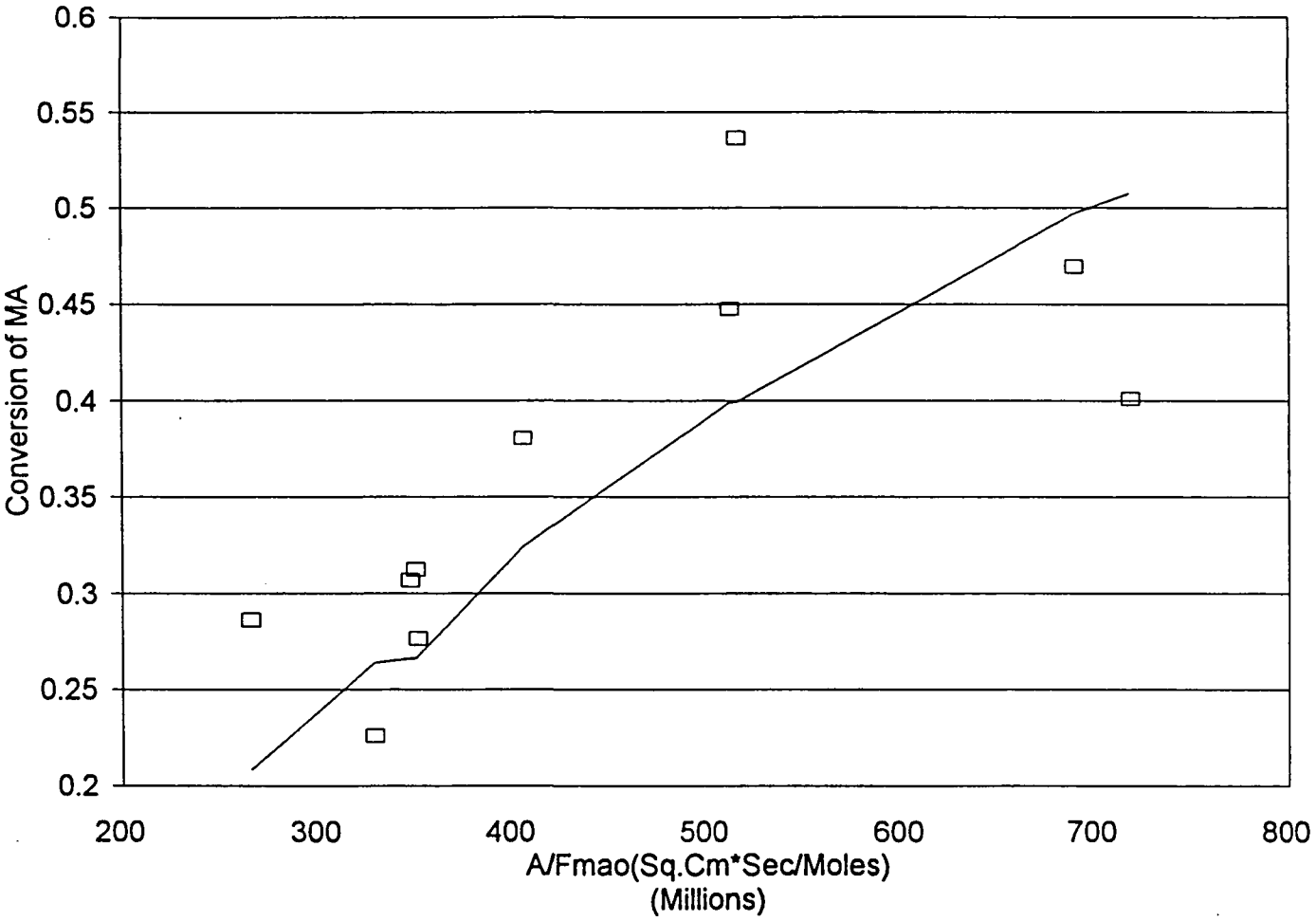

Figure 26. Conversion vs A/F_{MA0} at 330° C

Langmuir-Hinshelwood Model
Temperature = 271°C
[MA] = 1225 ppm

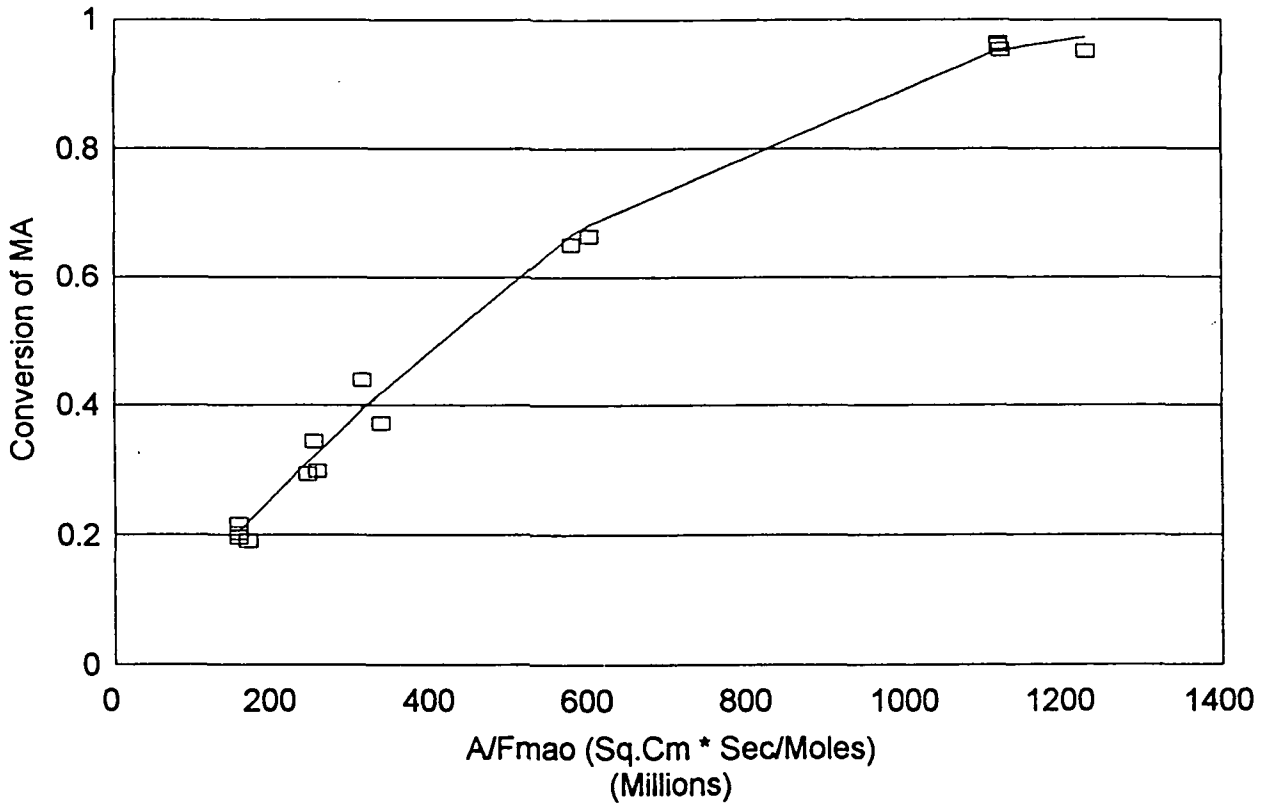

Figure 27. Conversion vs A/F_{MA0} at 271° C

Langmuir-Hinshelwood Model
Temperature = 280°C
[MA] = 1225 ppm

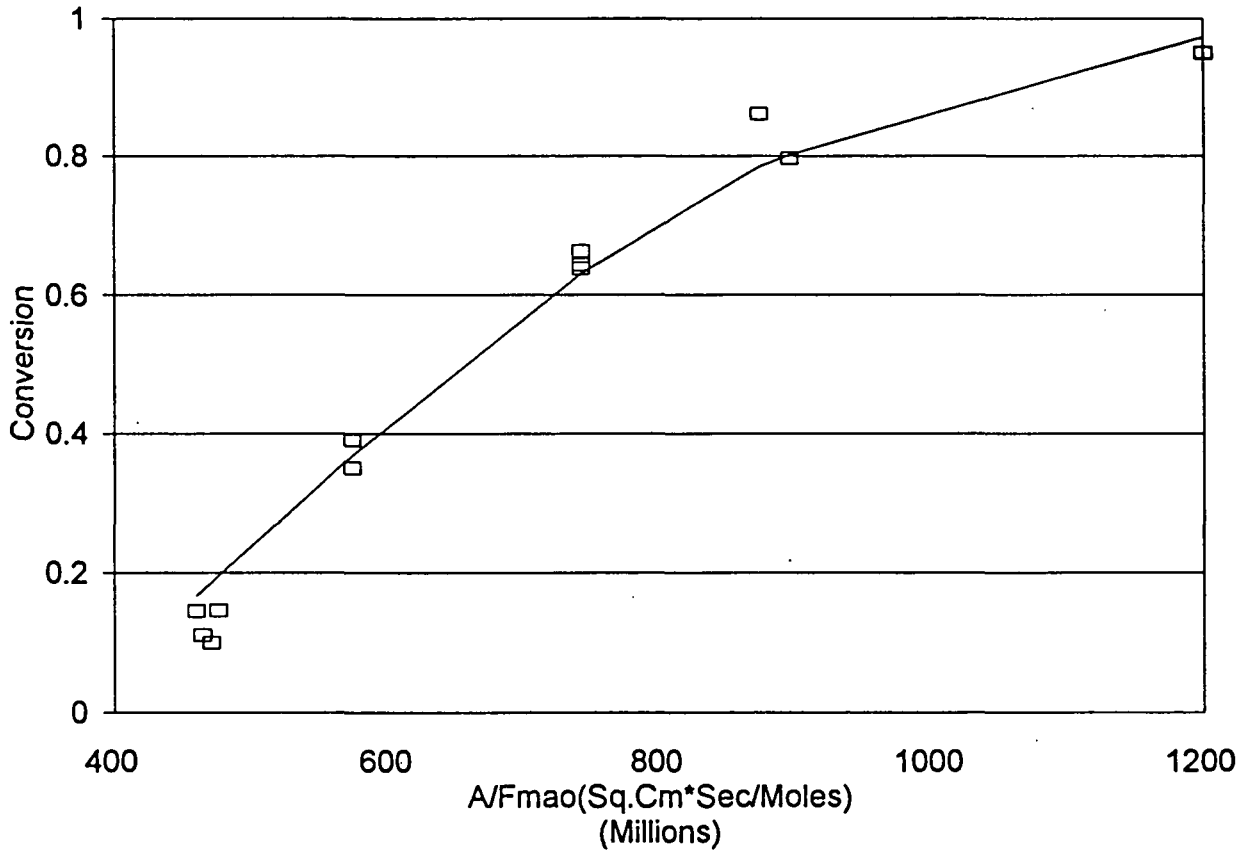

Figure 28. Conversion vs A/F_{MA0} at 280° C

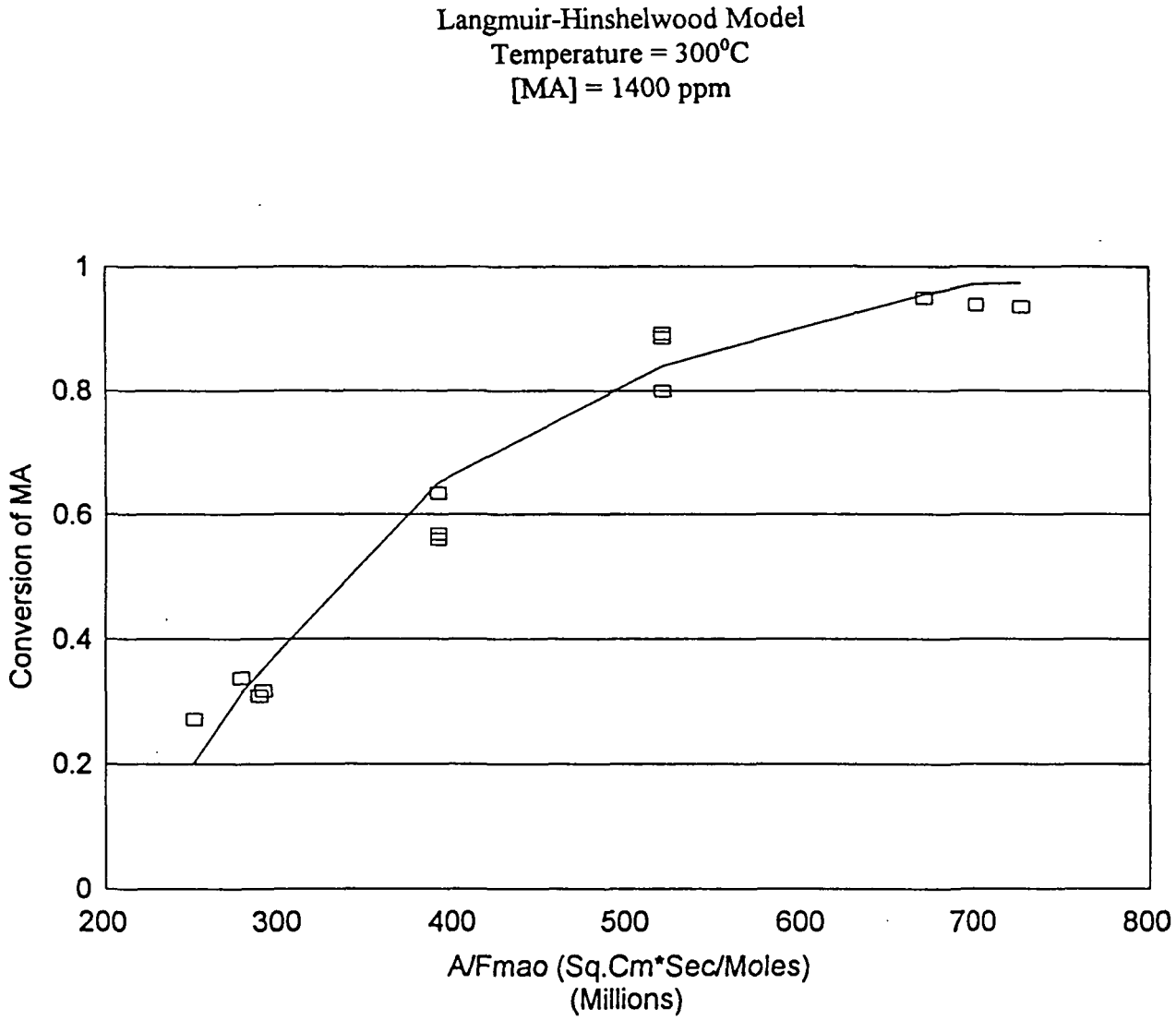

Figure 29. Conversion vs A/F_{MA0} at 300° C

Table 9.
Rate constants for Zero-Order Reaction

(Regression through an intercept)

Temperature (^{0}C)	Rate constant moles/(sec.cm^2)	R^2	Standard Error
*271	$7.644 \pm 0.43 \times 10^{-10}$	0.95	4.0×10^{-11}
*280	$1.166 \pm 1.3 \times 10^{-10}$	0.84	1.3×10^{-10}
285	$2.738 \pm 0.74 \times 10^{-10}$	0.72	7.5×10^{-11}
*300	$1.755 \pm 0.19 \times 10^{-9}$	0.87	1.9×10^{-10}
310	$3.805 \pm 0.13 \times 10^{-10}$	0.98	1.3×10^{-11}
320	$1.226 \pm 0.12 \times 10^{-9}$	0.92	1.2×10^{-10}
330	$7.565 \pm 0.38 \times 10^{-10}$	0.76	3.8×10^{-11}

*These experimental runs were performed after regeneration of the catalyst.

Table 10.

Rate constants for Zero-Order Reaction

(Regression computed through zero)

Temperature (^{0}C)	Rate Constant Moles/(sec.cm^2)	R^2	Standard Error
*271	6.176×10^{-10}	0.88	2.1×10^{-11}
*280	7.8×10^{-10}	0.58	4.4×10^{-11}
285	2.145×10^{-10}	0.69	2.1×10^{-11}
*300	1.464×10^{-9}	0.84	5.3×10^{-11}
310	3.06×10^{-10}	0.89	1.31×10^{-11}
320	6.565×10^{-9}	0.05	5.4×10^{-11}
330	7.565×10^{-10}	0.76	3.82×10^{-11}

*These experimental runs were performed after regeneration of the catalyst.

Table 11.

Rate constants for First-Order Reaction

(Regression computed through an intercept)

Temperature (°C)	Rate Constant L/(sec.cm^2 of catalyst)	R^2	Standard Error
*271	$6.322 \pm 0.26 \times 10^{-5}$	0.97	2.7×10^{-6}
*280	$7.202 \pm 0.76 \times 10^{-5}$	0.86	7.6×10^{-6}
285	$5.144 \pm 0.89 \times 10^{-5}$	0.87	8.9×10^{-6}
*300	$1.15 \pm 0.09 \times 10^{-4}$	0.93	9.0×10^{-6}
310	$4.496 \pm 0.26 \times 10^{-5}$	0.96	2.7×10^{-6}
320	$7.793 \pm 1.18 \times 10^{-5}$	0.84	1.2×10^{-6}
330	$3.943 \pm 0.72 \times 10^{-5}$	0.77	7.3×10^{-6}

*These experimental runs were performed after regeneration of the catalyst.

Table 12.

Rate constants for First-Order Reaction

(Regression computed through zero)

Temperature (^{0}C)	Rate Constant L/(sec.cm^2 of catalyst)	R^2	Standard Error
*271	3.88×10^{-5}	0.13	2.65×10^{-6}
*280	3.86×10^{-5}	0.22	7.61×10^{-6}
285	3.47×10^{-5}	0.59	8.92×10^{-6}
*300	6.75×10^{-5}	0.25	9.00×10^{-6}
310	3.055×10^{-5}	0.49	2.67×10^{-6}
320	3.295×10^{-5}	no good	1.18×10^{-5}
330	3.363×10^{-5}	0.75	7.25×10^{-6}

*These experimental runs were performed after regeneration of the catalyst.

Table 13.

Rate Constant k for Langmuir-Hinshelwood Model

Temperature (^{0}C)	Rate constant $L/cm^2_{Area\text{-}cat}.Sec$)	R^2	Standard Error
*271	$1.088 \pm 0.18 \times 10^{-4}$	0.988	1.9×10^{-5}
*280	$1.570 \pm 0.74 \times 10^{-4}$	0.876	7.5×10^{-5}
*300	$1.506 \pm 0.48 \times 10^{-4}$	0.933	4.9×10^{-5}

*These experimental runs were performed after regeneration of the catalyst.

Table 14.

Adsorption Equilibrium Constants for Langmuir-Hinshelwood Model

Temperature (^{0}C)	Adsorption Equilibrium Constant (L/mole)	R^2	Standard Error
*271	5.8528×10^4	0.988	2.81×10^4
*280	4.7229×10^4	0.876	8.56×10^4
*300	1.2442×10^4	0.933	3.72×10^5

*These experimental runs were performed after regeneration of the catalyst.

Discussion of Results

From an examination of Figures 13 through 19, it is seen that the zero-order model is not suitable for methyl acetate oxidation through the monolithic reactor. Tables 9 and 10 for this model indicate values of R^2 significantly different from unity.

On the other hand, the graphs of Figures 20 through 26 and the R^2 values of Tables 11 and 12 indicate that these data generally fit the first-order rate equation. For this case the R^2 values are near unity, and the model-predicted conversions are, in general, consistent with the experimental data.

For the Langmuir-Hinshelwood model, Figures 27 through 29, indicate that the experimental conversion, x, is very close to the model-predicted conversion, x_2. The values of R^2, as indicated in Table 13, are also close to 1. This is correct for inlet methyl acetate concentrations higher than 1200 ppm. At lower concentrations of methyl acetate, the regression results are unsatisfactory. Therefore in this region of lower concentration, the first-order model was used.

It is observed that the rate constant, k, increases with temperature while the adsorption equilibrium constant, K_a, decreases with an increase in temperature (Table 13 and Table 14). This result is quite reasonable, as at higher temperature there is less adsorption. All of the above results indicate that the data fit well into the Langmuir-Hinshelwood model at higher concentrations (> 1200 ppm) of methyl acetate.

Arrhenius Plot

The Arrhenius equation provides a relationship between rate constant and temterature. The equation is given below.

$$k(T) = Fe^{-E/RT} \tag{10}$$

where F = frequency factor, $L/(cm^2\ sec)$
E = activation energy, cal/mole, and
T = temperature in degrees kelvin.

For the first-order model, by using the rate constant k and the corresponding temperature, a frequency factor F and activation energy E are calculated. These are tabulated in Table 15 and also plotted in Figure 30.

Similarly, for the Langmuir-Hinshelwood model, the frequency factor F and activation energy E are calculated using temperature-dependent constants k and K_a constants, respectively. These results are tabulated in Table 16, and an Arrhenius plot is provided in Figure 31 for k, and in Figure 32 for K_d.

Table 15
Parameters for First order

First order
Rate equation rate = k C_{MA}
For rate constant
Frequency factor F = 12.17 L/(cm^2 X Sec) Activation energy = E = 13.186 kcal/mole R = 1.987 cal/mole.^{0}k

Arrhenius Plot for

First-Order Model

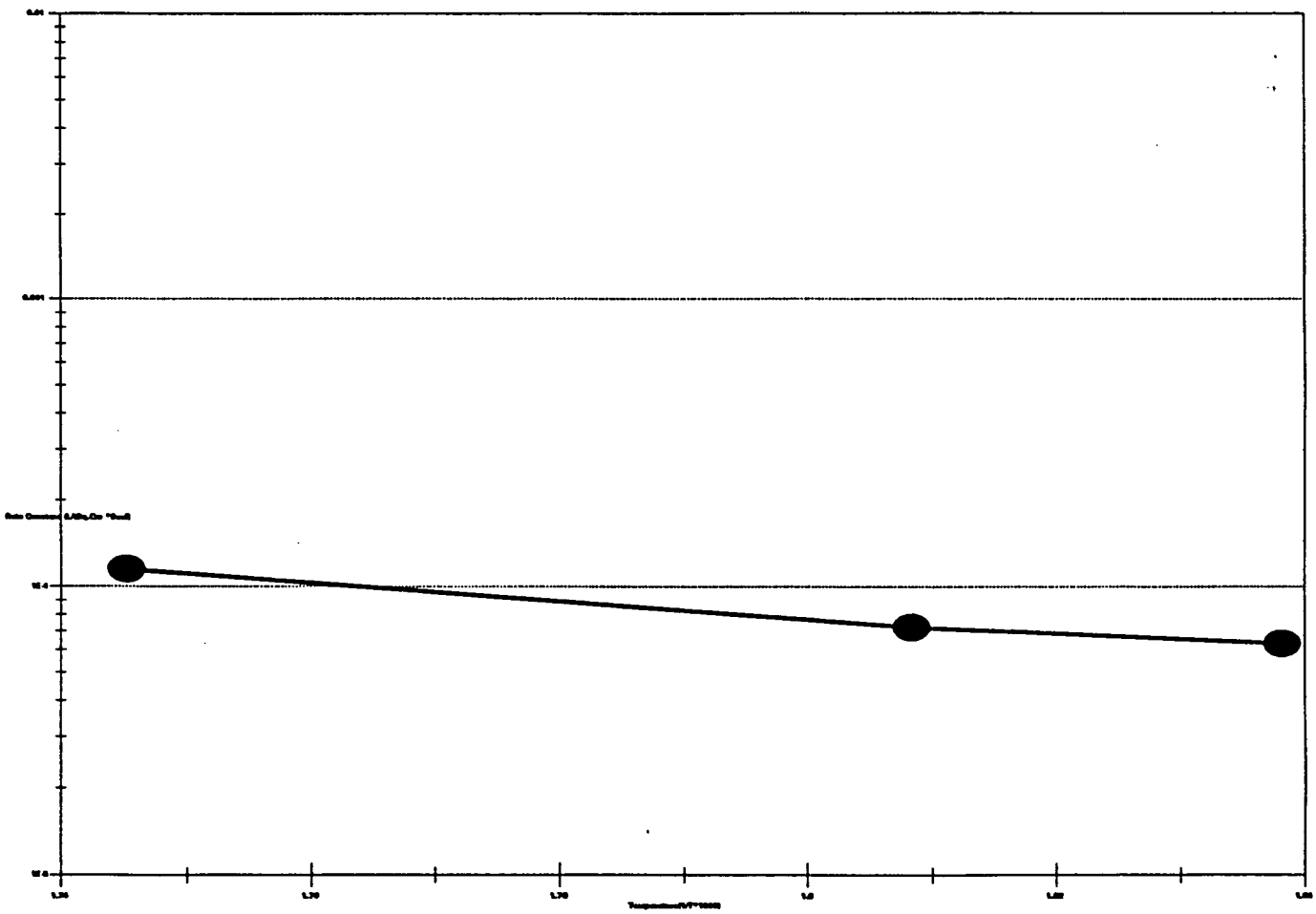

Figure 30. Arrhenius Plot of Rate Constant k versus Temperature

Table 16

Parameters for Langmuir-Hinshelwood model

Langmuir-Hinshelwood model	
Rate equation $$rate = k \frac{C_{MA}}{1 + K_a C_{MA}}$$	
Rate constant	Adsorption equilibrium constant
$F = 2.29 \times 10^{-2}$ L/(cm^2 X Sec)	$F = 6.45 \times 10^{-8}$ L/mole
E = 5658 cal/mole	E = -29.988 kcal/mole
R = 1.987 cal/mole.^{0}k	R = 1.987 cal/mole.^{0}k

Arrhenius Plot for

Langmuir-Hinshelwood Model

(for rate constant)

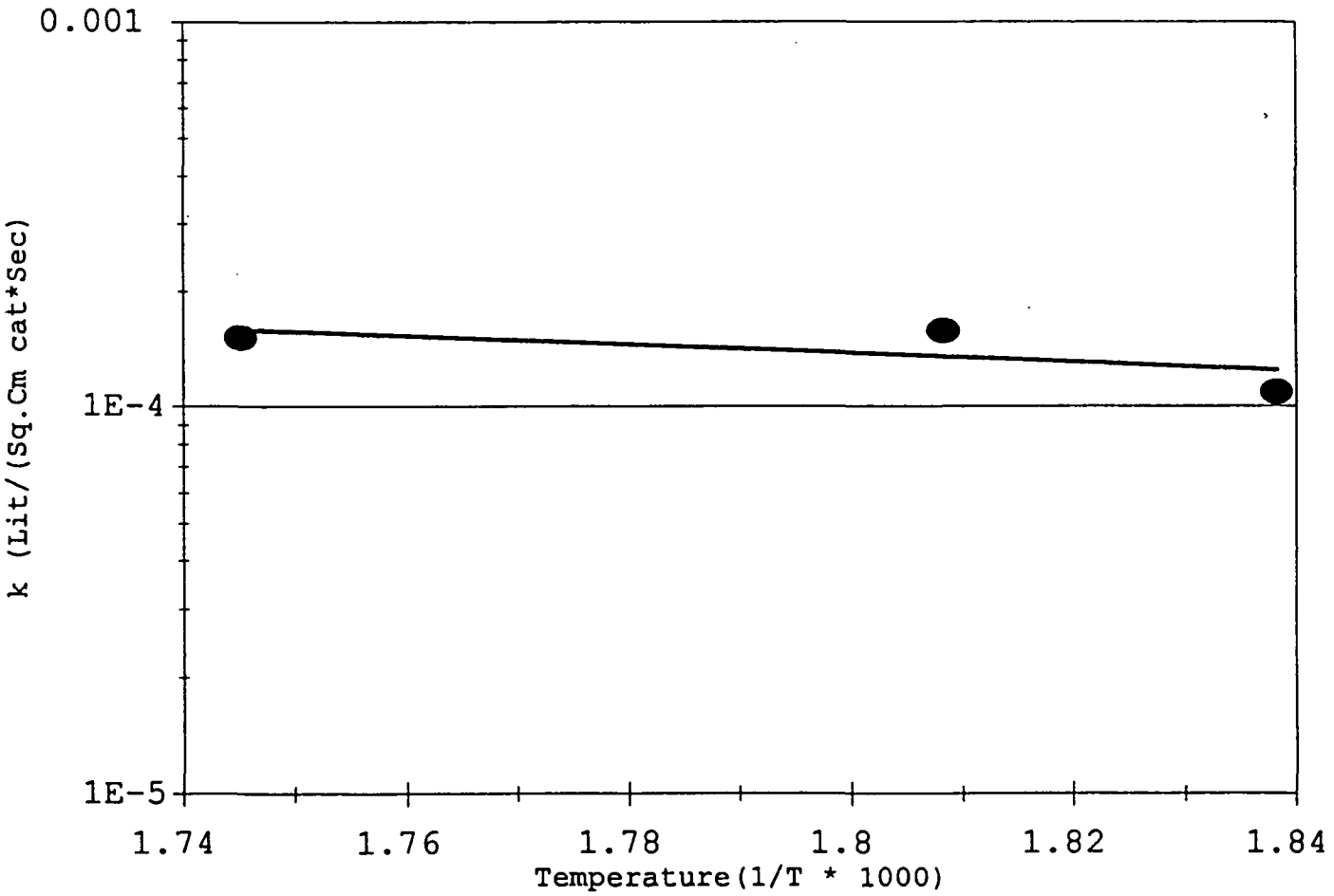

Figure 31. Arrhenius Plot for the Rate Constant k versus Temperature

Adsorption Equilibrium Constant for

Langmuir-Hinshelwood Model

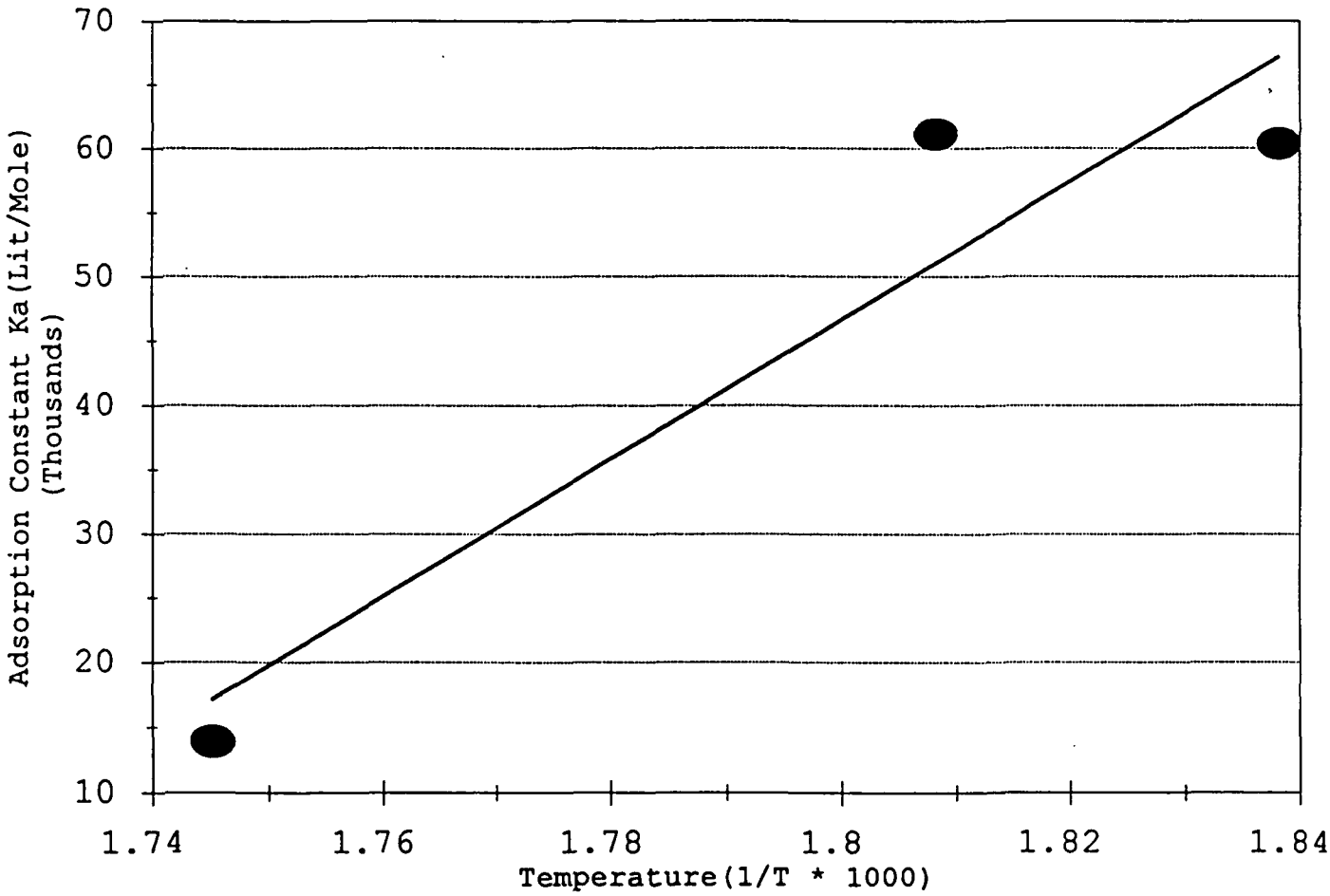

Figure 32. Adsorption Equilibrium Constant versus Temperature

Conclusion

1. The first-order power law and the Langmuir-Hinshelwood model were applied to develop a better explanation for the experimental data. Though the data can be approximated by both the first-order and Langmuir-Hinshelwood models at higher concentrations of methyl acetate, the Langmuir-Hinshelwood model is more accurate than the first-order model.

2. The first-order rate constant, with the Arrhenius relationship,

$$k(T) = Fe^{-E/RT}$$

was used to calculate the activation energy E and the frequency factor F. The values of F and E are 12.17 and 13,186 cal/mole,respectively.

3. For the Langmuir-Hinshelwood model, the Arrhenius relationship was used to calculate the activation energy E and the frequency factor, F, with rate constant k, and adsorption equilibrium constant K_a. For the rate constant, E = 109.96 kcal/mole and F = 9.63×10^{39} L/(cm^2 sec). For the adsorption equilibrium constant, E = -29.99 kcal/mole and F = 6.45×10^{-8} L/mole.

III.3 By-product Identification

The samples collected by the adsorbent tubes before and after the reactor were analyzed using identified by the Concentrator/GC/MS system. The GC-MS spectra of by-products are shown in Figures 33 through 35. In Figure 33, the two peaks with retention time 2.45 and 2.62 minutes were identified as methanol and methyl formate by the installed HP-G1034B-MS ChemStation Library. In Figures 34 and 35, the unknown compound spectrum (upper plot) is compared with the reference compound spectra in the ChemStation Library. This spectrum similarity is measured by a quantity called match quality. An unknown compound spectrum can be compared with several different reference compounds of different match quality.

Table 17 lists the retention time of each byproduct. The identification of the compounds shown in Table 17 is made possible by the software based on the highest matching quality (usually 82 to 97%). To verify whether or not these suggested compounds match the retention time, the standard solutions of the suggested compounds were injected into the GC/MS. If the retention time of a suggested compound was different from that listed in Table 17, then it was recognized that the compound suggested by the Library with the highest matching quality may not be the correct one. In these cases, the standard solution of the second highest matching quality was tested, and so on, until the compound was identified. After these identification procedures, the true byproducts, shown in Table 18, were identified as methanol, methyl formate, acetone, 1-propanol, and acetic acid.

Table 17
List of Retention Time of Byproduct and the Suggested Compound

Retention Time	2.45	2.62	3.02	3.65	5.67
Suggested Compound	Methanol	Methyl Formate	Acetone	Ethyl Formate	Acetic Acid

Table 18
List of the Retention Time of the Suggested Compound

Highest Matching Quality Compound	Standard Solution	Methanol	Methyl Formate	Acetone	Ethyl Formate	Acetate Acid
	Retention Time	2.46	2.6	3.02	3.34	5.67
Second Matching Quality Compound	Standard Solution	-	-	-	1-Propanol	-
	Retention Time	-	-	-	3.65	-

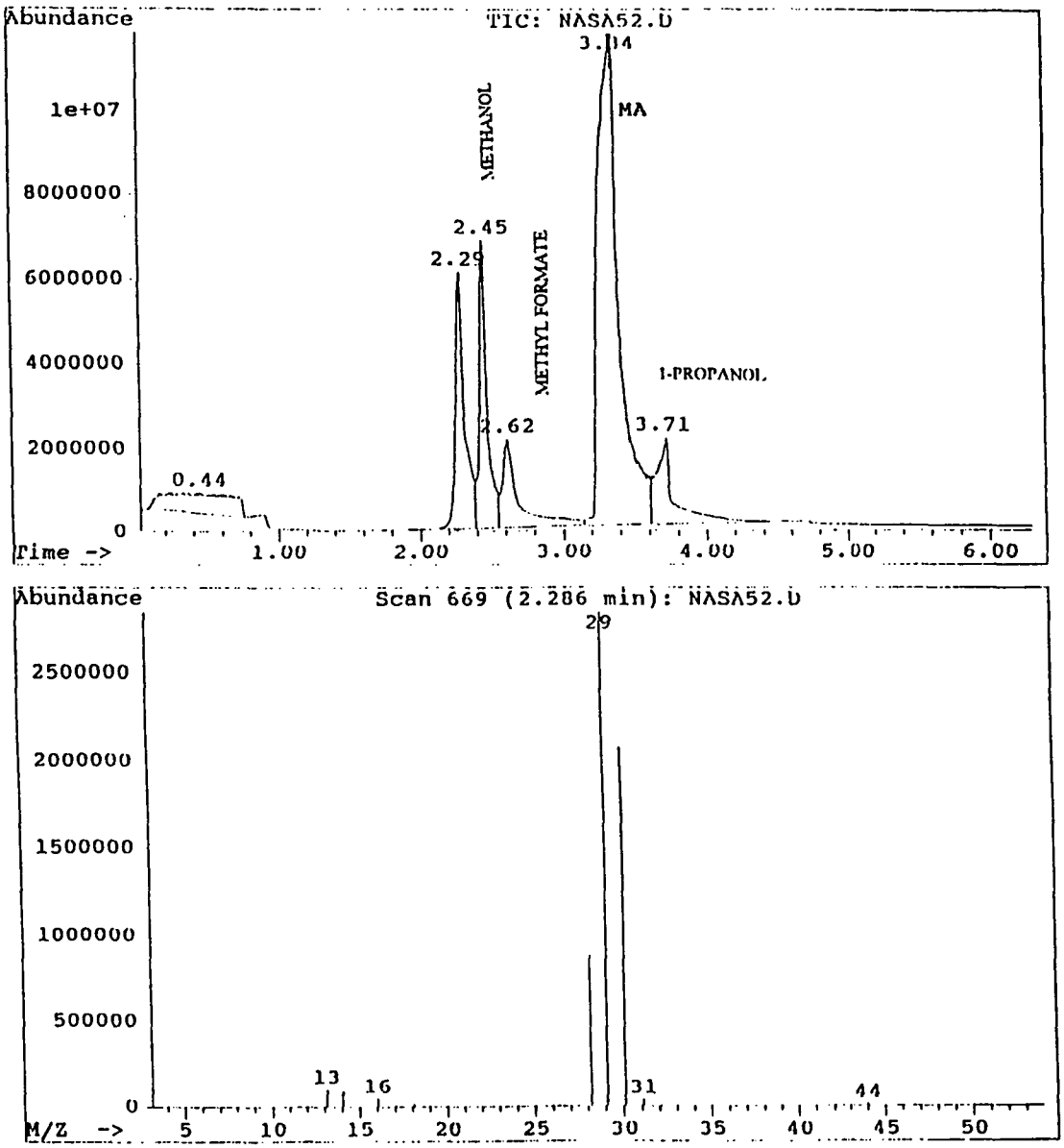

Figure 33 Byproduct Identification Downstream of Preheater

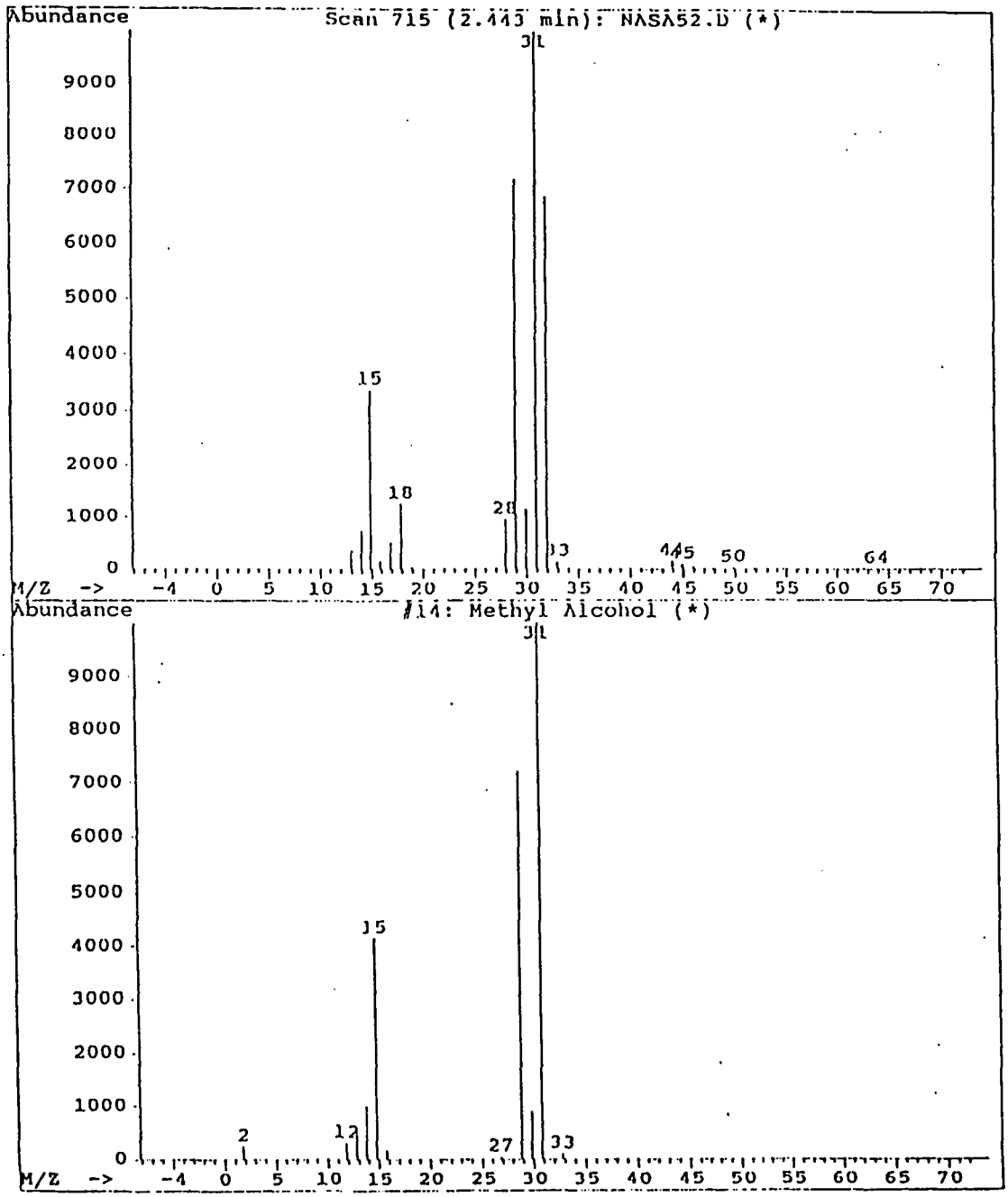

Figure 34 GC/MS Spectrum : Methanol Identification

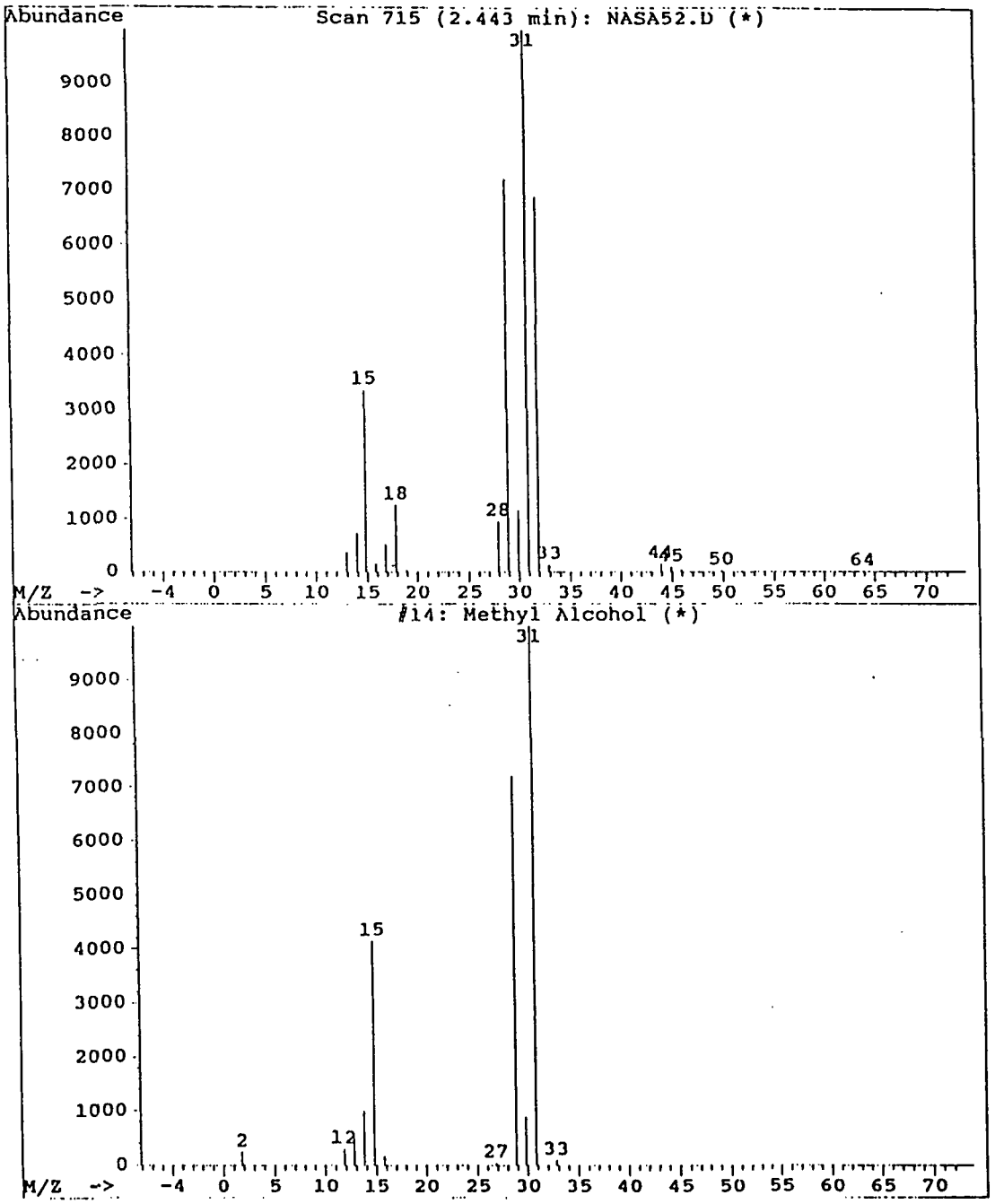

Figure 35 GC/MS Spectrum : Methyl Formate Identification

III. 4 Data Analysis by Taguchi Technique

The Taguchi method of experimental design is advantageous in analyzing a system with several uncertainties because it offers maximum information with minimum sets of experiments.

Analysis of Variance (ANOVA) Table

The purpose of this experiment was to identify specific reactor operating conditions (factors) which reduced the byproduct formation. It was necessary to decide which factor had a significant effect on the formation of the byproduct. The decision was usually made based on the analysis of variance (ANOVA). In lieu of pure judgment, the Taguchi analysis takes variation into account [Ross, 1988]. Table 19 is a typical Taguchi orthogonal array, L_9, data table and Table 20 is a typical ANOVA table [Montgomery, 1991].

Table 19
Typical Taguchi Designed Data

Set	A	B	C	D	Data
1	1	1	1	1	y_1
2	1	2	2	2	y_2
3	1	3	3	3	y_3
4	2	1	2	3	y_4
5	2	2	3	1	y_5
6	2	3	1	2	y_6
7	3	1	3	2	y_7
8	3	2	1	3	y_8
9	3	3	2	1	y_9

Level	A	B	C	D
1	A1	B1	C1	D1
2	A2	B2	C2	D2
3	A3	B3	C3	D3

Table 20
The Analysis of Variance Table

Source of Variation	Sum of Square	Degree of Freedom	Mean Square	F
Between Treatment	$SS_{Treatment}$	a-1	$MS_{Treatment}$	$F=MS_{Treatment}/MS_E$
Error (within treatment)	SS_E	N-a	MS_E	
Total	SS_T	N-1		

The terms in Table 20 are also described below.

$$y_{..} = \sum_{i=1}^{9} y_i \tag{11}$$

where A, B, C, D = treatment of experiment

$$SS_A = \frac{(\sum_{i=1,2,3} y_i)^2_{A1}}{3} + \frac{(\sum_{i=4,5,6} y_i)^2_{A2}}{3} + \frac{(\sum_{i=7,8,9} y_i)^2_{A3}}{3} - \frac{y_{..}^2}{N} \tag{12}$$

$$SS_B = \frac{(\sum_{i=1,4,7} y_i)^2_{B1}}{3} + \frac{(\sum_{i=2,5,8} y_i)^2_{B2}}{3} + \frac{(\sum_{i=3,6,9} y_i)^2_{B3}}{3} - \frac{y_{..}^2}{N} \tag{13}$$

$$SS_C = \frac{(\sum_{i=1,6,8} y_i)^2_{C1}}{3} + \frac{(\sum_{i=2,4,9} y_i)^2_{C2}}{3} + \frac{(\sum_{i=3,5,7} y_i)^2_{C3}}{3} - \frac{y_{..}^2}{N} \tag{14}$$

$$SS_D = \frac{(\sum_{i=1,5,9} y_i)^2_{D1}}{3} + \frac{(\sum_{i=2,6,7} y_i)^2_{D2}}{3} + \frac{(\sum_{i=3,4,8} y_i)^2_{D3}}{3} - \frac{y_{..}^2}{N} \quad (15)$$

$$SS_E = SS_T - SS_A - SS_B - SS_C - SS_D \quad (16)$$

$$MS_{Treatment} = \frac{SS_{Treatment}}{a-1} \quad (17)$$

N = a×n, the total number of observations,
a = number of level,
SS_T = total sums of squares,
$SS_{Treatment}$ = sums of squares due to the treatment A, B, C, or D,
SS_E = error sums of squares,
$MS_{Treatment}$ = mean square due to the treatment,
MS_E = error mean of squares,
$F_{\alpha,v1,v2}$ = F distribution (from percentage points of the F distribution table),
α = risk level,
Confidence = 1- risk,
v1 = degrees of freedom for numerator, and
v2 = degrees of freedom for denominator.

When F is bigger than $F_{\alpha,v1,v2}$, statistically, the estimated variances are believed to be unequal with at least (1- α) confidence [Rose 1988]. In this study, the F values are estimated based on the mean square of error, MS_E. This means that the variations due to the parameters (temperatures, flow rates, and concentrations) are significantly different from the variation of the random error. The judgment is based on a confidence level of (1- α).

MA Conversion over Pt/Al_2O_3 Pellet Catalysts

To study the variance of the parameters affecting MA conversion over the Pt/Al_2O_3 pellet catalyst, a Taguchi orthogonal array, L_{27}, (shown in Table 21) was constructed based on 3-level factors with interaction, v.i.z., reaction temperature (A), methyl acetate concentration (B), gas flow rate (C), and 3-level factors with no-interaction, v.i.z., pressure (D), carbon dioxide concentration (E), and oxygen concentration (F). The three

Table 21
Pellet Catalyst, Taguchi Experimental Design Orthogonal Array

Set	A	B	C	E	F	MA Conv.
1	1	1	1	1	1	0.09
2	1	1	2	2	2	0.03
3	1	1	3	3	3	0.05
4	1	2	1	2	3	0.088
5	1	2	2	3	1	0.09
6	1	2	3	1	2	0.05
7	1	3	1	3	2	0.04
8	1	3	2	1	3	0.06
9	1	3	3	2	1	0.04
10	2	1	1	3	2	0.57
11	2	1	2	1	3	0.33
12	2	1	3	2	1	0.24
13	2	2	1	1	1	0.47
14	2	2	2	2	2	0.30
15	2	2	3	3	3	0.27
16	2	3	1	2	3	0.25
17	2	3	2	3	1	0.25
18	2	3	3	1	2	0.15
19	3	1	1	2	3	0.93
20	3	1	2	3	1	0.83
21	3	1	3	1	2	0.81
22	3	2	1	3	2	0.89
23	3	2	2	1	3	0.84
24	3	2	3	2	1	0.76
25	3	3	1	1	1	0.87
26	3	3	2	2	2	0.75
27	3	3	3	3	3	0.61

level	A: Temp.	B: MA con.	C: flowrate	E: CO_2 con.	F: O_2 con.
1	250	100 ppmV	1.5 l/min	0%	21.0%
2	320	500 ppmV	3.0 l/min	3.0%	28.5%
3	420	2000 ppmV	4.5 l/min	8.5%	40.4%

levels of each factor are indicated in Table 21. The pressure factor was eliminated due to the difficulty of conducting a reduced-pressure test in this investigation. Experimental results, namely, conversion percentage of methyl acetate for the 27 experimental sets, were then obtained, and these are shown in Table 21.

Based on these experimental design results, an analysis of variance was then performed using Equations 11 through 17. The result indicated that the random error, and the error fluctuations from E, F and BxC factors, are very small. It is therefore convenient to lump these fluctuations into one random error term, and a simplified analysis of variance can be developed as shown in Table 22 [Li, et al, 1994; Gunst, 1980]. The F values were obtained from the ratio of mean square of the factor to that of the lumped random error. Results indicate that the reaction temperature (A-factor) is the most significant factor affecting the conversion. The next significant factor is the gas flow rate, followed by the methyl acetate concentration. The cross effect of either AxB or AxC is insignificant.

Table 22
Analysis of Variance, Simplified Combination of Taguchi Experimental Design

Factor	Degree of freedom	Sum of square	Mean squire	F*
A	2	26197.91	13098.95	533.78
B	2	481.16	240.58	9.80
C	2	832.99	416.45	16.97
AxB	4	189.74	47.44	1.93
AxC	4	292.71	73.18	2.98
e+E+F+BxC	12	294.46	24.54	
Total	26	28288.97		

* Confidence level	=	95%	99%
F(2,12)	=	3.88	6.93
F(4,12)	=	3.26	5.41

III.5 Analysis of Conversion of MA and Byproducts Through A Monolithic Reactor

To study the variance of the parameters affecting MA conversion and byproducts over Pt/Al_2O_3 monolithic catalysts, two Taguchi orthogonal arrays (OAs), both L_9, for the P-type monolithic catalyst and the E-type monolithic catalyst (shown in Tables 23 and 33) were constructed. The two OAs were based on 3-level factors with interaction, i.e., reaction temperature (A), methyl acetate concentration (B), and gas flow rate (C). The three levels of each factor are also indicated in the tables. Experimental results, namely, conversion data for MA and ppmV of the byproducts and ANOVA tables were then obtained, and these are shown separately from Tables 23 to 32 for the P-type monolithic catalyst, and from Tables 24 to 40 for the E-type monolithic catalyst. To avoid confusion these tables are put in two groups at the end of this section.

To investigate the effect of temperature on any byproduct, temperatures for the three levels were set as 160 °C, 320 °C, and 420 °C. Also, this temperature range is large enough to neglect experimental error. To better discern the influence of temperature at higher temperatures, both set 8 and set 9 were extended from 420 °C to 440 °C and 460°C. The results are shown in Table 25 (for P-type monolithic catalyst) and Table 35 (for E-type monolithic catalyst).

To analyze the effects of the factors, summaries of the ANOVA results were compiled in Tables 26 to 32 for the P-type monolithic catalyst, and Tables 36 to 40 for the E-type monolithic catalyst. The analysis of results for MA conversion and byproducts are discussed below.

Analysis of MA Conversion

From Table 23, Table 33 and the ANOVA summaries, Tables 26 and 36, it is seen that the reaction temperature (A-factor) is the most significant factor affecting the conversion of MA for both catalysts. For these monolithic catalysts, a very narrow flow rate range was observed when MA conversion was between 0 % and 100 % [Chalasani, 1994]. Because of the significant effect of temperature on MA conversion and this narrow flow rate range, the conversion of MA was either one or zero in this experimental investigation. For this reason, the flow rate and concentration (B and C factors) do not show any significant effect on MA conversion. In byproduct production, however, these two factors may show some effect. Details on this will be discussed later.

A comparison of Tables 23 and 33 indicates that the P-type monolithic catalyst exhibits better performance for MA conversion (at set 4, set 5, and set 6) than the E-type monolithic catalyst.

Table 23
P-type Monolithic Catalyst
Taguchi Experimental Design Orthogonal Array

SET	A	B	C	MA Conv.
1	1	1	1	0
2	1	2	2	0
3	1	3	3	0
4	2	1	2	1
5	2	2	3	0.58
6	2	3	1	1
7	3	1	3	1
8	3	2	1	1
9	3	3	2	1

Level	A:Temp.	B: MA Con.	C: Flowrate
1	160 °C	200 ppmV	1.5 l/min
2	320 °C	500 ppmV	3.0 l/min
3	420 °C	2000 ppmV	4.5 l/min

Analysis of Byproducts

When MA was forced through the preheater, thermal decomposition and/or catalytic oxidation occurred over the glass beads. The temperature of the preheater was not isothermal, as it varied from ambient temperature on one end to set point temperature on the other end. All byproducts and the MA passing through the preheater continued to pass through the monolithic catalyst to generate major products (CO_2 and H_2O). Analyses of data has produced the ANOVA data of Tables 26 to 32 for the P-type monolithic catalyst, and Tables 36 to 42 for the E-type monolithic catalyst. The F values were obtained from the ratio of the mean square of the factor to that of the lumped random error.

The experimental results indicate that temperature (A-factor) is the most significant factor affecting byproducts formation. Significant byproduct formation was observed at temperatures above 420°C. Also, complete combustion through the monolithic catalytic reactor was observed when all compounds passed through the reactor at a temperature higher than 420 °C (Tables 25 and 35).

However, when the reactor temperature was below 320 °C, byproducts were observed at the reactor exit. Under this condition, the concentration of MA (B-factor) is an important factor affecting the amount of byproduct. The data were shown as set 3 and set 6 in Tables 24 and 34. The flow rate (C-factor) has the least effect on MA conversion, as previously discussed.

In summary, the E-type monolithic catalyst exhibited better performance than the P-type monolithic catalyst in avoiding unwanted byproducts at low temperatures (320 °C and 160 °C) (Tables 24 and 34). Additionally, for the P-type monolithic catalyst reactor, the byproduct acetone was generated in a trace amount from MA oxidation over the reactor (set 5 in Table 24). However, with the E-type monolithic catalyst, this byproduct was not observed. This suggests that the E-type monolithic catalyst may contain a higher percentage of active platinum than that of the P-type monolithic catalyst.

Table 24
P-type Monolithic Catalyst
Identified Byproduct Amount from GC/MS

Set	Before Reactor				After Reactor				
	AA	MOH	MF	1-PL	AA	MOH	MF	1-PL	AT
1	0*	0	0	0	0	0	0	0	0
2	0	5.5	0	0	0	5.2	0	0	0
3	2.6	35.4	0	0	2.1	29.4	0	0	0
4	0	4.2	0	0	0	0	0	0	0
5	3.8	4.1	0	0	2.4	4.4	0	0	0.2
6	0	34.0	0	0	2.2	21.0	0	0	0
7	0	41.3	13.9	2.9	0	0	0	0	0
8	0	87.4	30.2	19.0	0	0	0	0	0
9	26.9	161.0	58.2	46.7	0	0	0	0	0

AA: Acetic Acid
MOH: Methanol
MF: Methyl Formate
1-PL: 1-Propanol
AT: Acetone
* Concentration at ppmV

Table 25
P-type Monolithic Catalyst
Identified Byproduct Amount from GC/MS at High Temperature Range

Set	Before Reactor				After Reactor			
	AA	MOH	MF	1-PL	AA	MOH	MF	1-PL
SET 8 (420 C)	0	87.5	30.2	19.0	0	0	0	0
SET 8 (440 C)	0	86.1	47.4	29.5	0	0	0	0
SET 8 (460 C)	9.3	109.2	91.1	51.5	0	0	0	0
SET 9 (420 C)	26.9	161.0	58.2	46.7	0	0	0	0
SET 9 (440 C)	11.9	232.4	60.1	66.5	0	0	0	0
SET 9 (460 C)	55.6	417.9	125.4	112.4	0	0	0	0

Table 26
P-Type Monolithic Catalyst, Methyl Acetate Conversion
Analysis of Variance Table

Factor	Degree of Freedom	Sum of Square	Mean Square	F*
A	2	1.7592	0.8796	44.88
B	2	0.0392	0.0196	1
C	2	0.0392	0.0196	1
e	2	0.0392	0.0196	
Total	8	1.8768		

* Confidence Level = 95% 99%
F(2,2) = 19.00 99.00

Table 27
P-Type Monolithic Catalyst, Before Reactor Byproduct: Acetic Acid
Analysis of Variance Table

Factor	Degree of Freedom	Sum of Square	Mean Square	F*
A	2	125.6	62.8	0.64
B	2	170.5	85.2	0.88
C	2	132.0	66.0	0.68
e	2	193.8	96.9	
Total	8	621.8		

* Confidence Level = 95% 99%
F(2,2) = 19.00 99.00

Table 28
P-type Monolithic catalyst, Before Reactor Byproduct: Methanol
Analysis of Variance Table

Factor	Degree of Freedom	Sum of Square	Mean Square	F*
A	2	13678.9	6839.4	11.5
B	2	6070.6	3035.3	5.1
C	2	1351.2	675.6	1.14
e	2	1188.1	594.0	
Total	8	22288.8		

* Confidence Level = 95% 99%
F(2,2) = 19.00 99.00

Table 29
P-type Monolithic Catalyst, Before Reactor Byproduct: Methyl Formate
Analysis of Variance Table

Factor	Degree of Freedom	Sum of Square	Mean Square	F*
A	2	2325.6	1162.8	6.9
B	2	334.7	167.3	1
C	2	334.7	167.3	1
e	2	334.7	167.3	
Total	8	3329.7		

* Confidence Level = 95% 99%
F(2,2) = 19.00 99.00

Table 30
P-type Monolithic Catalyst, Before Reactor Byproduct: 1-Propanol
Analysis of Variance Table

Factor	Degree of Freedom	Sum of Square	Mean Square	F*
A	2	1045.8	522.9	3.2
B	2	327.2	163.6	1
C	2	327.2	163.6	1
e	2	327.2	163.6	
Total	8	2027.4		

* Confidence Level = 95% 99%
F(2,2) = 19.00 99.00

Table 31
P-type Monolithic Catalyst, After Reactor Byproduct: Acetic acid
Analysis of Variance Table

Factor	Degree of Freedom	Sum of Square	Mean Square	F*
A	2	3.5	1.8	227.3
B	2	3.1	1.6	199
C	2	3.4	1.7	217
e	2	0.016	0.008	
Total	8	10.0		

* Confidence Level = 95% 99%
F(2,2) = 19.00 99.00

Table 32
P-type Monolithic Catalyst, After Reactor Byproduct: Methanol
Analysis of Variance Table

Factor	Degree of Freedom	Sum of Square	Mean Square	F*
A	2	214.1	107.1	1.7
B	2	477.4	238.7	3.9
C	2	136.8	68.4	1.1
e	2	123.4	61.7	
Total	8	951.8		

* Confidence Level = 95% 99%
F(2,2) = 19.00 99.00

Table 33
E-type Monolithic Catalyst
Taguchi Experimental Design Orthogonal Array

SET	A	B	C	MA Conv.
1	1	1	1	0
2	1	2	2	0
3	1	3	3	0
4	2	1	2	0
5	2	2	3	0
6	2	3	1	0
7	3	1	3	1
8	3	2	1	1
9	3	3	2	1

Level	A:Temp.	B: MA Con.	C: Flowrate
1	160 °C	200 ppmV	1.5 l/min
2	320 °C	500 ppmV	3.0 l/min
3	420 °C	2000 ppmV	4.5 l/min

Table 34
E-type Monolithic Catalyst
Identified Byproduct Amount from GC/MS

Set	Before Reactor				After Reactor			
	AA	MOH	MF	1-PL	AA	MOH	MF	1-PL
1	0*	0	0	0	0	0	0	0
2	0	7.0	0	0	0	0	0	0
3	0	63.7	0	0	0	7.7	0	0
4	0	0	0	0	0	0	0	0
5	0	4.2	0	0	0	0	0	0
6	0	34.3	0	0	0	0	0	0
7	0	31.5	0	0	0	0	0	0
8	2.6	135.1	42.2	9.3	0	0	0	0
9	27.6	189	87.7	42.9	0	0	0	0

AA: Acetic Acid
MOH: Methanol
MF: Methyl Formate
1-PL: 1-Propanol
AT: Acetone
* Concentration at ppmV

Table 35
E-type Monolithic Catalyst
Identified Byproduct Amount from GC/MS at High Temperature Range

Set	Before Reactor				After Reactor			
	AA	MOH	MF	1-PL	AA	MOH	MF	1-PL
SET 8 (420 C)	2.6	135.1	42.2	9.3	0	0	0	0
SET 8 (440 C)	0	161.0	45.2	22.4	0	0	0	0
SET 8 (460 C)	0	156.8	67.6	18.7	0	0	0	0
SET 9 (420 C)	27.6	189.0	87.7	42.9	0	0	0	0
SET 9 (440 C)	12.3	121.8	57.1	0	0	0	0	0
SET 9 (460 C)	16.4	199.5	103.8	0	0	0	0	0

Table 36
E-type Monolithic Catalyst, After Reactor Product: Methyl Acetate Conversion
Analysis of Variance Table

Factor	Degree of Freedom	Sum of Square	Mean Square	F*
A	2	2	1	∞
B	2	0	0	0
C	2	0	0	0
e	2	0	0	
Total	8	2		

* Confidence Level = 95% 99%
F(2,2) = 19.00 99.00

Table 37
E-type Monolithic Catalyst, Before Reactor Byproduct: Acetic Acid
Analysis of Variance Table

Factor	Degree of Freedom	Sum of Square	Mean Square	F*
A	2	202.7	101.4	1.3
B	2	154.8	77.4	1
C	2	154.8	77.4	1
e	2	154.8	77.4	
Total	8	667.2		

* Confidence Level = 95% 99%
F(2,2) = 19.00 99.00

Table 38
E-type Monolithic Catalyst Before Reactor Byproduct: Methanol
Analysis of Variance Table

Factor	Degree of Freedom	Sum of Square	Mean Square	F*
A	2	20306.3	10153.2	6.0
B	2	10917.3	5458.7	3.2
C	2	1659.9	830	0.5
e	2	3378.2	1689.1	
Total	8	36261		

* Confidence Level = 95% 99%
F(2,2) = 19.00 99.00

Table 39
E-type Monolithic Catalyst Before reactor Byproduct: Methyl Formate
Analysis of Variance Table

Factor	Degree of Freedom	Sum of Square	Mean Square	F*
A	2	3749.8	1874.9	2.9
B	2	1282.5	641.2	1
C	2	1282.5	641.2	1
e	2	1282.5	641.2	
Total	8	7597.24		

* Confidence Level = 95% 99%
F(2,2) = 19.00 99.00

Table 40
E-type Monolithic Catalyst, Before reactor Byproduct: 1-Propanol
Analysis of Variance Table

Factor	Degree of Freedom	Sum of Square	Mean Square	F*
A	2	605.5	302.8	1.8
B	2	339.5	169.8	1
C	2	339.5	169.8	1
e	2	339.5	169.8	
Total	8	1624.1		

* Confidence Level = 95% 99%
F(2,2) = 19.00 99.00

IV. MECHANISMS OF MA OXIDATION THROUGH A PREHEATER

With the glass beads used inside the preheater for this investigation, byproducts from the reaction in the preheater were detected and identified. If the glass beads would have served simply as an inert heat carrier, the reaction mechanism of MA through this preheater could be a simple homogeneous thermal cracking reaction. However, if the glass beads (SiO_2) serve as a catalytic site, the reaction mechanism could have been a heterogeneous catalytic oxidation. A heterogeneous-homogeneous reaction mechanism has been proposed successfully to explain the experimental data for the oxidation of methane and formaldehyde over SiO_2 [Garibyan, 1990].

Heterogeneous steps

The SiO_2, as a catalyst, can have various defected forms: Si·, SiO·, Si:, and SiO (diamagnetic groupings) presented on the surface. The reactant molecule could be adsorbed and held to these groupings [Bobyshev, 1991]. These adsorbed molecules actually form a chemical bond with these sites and are more active than their original status. Several reaction steps may occur to form intermediates and/or byproducts. These reaction steps, shown in Figure 36, will be discussed in the following paragraph. A number inside parentheses indicates an adsorbed species, while a number inside a bracket indicates a byproduct.

The first reaction step, IV-R1, in Figure 36 is a chemisorption of an oxygen molecule to form the species $O_2 \cdot S$ (1). The species $O_2 \cdot S$ (1) are formed slowly and are decomposed rapidly; their concentrations are sufficiently low so as to be considered negligible.

$$O_2 \xrightarrow{S} \underset{(1)}{\overset{O_2}{\underset{|}{S}}} \qquad \text{IV-R1}$$

$$\underset{(1)}{\overset{O_2}{\underset{|}{S}}} \xrightarrow[\text{very fast}]{S} 2\ \underset{(2)}{\overset{O}{\underset{|}{S}}} \qquad \text{IV-R2}$$

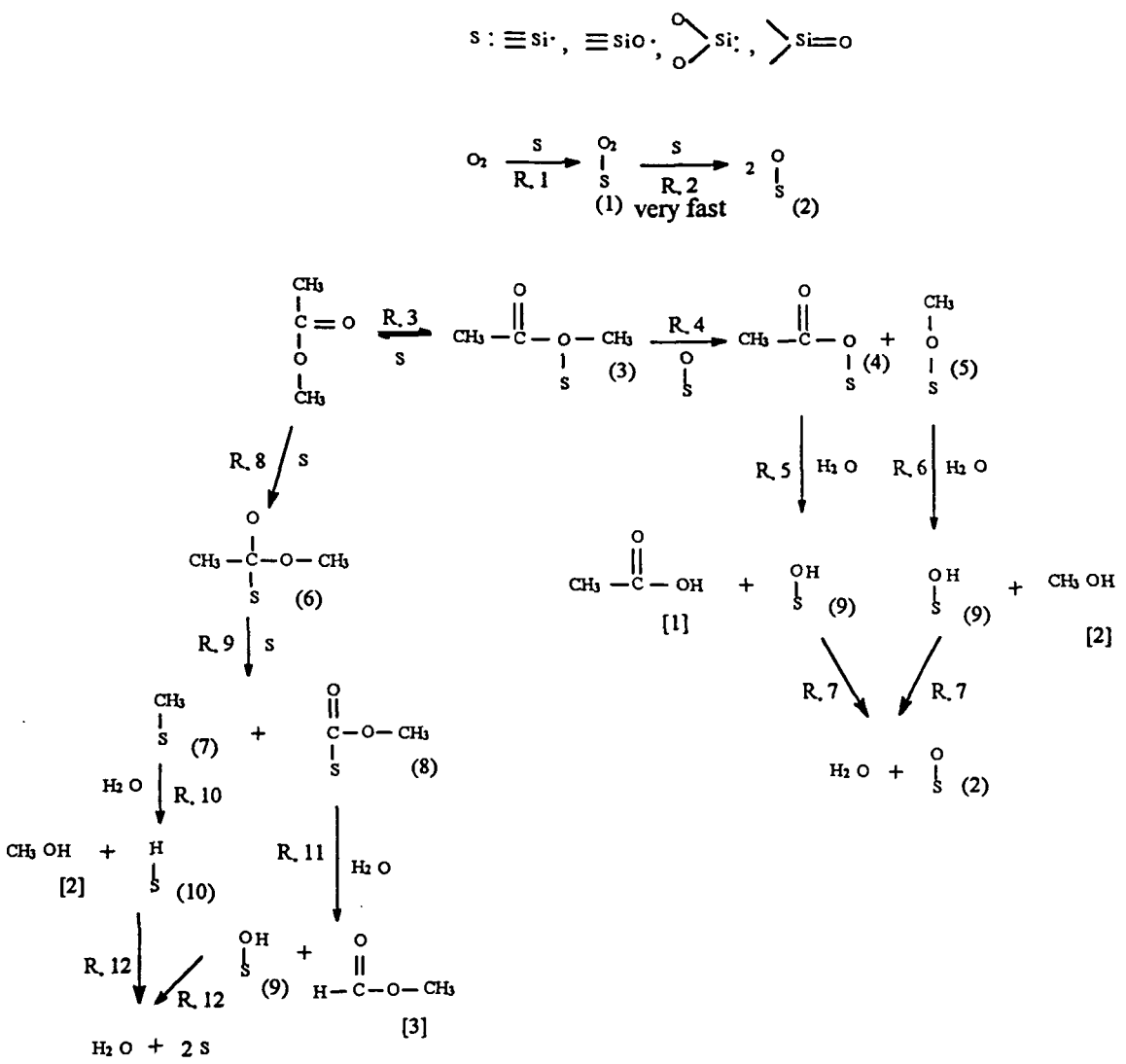

Figure 36

Scheme of Heterogeneous Steps of Methyl Acetate over SiO_2

(S represents a catalytic site)

The MA may be adsorbed on the active site through two independent pathways, IV-R3 and IV-R8 (Figure 36). Through the reaction step IV-R3, the MA is adsorbed on the site to form the species $CH_3CO(O{\cdot}S)CH_3$ (3). This reaction may be reversible. The species $CH_3CO(O{\cdot}S)CH_3$ is further oxidized by O·S through reaction step IV-R.4 to form $CH_3CO(O{\cdot}S)$ (4) and $CH_3(O{\cdot}S)$ (5). The bond between CO--CH_3 is broken because another adsorbed atomic oxygen, O·S, reacts with a methyl free radical, $\cdot CH_3$. Following an electron rearrangement, species (4) and (5) are formed through reaction step IV-R4. Species (4) may further react with H_2O (presented in the breathing air) to form a by-product, acetic acid [1], and another species (S·O)H. The byproduct acetic acid [1] has been identified by GC/MS analysis (Table 18). The reaction steps are shown below:

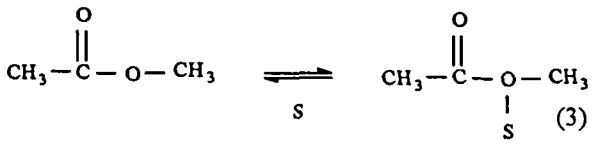

IV-R3

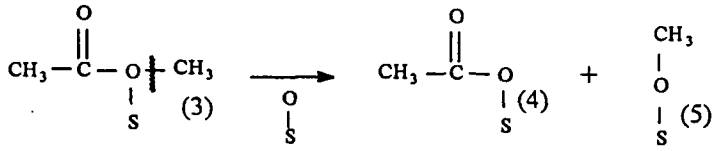

IV-R4

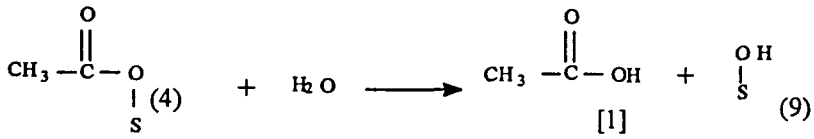

IV-R5

The species $CH_3O{\cdot}S$ (5) may react with H_2O through reaction stepIV-R6 to produce byproducts methanol, CH_3OH [2], and (S·O)H. The byproduct CH_3OH [2] also has been identified by GC/MS (Table 18) analysis. There are several reaction routes to form methanol. Other routes will be discussed later. This may explain why a significant amount of methanol was detected as the byproduct in this experiment. Reaction step IV-R7 indicates two S·OH may be combined to form water, H_2O , an O·S species and an empty site.

IV-R6

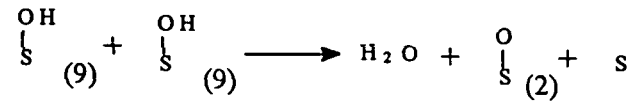

IV-R7

Reaction step IV-R8 indicates another reaction pathway which forms a different species, $CH_3(C{\cdot}S)OOCH_3$ (6). The $C\delta^-$-δ^+S bond is formed by one electron transfer from the C=O bond. Following reaction step IV-R9, the species (6) is dissociated to species $S{\cdot}CH_3$ (7) and species (8), $(S{\cdot}C)OOCH_3$. The species (7), from IV-R9, may go through reaction step IV-R10, react with H_2O and abstract a hydroxy group to form the byproduct methanol [2] and a species S·H. The byproduct methanol [2] has been identified by GC/MS (Table 18). Through reaction step IV-R11, the carbon of the species $(S{\cdot}C)OOCH_3$ (8) is attacked by H_2O and a hydrogen atom is substrated from H_2O to form the byproduct methyl formate [3] and a species (S·O)H. The byproduct methyl formate [3] has been identified by GC/MS as indicated in Table 5.3 (p. 87). The species S·H (10) may react with adjacent species (S·O)H (9) to form H_2O and two empty sites through reaction step IV-R12. The H_2O leaves the catalytic site and proceeds to the gas stream. The empty sites may adsorb other reactants.

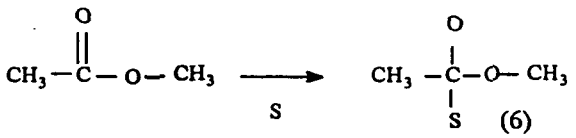

IV-R8

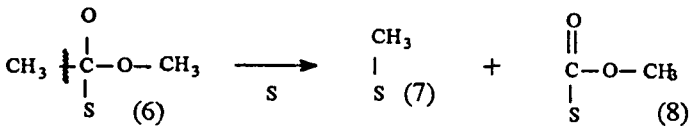

IV-R9

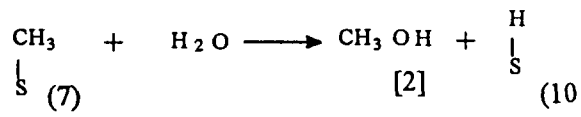

IV-R10

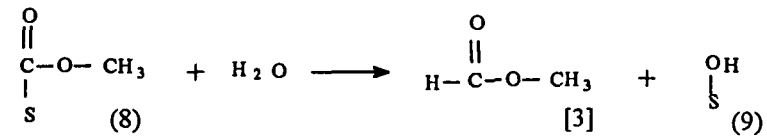

IV-R11

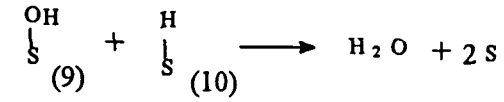

IV-R12

The byproduct 1-propanol may be formed only from a homogeneous reaction, since it is difficult to find reasonable heterogeneous reaction steps to explain the formation of 1-propanol. The homogeneous reaction steps are discussed in the following section.

Homogeneous steps

The reaction pathways of homogeneous thermal decomposition of MA to form the byproducts are complex. These pathways may include many different free radical reactions. These free radical reactions may involve chain-initiation, hydrogen-abstraction, radical-decomposition, radical-addition to unsaturated molecules, chain-termination, purely molecular reaction, radical-isomerization, etc. In order to propose the possible reaction routes, the bond strength (Table 41) [Vinogradov, 1971; Mortimer, 1962; Pauling, 1960] and the methyl acetate fragments (Table 42) are used as reference. The details of reaction pathways will be discussed later.

Table 41
The Bond Strengths

Bond	Bond Strength (kcal/mole)
C-O	84
C=O	176
C-C	83
C=C	146
C-H	99
O-H	111
H-H	104
HOH···O-H (gas) H	3-6
C=O > C=C > O-H > H-H >C-H > C-O > C-C > H··· O	

Table 42
Methyl Acetate Fragment List

M/e	
	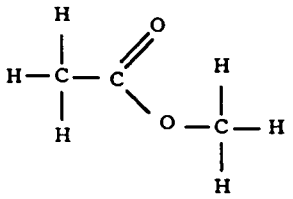
15	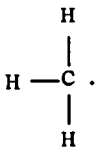
28	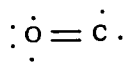
31	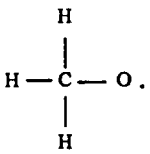
43	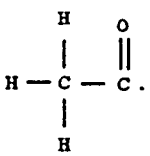
44	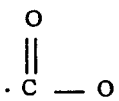
59	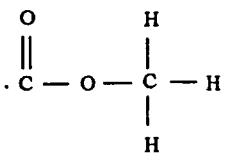

The possible homogeneous reaction pathways are shown in Figure 37. A number inside parentheses indicates an intermediate, and a number inside a bracket indicates a by-product. The MA may have three different independent reaction routes, IV-R1', IV-R4' and IV-R7' to form different byproducts. In the reaction step IV-R1', the MA is undergoing a thermal cracking reaction to form a $CH_3COO\cdot$ free radical (1) and a $CH_3\cdot$ free radical (2), since the bond energy between O--CH_3 is low (Table 41). Following reaction step IV-R2', the $CH_3COO\cdot$ free radical (1) from IV-R1' may be attacked by a water molecule and abstract a hydrogen atom from H_2O to form the byproduct acetic acid, CH_3COOH [1], and a hydroxy free radical. Because the electronegativity of a $CH_3COO\cdot$ free radical (1) (two oxygen atoms) is greater than that of H_2O (one oxygen atom), this hydrogen abstraction reaction occurs easily. The byproduct acetic acid [1] has been identified by GC/MS (Table 18). The hydroxy free radical, $\cdot OH$, is a very strong oxidant. It is second only to fluorine in oxidative power. It reacts easily with other free radicals, such as $CH_3\cdot$ free radical (2) or a hydrogen free radical to produce methanol or H_2O. These details are discussed below.

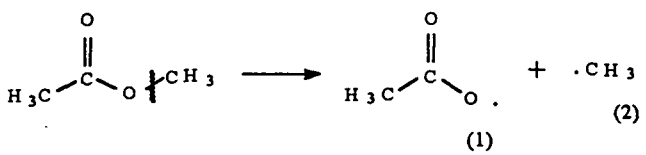

IV-R1'

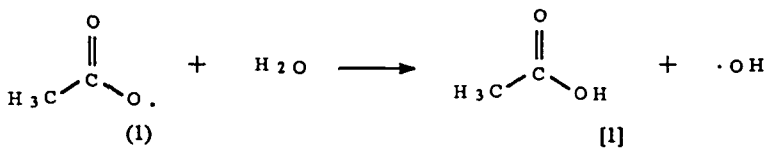

IV-R2'

The methyl free radical is extremely unstable and active, and for the same reason, it tends to complete its octet, to lose energy by forming a new bond. The reaction step IV-R3' indicates the $CH_3\cdot$ (2) may quickly react with H_2O and abstract a hydroxy from H_2O to form the byproduct methanol [4] and a hydrogen free radical. The methanol [4] has been identified by GC/MS (Table 18). The hydrogen free radical may quickly react with a hydroxy free radical to form H_2O.

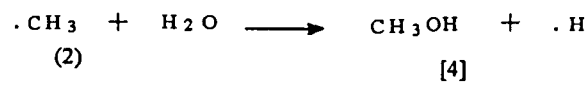

IV-R3'

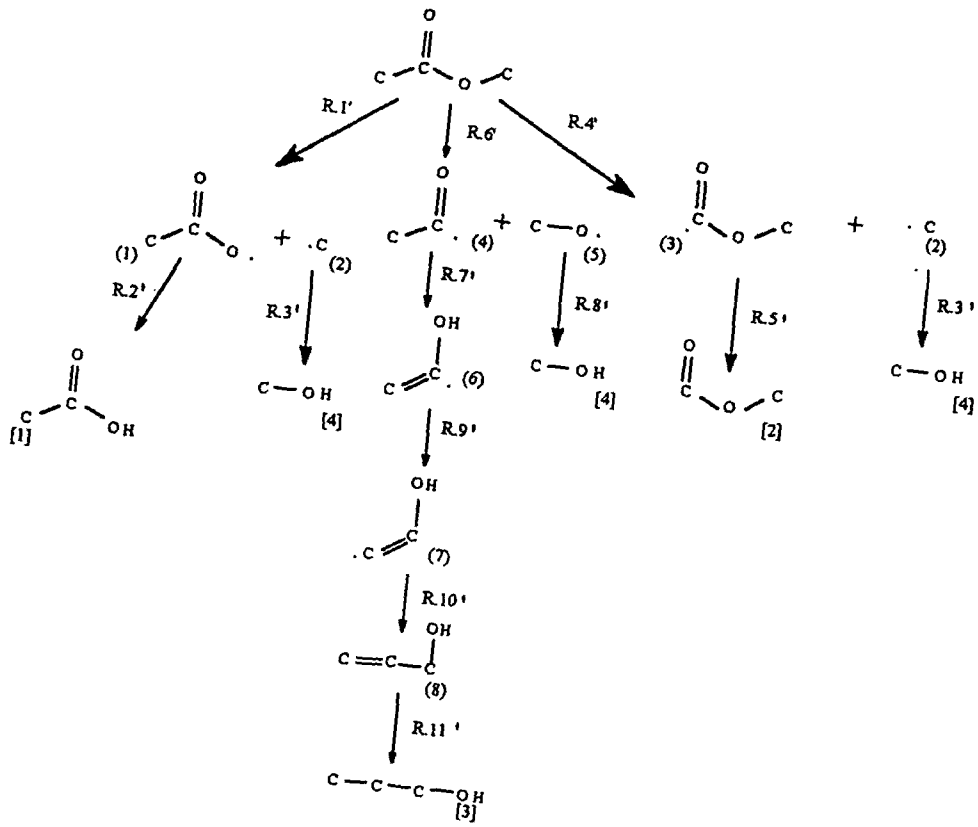

Figure 37

Scheme of Homogeneous Steps of Methyl Acetate over SiO_2

The MA may also go through reaction step IV-R4', a chain initiation reaction, to produce a ·$COOCH_3$ free radical (3) and a methyl free radical (2) because of the low bond energy between C--CH_3. The ·$COOCH_3$ free radical (3) may further react with H_2O and abstract a hydrogen atom from H_2O through reaction step IV-R5', a hydrogen abstraction reaction, to form the byproduct methyl formate, $HCOOCH_3$ [2] and a ·OH free radical. This methyl formate [2] has been identified by GC/MS (Table 18). The ·OH free radical may quickly react with ·H free radical to form H_2O. The methyl free radical (2), coming from IV-R4', may react with H_2O and abstract a hydroxy to product methanol [4] and a ·H free radical through reaction step IV-R3'. The methanol [4] has been identified by GC/MS. The hydrogen free radical may quickly react with the hydroxy free radical to form H_2O.

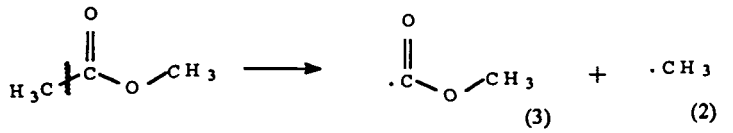

IV.R4'

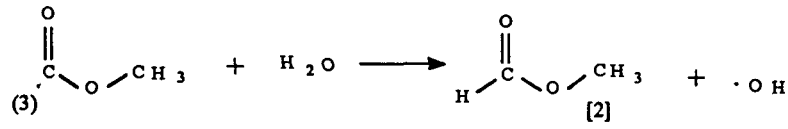

IV.R5'

The MA can also go through reaction step IV-R6'. The reaction step IV-R6' indicates the bond between C--O is broken due to the low bond energy between C--O. Then, the MA is initiated to form the CH_3CO· free radical (4) and a CH_3O· free radical (5). The CH_3O· free radical (5), coming from reaction step IV-R6', may abstract an H· free radical from H_2O through reaction step IV-R8', a hydrogen-abstraction reaction, to form the byproduct methanol [4] and a hydrogen free radical. The byproduct methanol [4] has been identified by GC/MS (Table 18). The hydrogen free radical may quickly react with the hydroxy free radical to from H_2O.

Reaction step IV-R7' indicates the CH_3CO· free radical (4), from reaction step IV-R6', is under keto-enol tautomerism to form a CH_2COH· free radical (6). The keto-enol tautomerism is an easy and rapid equilibrium between enol, a structure with -OH attached to doubly-bonded carbon, and the keto structure, one containing the C=O group [Morrison, 1983].

Following reaction step IV-R9', the CH_2COH· free radical (6) may go through a free radical isomerization to become the free radical (7). Reaction step IV-R10' indicates

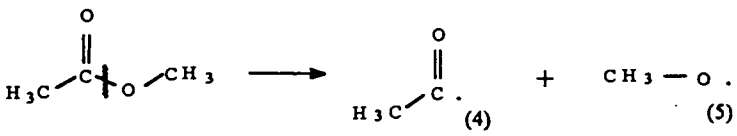

IV-R6'

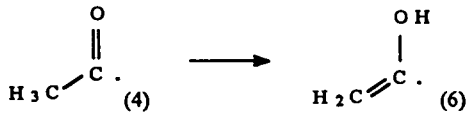

IV-R7'

IV-R8'

IV-R9'

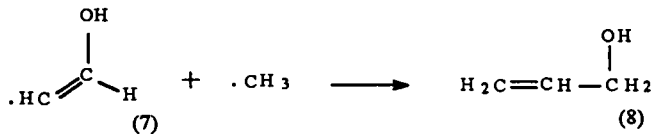

IV-R10'

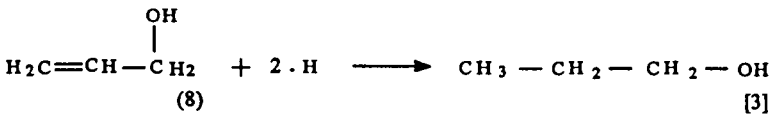

IV-R11'

that the free radical (7) may further react with a methyl free radical, which comes from reaction step IV-R1' and reaction step IV-R4', following a hydroxy rearrangement, to form 2-propen-1-ol, CH_2CHCH_2OH (8). Reaction step IV-R11' indicates the 2-propen-1-ol may quickly react with two hydrogen free radicals, which come the reaction IV-R3', to form the byproduct 1-propanol [3]. The 1-propanol [3] has been identified by GC/MS (Table 18). The homogeneous reaction mechanism may explain the formation of the by-product 1-propanol [3], which may not be explained from a heterogeneous reaction mechanism.

V. MECHANISMS OF MA OXIDATION THROUGH A MONOLITHIC REACTOR

Reaction Mechanism

To establish a mechanism, information concerning the absorbed species and how they react is required. The reaction mechanism of methyl acetate oxidation over Pt/Al_2O_3 has never been reported. However, the reaction mechanisms of ethanol, ethyl acetate, and n-heptane oxidation over Pt/Al_2O_3 have been proposed [Barresi, 1993; Swaver, 1994; Volter, 1987]. According to the above references and the experimental data obtained in this laboratory, hypothetical methyl acetate oxidation over Pt/Al_2O_3 schemes are proposed, as depicted in Figure 38, where S represents a free active catalytic site. The details of reaction steps are discussed in the following paragraphs. Numbers inside parentheses indicate an absorbed species, whereas numbers inside brackets indicate a byproduct.

Various studies indicate that platinum is very active in the oxidation of organics to form main products such as CO_2 and H_2O [Golodets, 1983; Barresi, 1992]. Since platinum was dispersed in the monolithic catalysts used in this study, the reaction rate of MA oxidation, as expected, was very fast. The intermediate concentrations were very low because most of the organics were oxidized to form CO_2 and H_2O.

The first reaction step V-R1, in Figure 38 is a chemisorption of an oxygen molecule to form the species $O_2 \cdot S$ (1). The species $O_2 \cdot S$ (1) is formed slowly in reaction step V-R1 and is destroyed rapidly in reaction step V-R1', therefore its concentration is sufficiently low that it can be neglected.

$$O_2 \xrightarrow{S} \underset{(1)}{O_2\text{-}S} \qquad \text{V-R1}$$

$$\underset{(1)}{O_2\text{-}S} \xrightarrow[\text{very fast}]{S} 2\,\underset{(2)}{O\text{-}S} \qquad \text{V-R1'}$$

When methyl acetate is fed through Pt/Al_2O_3, the oxygen atom of the MA may form a δ bond with an active site through reaction stepV-R2. This reaction may be a reversible adsorption reaction if the adsorption of MA is weak.

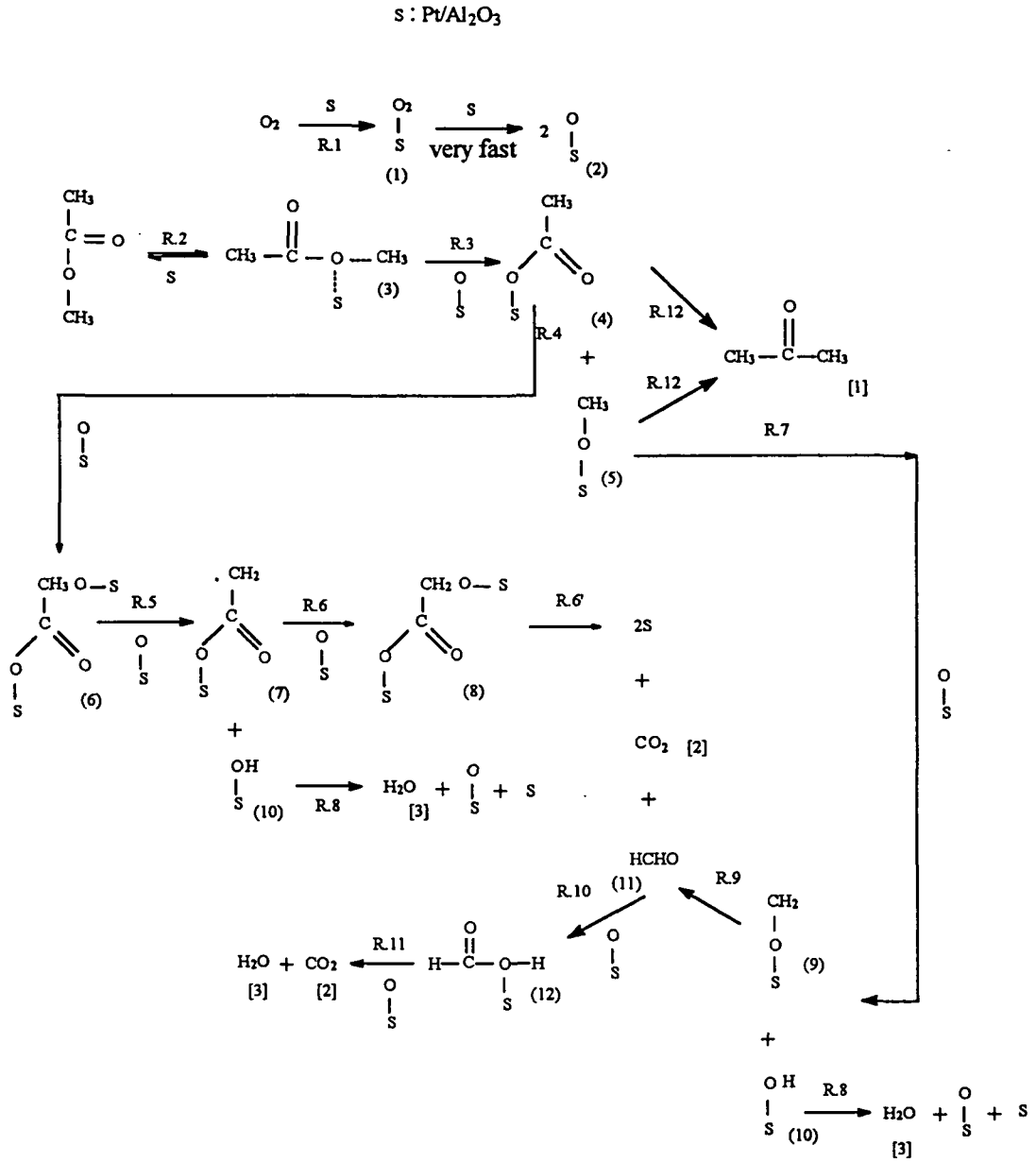

Figure 38

Scheme of Methyl Acetate Reaction over Pt/Al_2O_3 Catalyst

(S represents a catalytic site)

After MA is adsorbed on the site, an intermediate species, MA·S (3), is formed from reaction step V-R2. Then the adsorbed species O·S reacts with the adsorbed species MA·S (3) through a surface interaction reaction, to form the species $CH_3CO(O{\cdot}S)$ (4) and $CH_3(O{\cdot}S)$ (5). The bond between CO--CH_3 inside MA·S (3) is broken because another adsorbed atomic oxygen O·S reacts with the methyl free radical $\cdot CH_3$. Following an electron rearrangement, species (4) and (5) are formed through reaction step V-R3. Reaction step V-R3 is proposed as the rate-limiting step.

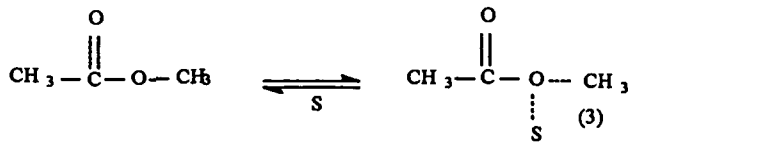

V.R2

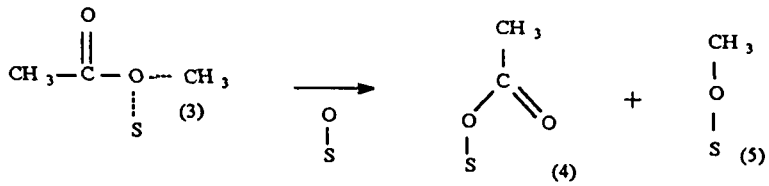

V.R3

The reaction is then assumed to follow Langmuir-Hinshelwood kinetics. The rate equation will be deduced in next section. Reaction step V-R4 indicates that species (4) $CH_3CO(O{\cdot}S)$, formed from reaction step V-R3, may rapidly react with O·S to produce $(S{\cdot}O)CH_3CO(O{\cdot}S)$ (6). Following reaction step V-R5, a hydrogen atom connected with the carbon atom of species (6) is transferred to connect with oxygen inside the species S·O. Also, because of the low bond energy between H_3C--O, species (6) is dissociated into $\cdot CH_2CO(O{\cdot}S)$ (7) and (S·O)H (10). Species (7) may further react with O·S to form species $(S{\cdot}O)CH_2CO(O{\cdot}S)$ (8) through reaction step V-R6. Rapidly, through reaction step V-R6', species (8) may further be dissociated into CO2 [2], HCHO (11) and two reduced catalyst sites because of the low bond energy of S--O and C--C. The CO2 [2] is a final product. Species (11) was not detected. It may have been oxidized immediately; details are discussed below.

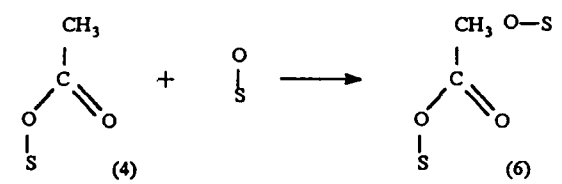

V.R4

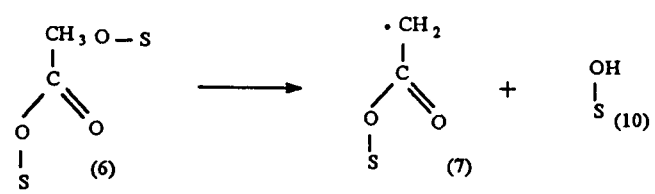

V.R5

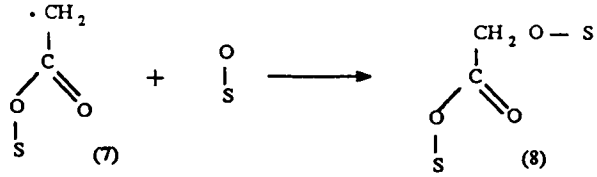

V.R6

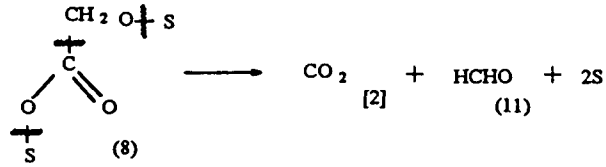

V.R6'

Reaction step V-R7 indicates the species $CH_3(O{\cdot}S)$ (5) from reaction step V-R3 may react with species O·S to form $CH_2(O{\cdot}S)$ (9), and (S·O)H (10) by a hydrogen atom transfer.

V.R7

Reaction step V-R8 indicates two species, S·OH (10) from reaction steps V-R5 and V-R7, may be combined to form water, H_2O [3], a species O·S, and a vacant site. Reaction stepV-R9 indicates the species $CH_2(O{\cdot}S)$ (9), coming from reaction steps V-R5 andV-R7, may form a component HCHO (11) and an empty site by a desorption reaction. Following reaction step V-R10, the HCHO(11) from reaction steps V-R6 and V-R9 may quickly react with species O·S to form HCO(O·S) H (12) with hydrogen atom isomerization.

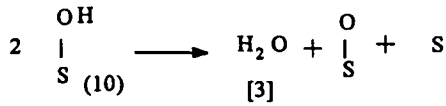

V.R8

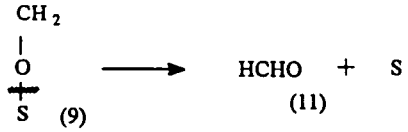

V.R9

V.R10

Reaction step V-R11 indicates the HCOOH·S (12), from V-R10, may react with S·O to produce the final products, CO_2 [2], H_2O [3] and two empty sites, by hydrogen atom isomerization and a desorption reaction.

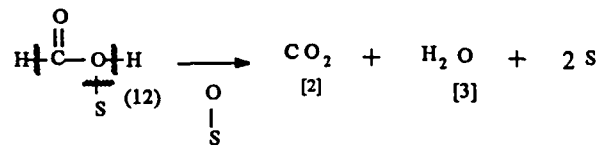

V.R11

Reaction step V-R12 indicates that $CH_3CO(O·S)$ (4) and $CH_3(O·S)$ (5), from reaction step V-R3, may be combined to form the byproduct acetone [1] and two species O·S. The acetone has been identified by GC/MS. However, acetone [1] was detected from the catalytic oxidation of MA on the P-type monolithic catalyst, but was not detected on the E-type monolithic catalyst.

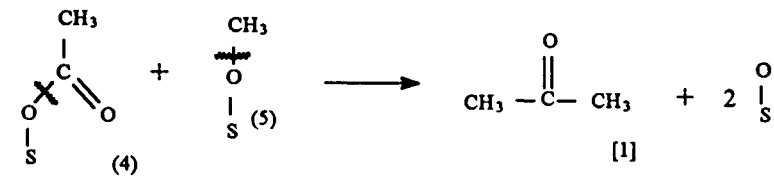

V.R12

Rate Equation Deduction for Dilute Concentration of MA

To deduce the rate equation, the following hypotheses are advanced in a discussion of the reaction mechanism.

1. The surface reaction rates of chemisorbed methyl acetate and oxygen are much slower than that of the adsorption and desorption processes. Consequently, equilibrium adsorption probably dominates and a Langmuir-Hinshelwood-type kinetic process is observed, with competitive adsorption of the MA [Barresi, 1992]. A Langmuir-Hinshelwood model has been proposed for methyl acetate over Pt/Al_2O_3 catalyst [Li, 1993]. The advantages of the Langmuir-Hinshelwood method are: (1) the resultant rate equation may be extrapolated more accurately to concentrations beyond the range of experimental measurements used; and (2) the method does take into account adsorption

and surface reactions (which must occur) in a consistent manner.

2. The reaction occurred on a uniform surface with the participation of weakly bound oxygen in the form of $O_2 \cdot S$.

3. The adsorption of oxygen and the interaction of $O \cdot S$ with the methyl acetate is irreversible.

4. The formation of CO_2 and H_2O is assumed not to inhibit the overall rate of oxidation of MA.

5. The theorems of two-step catalytic reaction are used to deduce the rate equation of MA oxidation.

6. Each elementary step involving interaction of intermediates is irreversible on the oxidized surface of the Pt/Al_2O_3 catalyst.

The elementary steps of adsorption, surface reaction, and desorption of MA oxidation may be expressed as follows:

$$O_2 + 2S \xrightarrow{k_1} O_2S + S \xrightarrow{fast} 2O \bullet S \qquad \text{V.R13}$$

$$CH_3COOCH_3 + S \underset{k_3}{\overset{k_2}{\rightleftharpoons}} CH_3COOCH_3 \bullet S \qquad \text{V.R14}$$

$$CH_3COOCH_3 \bullet S + O \bullet S \xrightarrow{k_4} CH_3COO \bullet S + CH_3O \bullet S \qquad \text{V.R15}$$

$$CH_3COO \bullet S + O \bullet S \xrightarrow{fast} S \bullet OCH_3COO \bullet S \qquad \text{V.R16}$$

$$S \bullet OCH_3COO \bullet S \xrightarrow{fast} S \bullet OH + CH_2COO \bullet S \qquad \text{V.R17}$$

$$CH_2COO \bullet S + O \bullet S \xrightarrow{fast} S \bullet OCH_2COO \bullet S_{(transition)} \qquad \text{V.R18}$$

$$S \bullet OCH_2COO \bullet S_{(transition)} \xrightarrow{fast} 2S + CH_2O + CO_2 \qquad \text{V.R18'}$$

$$CH_3O{\bullet}S+O{\bullet}S \xrightarrow{fast} CH_2O{\bullet}S+OH{\bullet}S \qquad \text{V.R19}$$

$$2OH{\bullet}S \xrightarrow{fast} H_2O+O{\bullet}S+S \qquad \text{V.R20}$$

$$CH_2O{\bullet}S \xrightarrow{fast} HCHO+S \qquad \text{V.R21}$$

$$HCHO+O{\bullet}S \xrightarrow{fast} HCOOH{\bullet}S \qquad \text{V.R22}$$

$$HCOOH{\bullet}S+O{\bullet}S \xrightarrow{fast} CO_2+H_2O+2S \qquad \text{V.R23}$$

The net oxidation reaction of MA is given as:

$$CH_3COOCH_3+7/2O_2 \rightarrow 3CO_2+3H_2O \qquad \text{V.R24}$$

Since reaction V.R15 is a rate control step, equilibrium adsorption may take place. Because of the fast reaction rate for intermediates, the concentrations of all intermediates compared with that of MA·S and O·S are so low that they are negligible. Only k_1 and k_4 are significantly smaller than other rate constants of reaction of intermediates. Therefore, the theorems of two-step catalytic reaction are used to develop the kinetic model from the possible mechanisms for the oxidation of MA. When the system reaches a steady state process in an ideally absorbed layer, the equations below are then obtained.

Let the occupied fraction of sites on which adsorption of oxygen atom and MA be θ_o and θ_{MA}, and the fraction of vacant sites be θ_v. In this case, $\theta_{MA} = b\, C_{MA}$ (the Henry region). Therefore, the rate equation is presented as:

$$rate,\ \frac{(moles)}{(time)(area)} = k_4\theta_{MA}\theta_O \qquad (18)$$

The MA is in the ppmV level in this study. With the Henry region (θ_{MA}= b C_{MA}), the θ_{MA} is so small that it can be neglected. Therefore, the fraction of vacant sites plus the fraction of sites occupied by oxygen shall be equal to one. Thus,

$$1 = \theta_O + \theta_V \tag{19}$$

When a steady state between reaction step V.R13 and V.R15 is reached, the rate of adsorption of oxygen molecules is equal to the rate of adsorbed MA reacted with absorbed oxygen atoms. Thus,

$$k_1 P_{O_2} \theta_V = \nu k_4 \theta_{MA} \theta_O \tag{20}$$

Combining Eqs 19 and 20,

$$\theta_O = \frac{k_1 P_{O_2}}{k_1 P_{O_2} + \nu k_4 b C_{MA}} \tag{21}$$

Eq 21 is then substituted into Eq 18 to obtain the following Langmuir-Hinshelwood rate equation:

$$rate = \frac{k_1 k_4 b P_{O_2} C_{MA}}{k_1 P_{O_2} + \nu k_4 b C_{MA}} \tag{22}$$

This Langmuir-Hinshelwood model has been correlated with the experimental data obtained in this investigation for high MA concentration (>1000 ppmV) over a monolithic catalyst [Chalasani, 1995].

If the oxygen coverage is very low and if the MA partial pressure is very high, i.e., $k_1 Po_2 << \nu k_4 b C_{MA}$ for the reaction condition,

$$rate = \frac{k_1 P_{O_2}}{\nu} \tag{23}$$

In this case the reaction rate no longer depends on the MA concentration.

If the oxygen coverage is very high and MA coverage is very low, i.e., $k_1 Po_2 >> \nu k_4 b C_{MA}$, the reaction rate is then reduced to Eq 24:

$$rate = k_4 b C_{MA} \tag{24}$$

where k_1 = reaction rate constant of 7.R1
k_4 = reaction rate constant of 7.R3, mole/area time pressure
b = Henry coefficient (hydrocarbon adsorption), pressure^{-1}
θ_o = fraction of sites occupied by oxygen atoms, dimensionless
θ_v = faction of vacant sites, dimensionless
θ_{MA} = fraction of sites occupied by MA, dimensionless
C_{MA} = concentration of MA, mole/volume
P_{o2} = partial pressure of O2
ν = stoichiometric coefficient of oxygen, 7/2 mole/mole for MA.

and is a first-order equation with respect to MA concentration. The first-order model has also been observed from the experimental data obtained in this investigation for low MA concentration (<1000 ppmV) over a monolithic catalyst [Chalasani, 1995].

VI. CONCLUSIONS

The follwoling conclusions may be drawn from this investigation:

1. Both monolithic and pellet catalysts coated with Pt/Al_2O_3 are demonstrated to be able to completely oxidize methyl acetate at high temperature (≥420°C) to form carbon dioxide and water. Trace amounts of byproducts (acetic acid, methanol, and acetone), ranging from 1 to 30 ppmV, have been detected in the reactor exit stream at low temperature (≤ 420°C), high MA concentrations (> 500ppm), and high gas flowrates (>3.0 l/min).

2. The preheater packed with glass beads causes both thermal and catalytic decomposition of methyl acetate to form four byproducts: methanol, methyl formate, acetic acid, and 1-propanol. The preheater produces higher concentrations of byproducts at higher temperatures.

3. Results form the Taguchi experimental design indicate that the reaction temperature is the most significant factor affecting the conversion of MA. The next most significant factor is gas flow rate, followed by methyl acetate concentration. Both concentrations of carbon dioxide and oxygen have insignificant effect on the conversion of methyl acetate.

4. Kinetic data of methyl acetate oxidation through a monolithic catalytic reactor indicate that a both first-order and the Langmuir-Hinshelwood models are fitted equaly well at low MA concentration. However, at higher concentrations of MA, Langmuir-Hinshelwood model is better than that of the first-order model.

5. Based on the adsorption of oxygen and MA molecules on active catalytic sites, a reaction mechanism is proposed to explain the oxidation of MA to form carbon dioxide, water, and byproducts. The rate law derived from this mechanism confirms that the kinetics of the catalytic oxidation of MA fits the a Langmuir-Hinshelwood model.

VII. LITERATURE CITED

Barresi, A. A. and Baldi, G.(1992). Deep Catalytic Oxidation Kinetics of Benzene-Ethenylbenzene Mixture. Chemical Engineering Science, 47(8), 1943-1953.

Barresi, A. A. and Baldi, G. (1993). Reaction Mechanisms of Ethanol Deep Oxidation over Platinum Catalyst. Chemical Engineering Communication, 123, 17-29.

Becker, E. R., and Pereira, C.J.(1989). Catalyst and Reactor Design for Emission Control. AIChE Advanced Seminar Series.

Bobyshev, A. A. and Radtsig V.A. (1990). Free-Radical Centers with Preassigned Structure on the Surface of Silicon Dioxide, and Their Reactivity in Substitution Reactions. Kinetics and Catalysis: 31(4), 810-815.

Chalasani, P. (1994). The Kinetic Study of Methyl Acetate Oxidation over Platinum Coated Monolithic Catalyst. Unpublished Master's Thesis, Lamar University, Beaumont, TX.

Chen, Shi-Min (1995).Catalytic Oxidation of Methyl Acetate Conversion and Byproduct Identification. Inpublished Master's Thesis, Lamar University, Beaumont, TX.

Czitrom, V. (1989). Taguchi methods: Linear Grapgs of High Resolution. Communications in Statistics. Part A, Theory and methods, 18(12), 4583-4606.

Dwidevi, P. N., and Upadhyay, S. N., "Processes Development for Catalysis (1977). "Industrial and Engineering Chemistry. Process Research and Development, 16,157-165.

Elikan, L.(1966). "An Approach to Water Management for Long Duration Manned Space Flights," Aerospace Life Support volume of Chemical Engineering Progress Symposium Series Number 63, Volume 62, American Institute of Chemical Engineers, New York, NY.

Froment, G. F., and Bischoff, K. B.(1979). Chemical Reactor Analysis and Design. New York: John Wiley & Sons, Inc..

Garibyan, T. A. and Margolis, L. Y. (1990). Heterogeneous-Homogeneous Mechanism of Catalytic Oxidation. Catalysis Reviews and Science Engineering, 31(4), 355-384.

Golodets, G. I. (1983). Heterogeneous Catalytic Reactions Involving Molecular Oxygen. New York: Elsevier Amsterdam.

Gunst, R. F., and Mason, R. L.(1980).Regression Analysis and Its Application. New York: Marcel Dekker, Inc..

Henninger, D.(1993). "Controlled Ecological Life Support Systems (CELSS) Research and Technology Development at the Johnson Space Center," CELSS Conference of 1993, Alexandria, Virginia, March 1-3.

Kesselring, J. P.(1986) "Catalytic Combustion", Advanced Combustion Method. London: Acdemic Press, 237-275.

Lange, K. E.(1991)."Summarized Work on the Analysis of a Proposed Metabolic Simulator", NASA/JSC Document.

Lange, K. E.(1992)."Requirements for the Test Bed Metabolic Simulator," Report to NASA-JSC,

Li, Jeffrey S.(1993). "The Kinetic Study of Methyl Acetate Oxidation over Platinum Alumina

Catalyst", Masters Thesis, Lamar University, Beaumont, Texas.

Li, K. Y., et al, (1994) "Kinetic Study of Methyl Acetate Oxidation in a Pt/Al2O3 Fixed-Bed Reactor", Dual-Use Space Technology Transfer Conference and Exibition, NASA Conference Publication 3263, Vol. 1, pp. 226-235.

Lin, C. H.(1982). "Space Station Environmental Control and Life Support System Preliminary Conceptual Design," NASA/JSC Doc. No. CSD-SS-059.

Maurel, J.-L., and J.-L. Vernet (1982). "Catalyse. - Etude de la Combustion Catalytique du Formlate et de l'Acetate de Methyle," C. R. Seances Acad. Sci. Ser. 2, 294(1) 25-28

Mears, D. E. (1971). "Test for Transport Limitations in Experimental Catalytic Reactors," Industrial and Engineering Chemistry Process Design and Development. 10, 541-548,

Morrison, R. T. and Boyd, R. N. (1983). Organic Chemistry. Boston, MA: Allyn and Bacon, Inc.

Ross, P. T. (1988). "Taguchi Techniques for Quality Engineering", McGraw Hill.

Roy, R (1990). "A Primes on the Taguchi Method," Van Nostrand Reinhold.

Simon, W.E. et al., (1994). "Advanced Support Systems Development and Supporting Technologies for Controlled Ecological Life Support Systems (CELSS)," Final Report, NASA Grants NAG9-620 and NAG9-640, August 31, 1994.

Satterfield, C. N. (1970). Mass Transfer in Heterogeneous Catalysis, Robert E. Kriegger Publishing Co.

Schwartzkopf, S. H.(1992). "Design of a Controlled Ecological Life Support System," BioScience, Vol 42, No. 7, 526.

Sawyer, J. E. and Abraham M. A. (1994). Reaction Pathways during the Oxidation of Ethyl Acetate on a Platinum/Alumina Catalyst. Industrial Engineering Chemical Product Research Development, 33, 2084-2089.

Volter, J., Lietz, G., Spindler, H., and Lieske, H. (1987). Role of metallic and Oxidic platinum in the catalytic combustion of n-heptane. Journal of Catalysis, 104, 375-380.